*Astronomy & Astrophysics* manuscript no. output
May 5, 2025


# Luminaries in the Sky: The TESS Legacy Sample of Bright Stars

## I. Asteroseismic detections in naked-eye main-sequence and sub-giant solar-like oscillators

Mikkel N. Lund[1], Ashley Chontos[2], Frank Grundahl[1], Savita Mathur[3,4], Rafael A. García[5], Daniel Huber[6,7], Derek Buzasi[8], Timothy R. Bedding[7], Marc Hon[9,6], and Yaguang Li[6]

[1] Stellar Astrophysics Centre, Department of Physics and Astronomy, Aarhus University, Ny Munkegade 120, DK-8000 Aarhus C, Denmark
[2] Department of Astrophysical Sciences, Princeton University, 4 Ivy Lane, Princeton, NJ 08540, USA
[3] Instituto de Astrofísica de Canarias (IAC), E-38205 La Laguna, Tenerife, Spain
[4] Universidad de La Laguna (ULL), Departamento de Astrofísica, E-38206 La Laguna, Tenerife, Spain
[5] Université Paris-Saclay, Université Paris Cité, CEA, CNRS, AIM, F-91191, Gif-sur-Yvette, France
[6] Institute for Astronomy, University of Hawai'i, 2680 Woodlawn Drive, Honolulu, HI 96822, USA
[7] Sydney Institute for Astronomy (SIfA), School of Physics, University of Sydney, NSW 2006, Australia
[8] Department of Astronomy & Astrophysics, University of Chicago, Chicago, IL 60637, USA
[9] Department of Physics and Kavli Institute for Astrophysics and Space Research, Massachusetts Institute of Technology, 77 Massachusetts Ave, Cambridge, MA 02139, USA

Received September 15, 1996; accepted March 16, 1997

**ABSTRACT**

*Aims.* We aim to detect and characterise solar-like oscillations in bright naked-eye ($V$<6) main-sequence and subgiant stars observed by the Transiting Exoplanet Survey Satellite (TESS). In doing so, we seek to expand the current benchmark sample of oscillators, provide accurate global asteroseismic parameters for these bright targets, and assess their potential for future detailed investigations – including missions such as the Habitable Worlds Observatory (HWO) and PLAnetary Transits and Oscillations of stars (PLATO).
*Methods.* Our sample of bright stars was selected from the Hipparcos/Tycho catalogues. We analysed TESS photometry from both 120-s and 20-s cadences using the standard TESS Science Processing Operations Center (SPOC) light curves and custom apertures extracted from target pixel files. After applying a filtering of the light curves, we extracted global asteroseismic parameters ($\nu_{\rm max}$ and $\Delta\nu$) using the `pySYD` pipeline. Results were cross-validated with independent pipelines and compared to predictions from the Asteroseismic Target List (ATL), while noise properties were evaluated to quantify improvements from a 20-s observing cadence.
*Results.* We detect solar-like oscillations in a total of 196 stars—including 128 new detections – with extracted $\nu_{\rm max}$ and $\Delta\nu$ values showing strong conformity to expected scaling relations. This corresponds to an increase by more than an order of magnitude in the number of main-sequence stars with detection of solar-like oscillations from TESS. Importantly, our sample of newly detected solar-like oscillators includes nearly 40% of the prime targets for HWO, paving the way for a systematic determination of asteroseismic ages that will be important for the possible interpretation of atmospheric biosignatures. Our analysis confirms that 20-s cadence data yields lower high-frequency noise levels compared to 120-s data. Moreover, the precise stellar parameters obtained through asteroseismology establish these bright stars as benchmarks for seismic investigations and provide useful constraints for refining stellar evolution models and for complementary analyses in interferometry, spectroscopy, and exoplanet characterisation.

**Key words.** Asteroseismology – Stars: oscillations – Stellar properties – Catalogues – Binaries: general – Planetary systems – Methods: data analysis

## 1. Introduction

Asteroseismology from space-based photometric missions has, in the last decade-and-a-half, heralded a revolution in our understanding of stars, exoplanet characterisation, Galactic archaeology, and many more fields within the broad landscape of astrophysics (Chaplin & Miglio 2013; García & Ballot 2019). This revolution was pioneered by the CoRoT (Convection, Rotation, and planetary Transits, Baglin et al. 2006; Michel et al. 2008) and *Kepler*/K2 missions (Borucki et al. 2010; Howell et al. 2014) and the field is now steadily maturing with the ongoing observations by the Transiting Exoplanet Survey Satellite (TESS; Ricker et al. 2014), which we are hopeful will continue for many years to come.

Although TESS, with its larger pixel size, shorter continuous observation periods, and higher background noise compared to, e.g., *Kepler*, has not (yet) yielded the same specific breakthroughs in asteroseismology of main-sequence solar-like oscillators, it offers several unique advantages. TESS provides nearly full-sky coverage, enabling the study of a vast array of bright, well-characterized stars, and for specific regions of the sky the total observing baseline has now surpassed the 4 years from *Kepler*. A 10-min observing cadence now enables asteroseismic studies of stars down to the subgiant regime based on full-frame images, and targeted 120-s and 20-s cadence observations have

*Send offprint requests to*: MNL, e-mail: `mikkelnl@phys.au.dk`

pushed the photometric asteroseismic studies into the K-dwarf regime (Hon et al. 2024).

The bright stars that can be uniquely observed by TESS are crucial because they serve as important benchmarks for future missions, such as PLATO (PLAnetary Transits and Oscillations of stars, Rauer et al. 2024), and many of them will be included in the target list for the future Habitable Worlds Observatory (HWO) mission (Mamajek & Stapelfeldt 2024). Moreover, their brightness makes them ideal for follow-up ground-based observations, which can significantly enhance our understanding of stellar physics.

With this work, we present a catalogue of 196 asteroseismic detections for the brightest solar-like main-sequence (MS) and subgiant (SG) oscillators observed by TESS. Hereafter, we refer to this cohort of stars as the *TESS Luminaries Sample* (TLS). Of these, 128 are to our knowledge new detections, thereby more than doubling the number of known bright MS/SG oscillators, and include many of the stars predicted by Bedding et al. (1996) to show oscillation in the early days of asteroseismology. We have limited our sample to stars with $V < 6$, hence stars that, for most people, will be visible to the naked eye under favourable observing conditions. For MS/SG stars in the brightness range of interest here, asteroseismic analyses based on TESS data have to date mainly focused on single or few stars (see, e.g., Ball et al. 2020; Metcalfe et al. 2020; Nielsen et al. 2020; Chontos et al. 2021; Huber et al. 2022; Ball et al. 2022; Corsaro et al. 2024) – with the TLS catalogue we aim to provide a comprehensive asteroseismic catalogue of all the bright solar-like oscillators observed by TESS, and we will continue to update and extend the catalogue as more data from TESS become available. With its focus on MS/SG stars, the TLS catalogue can be seen as a complement to the HD-TESS catalogue by Hon et al. (2022) focusing on bright evolved stars observed by TESS. The adopted brightness limit is admittedly somewhat arbitrary, but our analysis suggests that most fainter stars have already been covered by the recent impressive catalogues by Hatt et al. (2023) and Zhou et al. (2024), both providing detections for thousands of solar-like oscillators from TESS, but mainly focusing on evolved solar-like stars (SG and RG). So, while we can generally confirm their detections for overlapping stars, we note that many of the brightest stars were not included in their analyses.

For the stars with detected oscillations, we provide measurements for the global asteroseismic parameters $\Delta\nu$ and $\nu_{\rm max}$ (Chaplin & Miglio 2013; García & Ballot 2019). With our results, we seek to highlight the opportunities for further detailed analysis from TESS for this cohort of stars that can prove valuable as benchmarks for stellar evolution theory and the asteroseismic method. Importantly, several of the stars that can be characterised asteroseismically by TESS, and in some cases by ground-based facilities such as SONG (Grundahl et al. 2017), will also be observed by the coming ESA PLATO mission and can here serve as key benchmarks for the quality of PLATO results (Sect. 5.3).

The brightness of the stars in this catalogue enables a detailed characterisation of their properties. This is both in terms of asteroseismology, with the current and future observation from TESS, and crucially also from ground-based observations such as spectroscopy (e.g., Tautvaišienė et al. 2022), interferometry (Vrard et al. 2024), spectropolarimetry (Metcalfe et al. 2023, 2024), measuring binary or multiple-star properties (Malla et al. 2024), and in some cases asteroseismic follow-up in radial velocity (Kjeldsen et al., submitted to A&A).

The paper is structured as follows: in Sect. 2 we outline the target sample, in Sect. 3 we describe our treatment of TESS data, while in Sect. 4 we describe our asteroseismic analysis methodology. Sect. 5 is devoted to presenting the results of our analysis and highlighting the potential use cases and interesting aspects of the stars in our sample, including synergies with PLATO and HWO, exoplanets, interferometry, binarity, solar analogues, and individual cases.

This paper is the first in a series, and follow-up papers in development will focus on the detailed peak-bagging and stellar modelling for the highest quality targets in the sample, a detailed analysis of the targets that overlap with PLATO fields, an analysis of the detectability of solar-like oscillators near the red-edge of the classical instability strip, updates to exoplanet parameters and analysis of HWO targets, and a detailed analysis of several individual stars/systems.

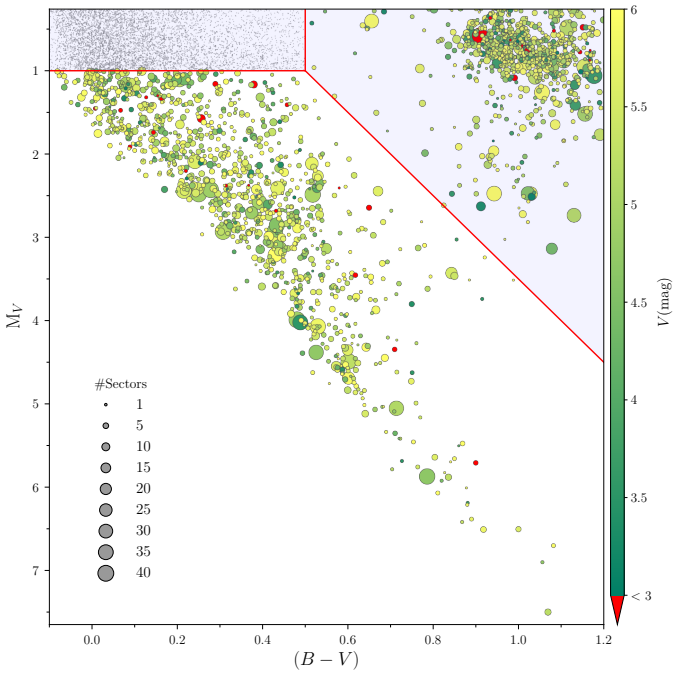


**Fig. 1.** HR-diagram showing the criteria for our selection of targets. The red line shows our limits on $M_V$ and $(B-V)$, and targets in the lower non-shaded region were selected for analysis. The marker colour indicates the $V$-band magnitude for the stars, while the marker size indicates the number of sectors TESS will have observed a given star in Cycle 6 (up to and including Sector 83). The stars in the top left shaded box are not expected to show solar-like oscillations and here we have not indicated $V$ nor the number of sectors. The stars in the top-right shaded region contain evolved stars that may well show solar-like oscillations – these will be the subject of a future study.

## 2. Targets

The starting points for building our sample are the Hipparcos and Tycho catalogues (Perryman et al. 1997; Hoeg et al. 1997; van Leeuwen et al. 1997; hip 1997). To limit our sample to stars visible to the naked eye, we first selected stars with a $V$-band magnitude below 6. Based on Hipparcos parallaxes we computed the absolute $V$-band magnitude, $M_V$, and used this in combination with the $(B-V)$ colour as a proxy for the effective temperature to select stars that reside on the main-sequence (MS) or subgiant branch (SGB) – our specific selection criteria are shown in Fig. 1. The adopted limits are conservative because many of the high-$M_V$ targets are expected to be classical pulsators. However,

we wanted to ensure that no solar-like oscillators near the red edge of the classical instability strip were excluded.

We also checked the Yale Bright Star Catalog (5th ed.; Hoffleit & Warren 1995) and the Gliese Catalogue of Nearby Stars (3rd ed.; Gliese & Jahreiß 1991) for targets that Hipparcos may have missed. However, none of the missing targets identified matched our selection criteria for $M_V$ and $B-V$. We note that for several targets that are members of binary systems, the Hipparcos (HIP) ID generally refers to the system rather than the individual components, as opposed to the TESS input catalogue (TIC; Stassun et al. 2019), which builds on *Gaia* (Gaia Collaboration et al. 2018) and the Two Micron All Sky Survey (Cutri et al. 2003) – for these targets we manually assigned the TIC ID for the main component of the binary to the HIP ID.

Finally, we excluded known oscillators $\alpha$ Cen A and B (Bouchy & Carrier 2001, 2002; Carrier & Bourban 2003; Kjeldsen et al. 2005), and $\alpha$ CMi (Procyon; Brown et al. 1991; Martić et al. 1999; Arentoft et al. 2008) from our analysis as these extremely bright targets require special treatment in the form of a recalibration of the target pixel files and the smear data[1].

From data availability, our sample is limited to stars with 120-s or 20-s cadence observations in at least one TESS sector up to and including Sector 77. These criteria leave us with 1060 stars to be analysed (see Fig. 1), and of these 311 have at least one sector with 20-s cadence observations.

By the end of TESS Cycle 7 (up to and including Sector 92) an additional 69 targets that match our $M_V$ and $B-V$ selection criteria will have been observed (the observing cadence will depend on their inclusion in Guest Investigator proposals), among which are well-known asteroseismic targets such as 18 Sco (Bazot et al. 2011) and 70 Oph (Carrier & Eggenberger 2006b). These targets are primarily located near the ecliptic plane in the constellations of Libra, Scorpius, Ophiuchus, and Sagittarius, and none of them overlap with the PLATO fields (Sect. 5.3). These targets will generally only be observed during a single sector and, in a few cases, 2–3 sectors, so for the most promising of these targets having access to 20-s cadence observations will be particularly important. Finally, 19 Hipparcos targets that match our $M_V$ and $B-V$ criteria have not been, and will not be, observed by TESS up to and including TESS Cycle 7. Table A.1 in Appendix A provides an overview of these targets.

## 3. Data

Our main source of data comes in the form of `PDCSAP` light curves generated by the TESS Science Processing Operations Center (SPOC; Jenkins et al. 2016). We used light curves with both a 120-s and, when available, 20-s cadence (introduced from Sector 27 onwards). All data were downloaded from the Mikulski Archive for Space Telescopes (MAST) using functionalities provided by `Astroquery` (Ginsburg et al. 2019) and `lightkurve` (Lightkurve Collaboration et al. 2018).

For the targets where a detection of oscillations was made from an initial inspection of the data, and/or where a detection was expected[2] from the asteroseismic target list (ATL; Schofield et al. 2019) in the updated version provided by Hey et al. (2024)[3], we also analysed the data contained in the star's target pixel files (TPFs; see Sect. 4). In the TPF analysis, we specifically focused on the light curve improvement from constructing custom apertures. We used the K2P$^2$ pipeline (Lund et al. 2015) to create apertures via the density-based clustering algorithm `DBSCAN`, as implemented in `scikit-image` (van der Walt et al. 2014), combined with a watershed algorithm to separate close targets. The clustering algorithm was applied to pixels with flux values greater than 3 times the standardised median absolute deviation (MAD) from the median flux level. This routine is, by construction, excellent at defining apertures that include pixels that are grouped, but the occasional long bleed trails from the blooming of brighter saturated stars are more difficult to handle. However, while the apertures defined by SPOC are often small near the centroid of the star, the bleed trails are generally well-covered. Therefore, in the end, we opted to construct apertures by combining those from K2P$^2$ and SPOC.

In certain instances, we could only make a positive seismic detection after adopting the custom joint aperture and, for several cases, the custom apertures significantly improved the data quality. Fig. 2 provides an example of a problematic SPOC aperture for the star $\psi^1$ Dra A (TIC 441804568). The scatter in the light curve introduced by the SPOC aperture, which is missing several bright pixels, inhibits the detection of a seismic signal. As seen, when adopting the larger custom aperture, the noise level in the power-density spectrum (PDS) is significantly reduced, and oscillations can be detected.

We noticed that the pixel stamp available for 20-s cadence data was sometimes significantly smaller than the corresponding 120-s cadence pixel stamp – examples of this are $\delta$ Eri (TIC 38511251), $\gamma$ Lep (TIC 93280676), and $\epsilon$ Eri (TIC 118572803). For these stars, the saturated bleed trails extend beyond the 20-s cadence stamp, causing the resulting light curves to have high noise levels. This inhibits the detection of oscillations from the 20-s data, while detections from the 120-s data are possible.

In some cases, mainly for the brightest stars in the sample (e.g. $\theta$ UMa; TIC 150226696), SPOC light curves are not available for all sectors. In these cases, TPF data are needed to make full use of the TESS observations. We refer to Appendix B for additional details on the comparison of SPOC and custom apertures.

In sectors where both 20- and 120-s light curves were available, we used the 20-s data binned to a 120-s cadence. As demonstrated by Huber et al. (2022), the 20-s data from TESS generally has lower noise than 120-s data, especially for bright stars, and with a reduction of scatter of the order ~25% at TESS magnitude 6 (see Sect. 5.2).

Before searching for oscillations, we processed the light curves using the KASOC filter (Handberg & Lund 2014) to correct for any spurious signals or long-term trends. In this filtering and the construction of new apertures, we followed the suggestion by Huber et al. (2022) to adopt the `default` quality bitmask defined by `lightkurve`[4] for 120-s cadence data and the `hard` bitmask for 20-s cadence data.

## 4. Asteroseismic analysis

To identify targets of interest for asteroseismic analysis, an initial inspection of SPOC and TPF data (Sect. 3) was conducted using a variety of methods, including visual inspection of all data, autocorrelation function (ACF) analysis of the PDS, échelle

[1] the `Python` module `mundy` (https://github.com/hvidy/mundey) by White & Pope could possibly achieve this.
[2] using the conservative criterion of a detection probability of $P_{\rm det} \geq 50\%$.
[3] available via the `Python` module `tess-atl` (v0.1) at https://github.com/danhey/tess-atl
[4] https://github.com/nasa/Lightkurve/blob/master/lightkurve/utils.py#L19

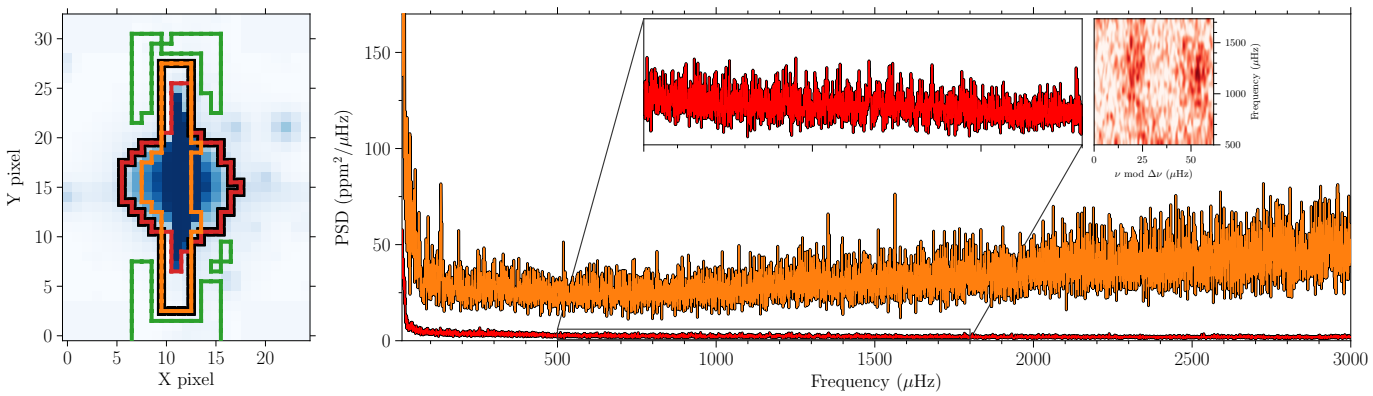


**Fig. 2.** Example of the effect of adopting custom apertures, here for $\psi^1$ Dra A (TIC 441804568) as observed during Sector 15 in 120-s cadence, where the SPOC aperture is missing several high-flux pixels. Similar apertures are seen for $\psi^1$ Dra A in other sectors. Left: The adopted aperture, shown with a black outline, combines the SPOC aperture in orange and the K2P$^2$ aperture in red. The green outline shows the aperture used to estimate the background. In blue the median pixel flux levels are shown on a log-scale. Right: Segments of the power-density spectra of the filtered SAP light curves from the apertures on the left, where the PDS obtained from the SPOC aperture is shown in orange and the one from the adopted custom aperture is shown in red. The inset shows a zoom of the region with identified oscillations from the custom aperture data. The small inset to the right shows the échelle diagram of the zoomed region after correcting for the background using a robust Siegel slope estimator.

diagrams, comparison to expectations from the ATL, etc. To obtain the first estimates of the global asteroseismic parameter $\nu_{\rm max}$ (the frequency of maximum oscillation power) we used a 2D-ACF method (see Verner & Roxburgh 2011), as implemented in `lightkurve`.

For stars with detected oscillations (or an expected detection of oscillations from the ATL) we used the `pySYD` pipeline (Chontos et al. 2022) to extract the global asteroseismic parameters $\Delta\nu$ and $\nu_{\rm max}$. The `pySYD` pipeline is an open-source adaptation of the closed-sourced `SYD` pipeline (Huber et al. 2009), which was extensively tested and benchmarked to *Kepler* LEGACY results (Lund et al. 2017). To summarise, `pySYD` first performs an automated optimisation to identify the best-fit background model due to stellar granulation on different timescales and with varying amplitudes, which can ultimately bias parameter estimates if not properly accounted for. The best-fit background model is then subtracted from the PDS to calculate a background-corrected power spectrum (BCPS), from which $\nu_{\rm max}$ and $\Delta\nu$ can be measured. The frequency corresponding to maximum power ($\nu_{\rm max}$) is adopted as the frequency with peak power in the heavily-smoothed BCPS. An autocorrelation function is then used to identify the characteristic frequency spacing ($\Delta\nu$), which corresponds to the average frequency separating modes of the same spherical degree ($l$) and consecutive radial order ($n$). Due to highly correlated data and the stochastic nature of solar-like oscillations, parameter uncertainties are estimated through a bootstrapping technique discussed in more detail in Huber et al. (2009).

As mentioned in Sect. 3, a detection of oscillations is not always possible from all data products, either because of problems with the aperture and systematics in the light curve or simply from too high noise levels from 120-s cadence data compared to 20-s cadence data. To this end, `pySYD` was applied to PDS prepared from each of the SPOC and custom aperture light curves. We tested on both 120-s cadence and, if available, 20-s cadence data. We calculated a variance-weighted PSD from the full light curves, as well as a PDS from the weighted PDS of individual sectors (weighted by the average variance in each sector). From the results obtained from the different data sets, we identified the ones that agreed within 3 standardised MAD of the median of all results in both $\nu_{\rm max}$ and $\Delta\nu$, checked that these agreed within errors with the initial assessment of $\nu_{\rm max}$, and that $\Delta\nu$ and $\nu_{\rm max}$ were in correspondence with the known relation between these parameters (Hekker et al. 2009; Stello et al. 2009; Huber et al. 2011). From the measurements meeting these requirements, we computed the variance-weighted averages of $\Delta\nu$ and $\nu_{\rm max}$ as our final reported parameters; see Sect. 5.1 for details.

As an additional validation of the identified detections we also applied the `A2Z` pipeline (Mathur et al. 2010b) to our data. Briefly, `A2Z` first blindly searches the modes by computing the power spectrum of the power spectrum in sliding boxes along the PDS. This allows us to measure $\Delta\nu$ along with the frequency range where the modes are detected. The background is then fitted with one Harvey model (Harvey 1985) for the granulation and a component for the photon noise. After subtracting the background a Gaussian function is fitted around the frequency range found in the first step to obtain $\nu_{\rm max}$. For cases with low SNR, the search of the modes was forced to the expected $\nu_{\rm max}$. The 196 stars in the sample represent the consolidated cohort of stars analysed.

## 5. Results

From our asteroseismic analysis, we detected oscillations in a total of 196 stars and provide the extracted global asteroseismic parameters $\Delta\nu$ and $\nu_{\rm max}$ in Table 1. Examples of PDS for some targets with detected oscillations, many of which are new detections, are shown in Fig. 3. In Fig. 4, the TLS is compared to the cohorts obtained from ground-based efforts, other studies based on TESS data, and the previous missions of CoRoT, *Kepler*, and K2.

As seen from Fig. 4, the main overlap with the TLS is from oscillators identified in ground-based efforts, and partly from the Hatt et al. (2023) and Zhou et al. (2024) samples, where our new detections extend these works to brighter stars. In terms of proximity, and thereby brightness, we see that the oscillators found from TESS are complementary to those found from *Kepler*, with K2 and CoRoT nearly closing the gap, at least for sub-giants and more evolved stars. Consequently, the overlap with these missions is very limited, and only includes the CoRoT target HD 49933 (Mosser et al. 2005; Appourchaux et al. 2008; García et al. 2010) and the two *Kepler* targets $\theta$ Cyg (Guzik et al.

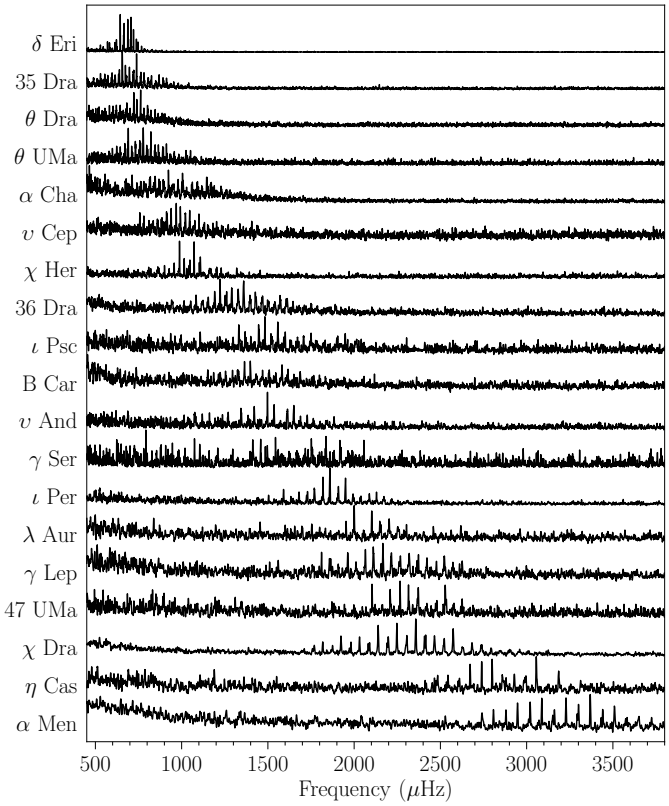


**Fig. 3.** Examples of PDS for a small subset of stars with detected oscillations, arranged according to increasing $\nu_{\rm max}$ (see Table 1 for details). The spectra have been smoothed by an Epanechnikov kernel (Epanechnikov 1969) with a width of $\Delta\nu/20$.

2016) and 16 Cyg A (Metcalfe et al. 2012). With continued observations from TESS, the fainter magnitude limit for seismic detections on the MS will further close the gaps between the samples (Campante et al. 2016). Although we did not investigate the seismic detectability in stars fainter than $V = 6$ in this study, a comparison with the extensive Hatt et al. (2023) and Zhou et al. (2024) catalogues suggests that very few additional MS targets would be detected from the current amount of data. All TLS stars with an earlier seismic detection are identified in Table 1, with reference given to the discovery paper.

### 5.1. Asteroseismic parameters

The correlation between the extracted $\Delta\nu$ and $\nu_{\rm max}$ values is shown in Fig. 5, together with the expected empirical relation obtained from *Kepler* by Huber et al. (2011). The measured values are generally well within expectations, indicated by the 1- and 2-$\sigma$ bands to the empirical relation. The right panel of Fig. 5 shows the kernel density estimates of the relative $\Delta\nu$ and $\nu_{\rm max}$ uncertainties, with median values of ∼1.6% in $\Delta\nu$ and ∼3.7% in $\nu_{\rm max}$. These typical uncertainties are comparable to similar analyses in the literature of MS/SG stars observed with Kepler and K2 (Verner et al. 2011; Viani et al. 2019; Lund et al. 2024; Sayeed et al. 2025). From our analysis, we find that the typical RMS deviation amongst the different values used in the reported weighted average is well below the typical uncertainties, at ∼0.5% in $\Delta\nu$ and ∼1.4% in $\nu_{\rm max}$. Notably, we also find no indications of systematic biases between the different analyses.

We note that the uncertainties obtained for $\Delta\nu$ and $\nu_{\rm max}$ from the individual data products are generally lower (∼0.8% in $\Delta\nu$ and ∼2% in $\nu_{\rm max}$) for 20-s cadence data (when available) or the combination of 120-s and binned 20-s data (depending on the amount of 20-s cadence data available). While these data naturally contribute proportionally more to the final value in the weighted average, the uncertainties are increased slightly by the inclusion of 120-s data and the averaged PDS. However, considering that our main focus is the detection of oscillations and given that not all stars have 20-s cadence data available, we opted to include these data products in the reported averages. Indeed, in some cases the detection and measurement of $\Delta\nu$ and $\nu_{\rm max}$ were only possible when using the averaged PSD (like for 19 Dra (h Dra/TIC 289622310) and $o^2$ Eri (TIC 67772871; Sect. 5.9)).

In addition to the global asteroseismic parameters, we estimate[5] that ∼63% (or ∼125 stars) will be amenable to peak-bagging and the extraction of individual mode parameters (e.g., Handberg & Campante 2011; Davies et al. 2016; Lund et al. 2017; Nielsen et al. 2021). Such a peak-bagging effort and modelling of the asteroseismic parameters will be the subject of future works.

#### 5.1.1. Comparison to the literature

As a check of our global asteroseismic parameters, we compared our values to those of Hatt et al. (2023), Zhou et al. (2024), and Corsaro et al. (2024) for the stars we have in common. In addition, we also compared to the predicted values from the ATL (which was included in the initial pruning of our sample), both versions 1 (Schofield et al. 2019) and 3 (Hey et al. 2024).

Our comparison for $\nu_{\rm max}$ is given in Fig. 6, and shows good overall agreement with the other studies using TESS data. The differences are generally within uncertainties, and we see no apparent bias in differences against $\nu_{\rm max}$. We find the ATL typically underestimates $\nu_{\rm max}$ compared to our values, at a level of ∼10% for ATL1 and ∼16% for ATL3. For ATL3, we can trace this to a general offset in the $\log g$ and $T_{\rm eff}$ values adopted from Gaia DR3 (Gaia Collaboration et al. 2023). We refer to Sect. 5.2 and Appendix C for further discussion on the ATL comparison, which should be considered in future target selection efforts.

In terms of our ability to detect oscillations, we note that for all stars in the Hatt et al. (2023) and Zhou et al. (2024) catalogues that overlap with our sample, we also obtain a detection. Indeed, we confirm all previous detections from single-star analyses of TESS data that we could find in the literature, except for two stars. These are HD 4628 (HIP 3765) and 111 Tau (HIP 25278), listed as confident detections in Corsaro et al. (2024) from TESS observations, for which we could not confirm a detection in our analysis.

Among stars with ground-based detections, we have identified only seven matching our selection criteria where a positive detection could not be made, namely 18 Sco (HIP 79672), 70 Oph (HIP 88601), $\tau$ Boo (HIP 67275), $\epsilon$ Indi (HIP 108870), $\tau$ Cet (HIP 8102), $\iota$ Hor (HIP 12653), and HD 219134 (HIP 114622). No TESS observations up to Sector 77, as considered in our analysis, are available for 18 Sco (Bazot et al. 2011) and 70 Oph (Carrier & Eggenberger 2006b), but both will be observed for one sector during TESS Cycle 7 (Table A.1). For $\tau$ Boo (Borsa et al. 2015) data are available from two sectors, although only with a 120-s cadence; $\epsilon$ Ind (Campante et al. 2024; Lundkvist et al. 2024) has data from two sectors, including one of 20-s cadence, and with more observations scheduled for Sector 95; $\tau$ Cet (Teixeira et al. 2009) also has data from two sec-

[5] This fraction is a heuristic estimate based on previous experience with analysis of comparable *Kepler*/K2 data.

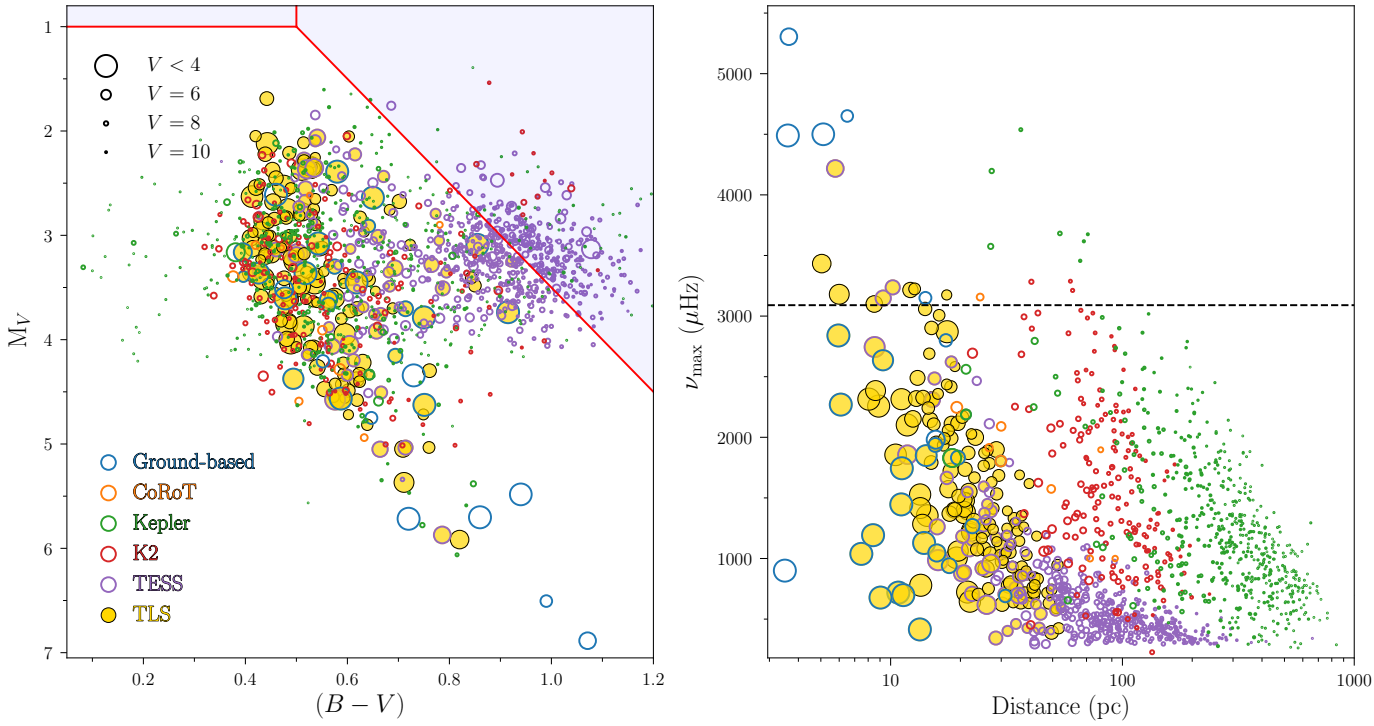


**Fig. 4.** Comparison of the TLS with solar-like detections in MS/SG stars from other missions. Left: position of solar-like oscillators in the HR-diagram, with an indication of the selection criteria in $M_V$ and $(B - V)$ used to define our sample (Sect. 2). The marker size indicates the $V$-band magnitude of the stars, while the marker edge colour indicates how or by which mission oscillations were first detected. Any stars with a detection of oscillations from this work are shown with a filled yellow marker. Stars with ground-based detections were identified from individual cases in the literature (see Table 1 and Sect. 5.1.1); the *Kepler* comparison sample was constructed from the compilations of Lund et al. (2017), Serenelli et al. (2017), Mathur et al. (2022), in addition to Kepler-444 (Campante et al. 2015) and $\theta$ Cyg (Guzik et al. 2016); the 9 stars from CoRoT were identified from individual cases in the literature (Barban et al. 2009, 2013; Appourchaux et al. 2008; Mosser et al. 2009; Mathur et al. 2010a, 2013; Ballot et al. 2011; Boumier et al. 2014; Castro et al. 2021); the stars forming the K2 sample are obtained from Lund et al. (2016, 2024); while the TESS sample was obtained from the catalogues of Hatt et al. (2023), Zhou et al. (2024), and Corsaro et al. (2024) (considering only their confident detections; their Table 1), in addition to individual cases from the literature (see Table 1). For the TESS and K2 comparison samples, we have limited these to stars with $\nu_{max} < 284\,\mu$Hz. Right: distribution of the stars in terms of distance and $\nu_{max}$, using only stars that in the left plot fall within the $M_V$ and $(B - V)$ boundaries defined in our target selection. We note that $\alpha$ Cen A+B, at a distance of ~1.35 pc, have been omitted from the plot. Distances and magnitudes used in this plot were adopted from the TESS Input Catalog (TICv8.2; Paegert et al. 2021). The horizontal dashed line indicates the solar $\nu_{max}$ for comparison.

tors, one with 20-s cadence, but unfortunately the 20-s cadence stamp is too small to contain the star's saturation trails, which adds significant noise to the photometry; $\iota$ Hor (Vauclair et al. 2008) has five sectors of data, of which three are of 20-s cadence; HD 219134 (Li et al. 2025) has four sectors of data, of which two are of 20-s cadence, and with additional observations scheduled for Sector 84. Of these five non-detections, $\epsilon$ Ind, $\tau$ Cet, and HD 219134 are cool dwarfs (spectral types G8, K5, and K3, respectively) and therefore have very low oscillation amplitudes.

### 5.2. Detectability and noise properties

From our asteroseismic analysis, we find that our two sources of light curves, those from SPOC and those extracted from TPFs using custom apertures (Sect. 3), greatly complement each other. Generally, the photometric quality is comparable, but with outliers and regions in visual magnitude where the custom data performs better, typically from an improved aperture that better conserves the stellar flux. As an example of this, Fig. 7 provides a comparison between 20-s cadence light curves (including all stars where custom apertures were computed) from SPOC and those from custom apertures. The two metrics shown are the 1-hour root-mean-square deviation (RMSD; calculated as the standardised MAD of the data binned to 1-hour) and the point-to-point (P2P) median difference variability (MDV; calculated as the median of the absolute point-to-point flux differences, binned to 120-s cadence), both plotted as a function of TESS magnitude. The 1-hour RMSD is similar to the metric estimated in Huber et al. (2022) (their Fig. 2b), and we find that the levels from our sample agree well with those from Huber et al. (2022) in the magnitude range around $T_{mag}$~5.5 where the samples overlap. The P2P-MDV metric is included to measure the high-frequency noise, which is particularly important for the detection of oscillations in MS/SG stars.

We confirm the lower noise of 20-s vs. 120-s cadence data, as demonstrated by Huber et al. (2022), and we can extend their reported improvement of 20-30% to stars down to $T_{mag}$~4.3. Brighter than this magnitude, we observe less improvement, but note that the sample size in this regime is limited to only 39 stars with data from both cadences. For the high-frequency noise, captured by the PTP-MDV, the improvement seems to be even greater, at a level of 30-40% in the median and remaining nearly constant across the magnitude range covered by our sample.

In Fig. 8 we show the minimum high-frequency noise levels (median between $3000\,\mu\text{Hz} < \nu < 4000\,\mu\text{Hz}$) from the power

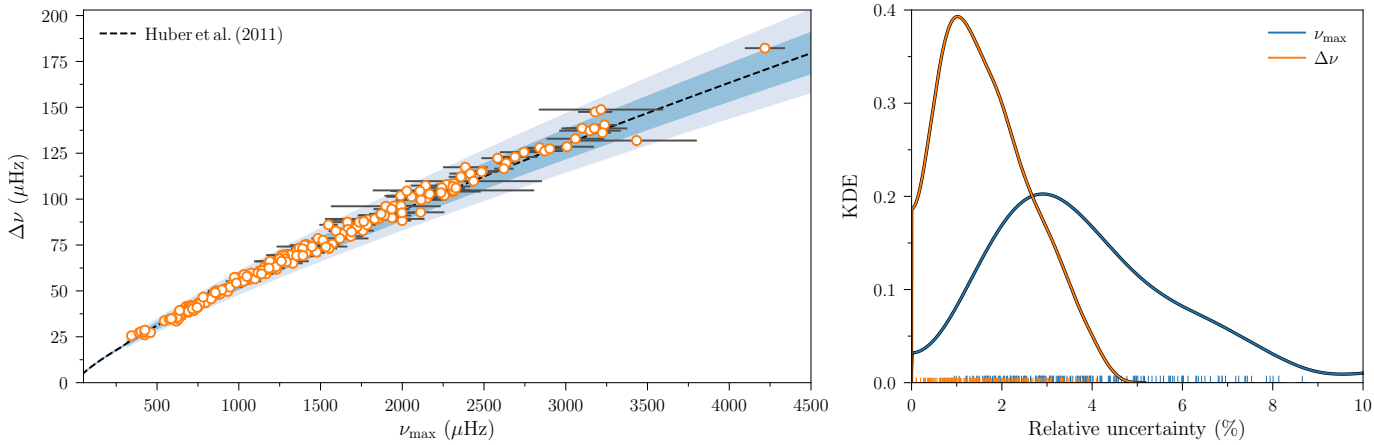


**Fig. 5.** Left: correlation between the measured global asteroseismic parameters $\Delta\nu$ and $\nu_{\rm max}$. The dashed line indicate the empirical relation from Huber et al. (2011) together with the 1- and 2-$\sigma$ confidence bands on their relation. Right: KDE of the relative uncertainties on $\Delta\nu$ and $\nu_{\rm max}$ for the sample, with median values of ∼1.6% in $\Delta\nu$ and ∼3.7% in $\nu_{\rm max}$. The ticks at the bottom of the panel indicate the individual values, coloured according to the legend.

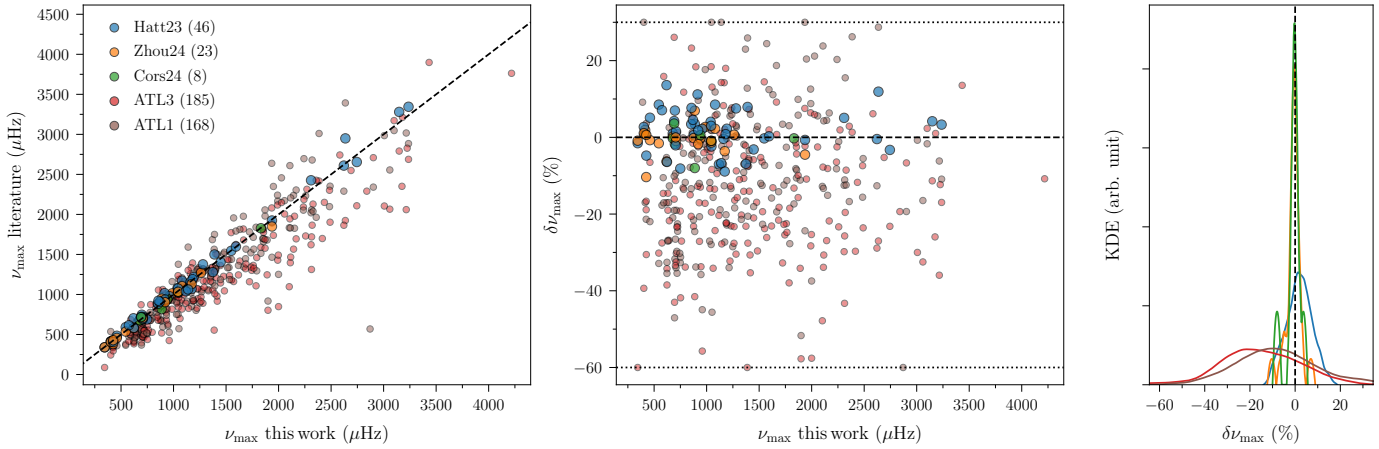


**Fig. 6.** Comparison of $\nu_{\rm max}$ values for the stars in our sample that overlap with those of Hatt et al. (2023), Zhou et al. (2024) and Corsaro et al. (2024), and with the predictions from the Asteroseismic Target List (ATL) versions 1 (Schofield et al. 2019) and 3 (Hey et al. 2024). Left: a direct comparison between our values and those published in the literature or predicted in the ATLs. The colour indicates the comparison source (see legend), while the numbers in the legend indicate how many stars are in common with the different comparison sources. Middle: the relative differences between the values. Values beyond either +30% or −60% have been adjusted to these values (dotted lines) for a better visual rendition. Right: the KDE of the relative differences.

density spectra considered in our analysis against the measured (blue) or predicted (green) $\nu_{\rm max}$ for the stars with a seismic detection or a detection probability in ATL3 of $P_{\rm det} \geq 50\%$ (based on whichever is highest if both 20-s and 120-s cadence observations are available). As expected, we see that stars with a positive seismic detection at a given $\nu_{\rm max}$ generally have lower noise levels than stars without a detection. If we look at the ATL3 detection probabilities, we see that only a single star (HD 49933) with a firm detection has a detection probability below $P_{\rm det} \sim 80\%$, and the vast majority has a rounded probability of 100%. As noted in Sect. 5.1.1 the ATL3 $\nu_{\rm max}$ values are generally underestimated, and hence $P_{\rm det}$ is overestimated, suggesting that most of the stars without a detection, but with high predicted detection probabilities, may indeed be overestimated. We also see that the stars with confirmed detections, but detection probabilities below 100% generally have slightly overestimated $\nu_{\rm max}$ values from ATL3 (hence underestimated detection probabilities). We refer again to Appendix C for further details on the ATL comparison. It is also worth noting that the ATL detectability calculation does not take into account that some targets could have an increased activity level, which is known to suppress the amplitudes of oscillation modes (García et al. 2010; Chaplin et al. 2011a; Mathur et al. 2019). This could also explain why oscillations are not detected in several stars where the noise level should be low enough for detection.

### 5.3. TLS and PLATO

From being or having the potential to become extremely well-characterised, the stars of the TLS are of particular interest as calibrators and benchmarks for future asteroseismology missions, such as the ESA PLATO mission scheduled for launch in late 2026 (Rauer et al. 2024).

PLATO's planned observing strategy is currently focused on two so-called "Long-duration Observation Phase" (LOP) fields, each of which will cover a 49°×49° region of the sky (Rauer et al. 2024). While subject to potential changes following the evaluation of initial observations, the nominal plan is to conduct obser-

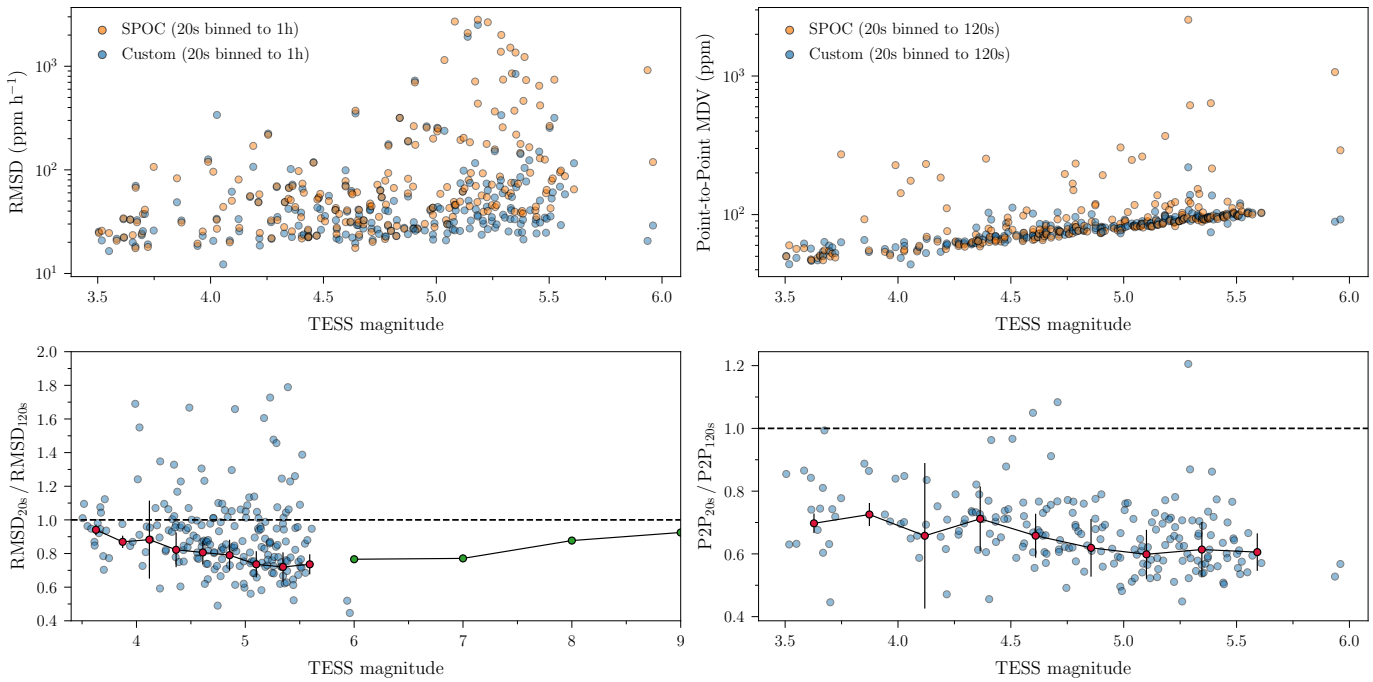


**Fig. 7.** Comparison of noise statistics between different light curve sources and observing cadences, including all stars with 20-s cadence observations where a custom aperture was constructed (cf. Sect. 3). Top left: Root-mean-square deviation (RMSD) of 20-s light curve flux binned to 1-hour against TESS magnitude for both SPOC and custom aperture data. Top right: Point-to-point (P2P) median difference variability (MDV) of 20-s light curve flux binned to 120-s against TESS magnitude. Bottom left: Ratio between the 1-hour RMSD from 20-s and 120-s cadence custom aperture data. The red markers indicate median-binned values, with uncertainties given by the standardised MAD, while the green markers give the ratios provided by Huber et al. (2022) (their Table 1). Bottom right: Ratio between P2P-MDV from 20-s (binned to 120-s) and 120-s cadence custom aperture data. Red markers again indicate median-binned values, with uncertainties given by the standardised MAD.

vations for each of the LOP fields for two years. The 24 "normal" cameras will observe at a cadence of 25 sec, while a cadence of 2.5 sec will be used for the two "fast" cameras, capable of observing towards the centre of the FOV. At the time of writing, only the southern LOP field (LOPS2; centred on $l = 255.9375°$, $b = -24.62432°$ in Galactic coordinates) is fully defined[6] and this is where observations are scheduled to start (Nascimbeni et al. 2025). For the northern LOP filed (LOPN1; $l = 81.56250°$, $b = 24.62432°$) we adopt the current suggested definition by Nascimbeni et al. (2022).

In Fig. 9 we show the sky distribution of the TLS, including the overlap with the PLATO LOP fields[7]. Table 2 provides an overview of the targets within the current LOP field definitions and targets near the fields (defined as being within 5° of the field edges). To check if a given target will be within the LOP fields we tested against the field edges obtained from the LOP field versions `pLOPN1PIC2.0.0.1-t` and `pLOPSsPIC2.0.0.1-t` of the PLATO Input Catalog (PIC; Montalto et al. 2021). We find that 10 targets are within the LOPS2 field, while 24 targets are within the current LOPN1 field. Interestingly, we identify several of the targets as spectroscopic and/or visual/astrometric binaries where independent constraints can be placed on the stellar masses (see Sect. 5.7, Table 5), and in some cases also on radii from interferometry (see Sect. 5.6, Table 4).

Based on the brightness of our sample and our target selection strategy (Sect. 2), most (if not all) of the stars overlapping the PLATO fields should meet the requirements for the P2 "bright-star" sample (Montalto et al. 2021; Rauer et al. 2024; Goupil et al. 2024). We note, however, that the stars will generally be best suited for observations with the two fast cameras whose dynamical range lies between $4 < V < 8$. For the normal cameras, optimised for stars fainter than $V = 8$, it remains to be seen how well photometric observations can be extracted for heavily saturated stars, e.g. from extended imagettes, that will experience significant blooming (e.g., Jannsen et al. 2024).

It would be instructive for the stars that, in addition to now being known asteroseismically, are well-characterised binaries, to be considered for the science calibration and validation PIC (scvPIC; Gaulme 2023) and possibly for the so-called "prime" sample of stars that will receive the highest priority throughout the mission (Rauer et al. 2024). The TLS should also be taken into consideration for the final definition of the northern LOP field by the PLATO Science Working Team (PSWT). Concerning the use of the TLS for the future final definition of the northern LOP field, we note that $\mu^1$ Her (HIP 86974), which with more than 10 years of ground-based RV observations from SONG (Grundahl et al. 2017) is en-route to becoming one of the best characterized asteroseismic subgiants, is near (i.e., $\leq 5°$ away from) the current LOPN1 field definition. A dedicated in-depth analysis of the TLS stars in or near the PLATO fields will be the subject of subsequent analysis (Panetier et al., in prep.). We also refer the reader to Eschen et al. (2024) and Nascimbeni et al. (2025) for additional analysis of the target content of the PLATO LOP2S field.

[6] https://www.cosmos.esa.int/web/plato/first-sky-field

[7] The PLATO field plots are made using functionalities of the `platopoint` code by Hugh P. Orborn, in the modified version used by Boettner et al. (2024) (https://github.com/ChrisBoettner/plato/tree/main/plato/instrument/platopoint.py)

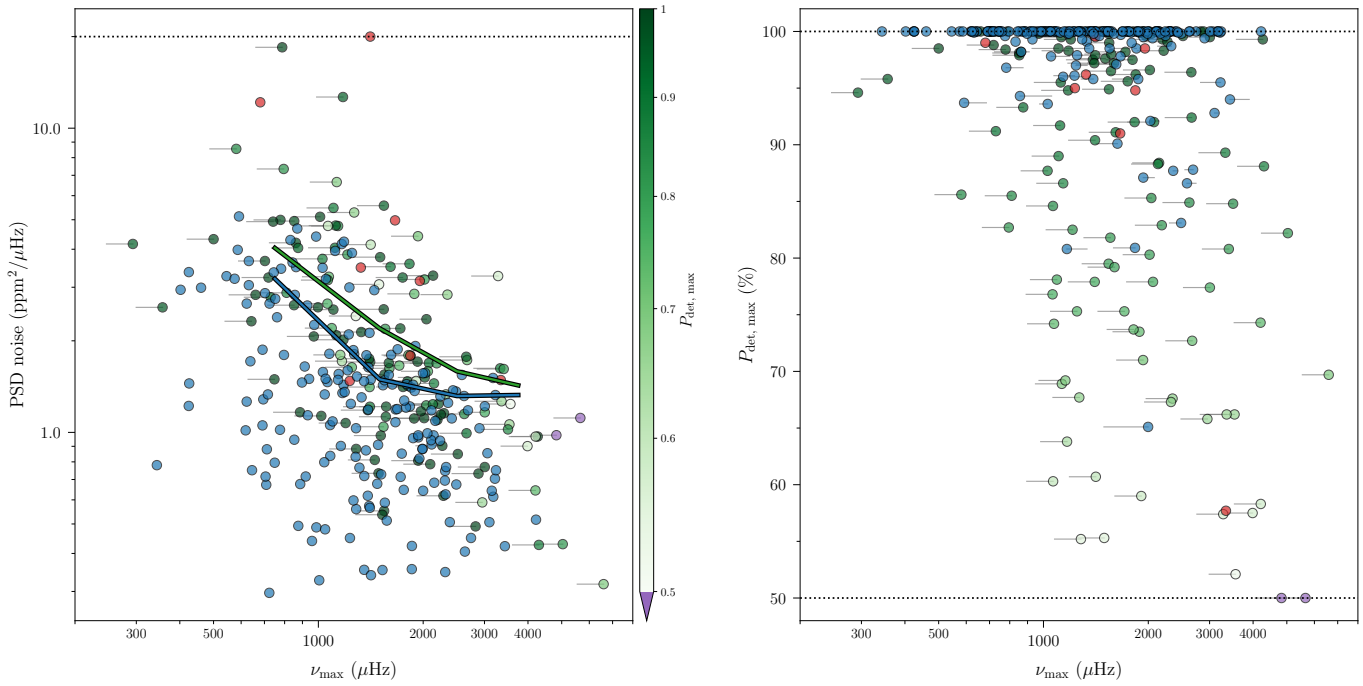


**Fig. 8.** Comparison of noise levels and predicted detectability in ATL3 for stars with and without seismic detections. Left: correspondence between the global asteroseismic $\nu_{max}$ parameters and the high-frequency PSD noise level for stars with positive seismic detections in blue, for stars identified as classical pulsators (e.g. $\delta$ Sct/$\gamma$ dor) in red, and for stars without a seismic detection in green. The $\nu_{max}$ and colouring of the non-detection cases are given by the $\nu_{max}$ and detection probability ($P_{det}$) returned by the ATL3 (Hey et al. 2024), and except for a few cases we have only included stars with $P_{det} > 50\%$. The non-detection $\nu_{max}$ values have been offset (horizontal line indicates the offset from the original position) by increasing $\nu_{max}$ by 16%, corresponding to the apparent overall bias of the ATL3 values, as seen from Fig. 6. Stars with a noise level above 20 ppm$^2$/$\mu$Hz have been offset to this value (dotted line). The coloured lines give the median binned noise levels of stars with (blue) and without (green) detections against $\nu_{max}$. Right: correspondence between the maximum ATL3 $P_{det}$ (for either 20- or 120-s cadence) against $\nu_{max}$, with the same colouring and $\nu_{max}$ as in the left panel. Stars with a $P_{det}$ below 50% have been offset to this value (dotted line). For the stars with seismic detection (blue) we have indicated with the small horizontal lines the ATL3 predicted $\nu_{max}$

### 5.4. TLS and the Habitable Worlds Observatory (HWO)

HWO is a planned NASA 6-meter-class UV/optical/IR space observatory capable of high-contrast imaging and spectroscopic characterisation of potentially habitable exoplanets in reflected light. The HWO concept was the top priority of the 2020 Decadal Survey on Astronomy and Astrophysics and is currently envisioned to launch in the early 2040s.

The primary targets for HWO are nearby, bright Sun-like stars for which the inner working angle allows the detection of planets on angular separations consistent with the habitable zone. Possible targets for HWO are described in a catalogue of HWO Precursor Science Stars by the NASA Exoplanet Exploration Program (ExEP) (Mamajek & Stapelfeldt 2024) and the HWO Input Catalog (Tuchow et al. 2024). The former consists of 164 stars divided into tiers (A, B, or C) based on their expected suitability for detection of Earth-like exoplanets.

Of the 164 ExEP HWO targets we have identified 139 matching the selection criteria adopted in this analysis (Sect. 2). The remaining stars include $\alpha$ Cen A+B, which were ignored in our analysis and then stars fainter than the $V = 6$ selection cut – generally, these also turn out to be of spectral type later than K0V (hence, with low probability of detecting oscillations). Of the 139 stars matching our selection criteria, two stars ($\tau^6$ Eri and 12 Oph) have not been, and are not scheduled to be, observed by TESS, while eight stars[8] did not have any data up until Sector 77 as considered in this analysis. From the remaining 129 stars with data, we detected oscillations in 67 stars, including 20 from tier A, 22 from tier B, and 25 from tier C. The HWO sample is shown in Fig. 10 in terms of luminosity against distance (mimicking the illustration of the sample in Mamajek & Stapelfeldt (2024)) with indications of which stars have detections. In Table 1 we have for all stars with seismic detections indicated their tier if they overlap with the HWO sample. The detections presented here, combined with asteroseismology of cooler HWO targets with extreme precision radial velocities (e.g., Campante et al. 2024; Hon et al. 2024; Li et al. 2025), will allow the systematic determination of precise ages of HWO targets, which are critical for the interpretation of possible biosignatures on directly imaged planets (Bixel & Apai 2020). A future paper in this series will focus on the asteroseismic age distributions for the HWO sample (Chontos et al., in prep.). Continued 20-second data of bright nearby stars in future TESS extended missions will be important to increase the sample of detections presented here.

### 5.5. Exoplanets, disks, and substellar objects

In addition to using asteroseismology for known binaries, a detailed stellar characterisation from asteroseismology of known exoplanet hosts is naturally of great interest, particularly for mass estimates of RV exoplanets, information on system ages, obliquity, etc. (Van Eylen et al. 2014; Huber 2018; Lundkvist et al. 2018; Lund et al. 2019).

Of the oscillating stars in the TLS (Table 1), we have identified 24 of them to be known exoplanet hosts, of which 13 are

[8] HD 131977, 18 Sco, 36 Oph A+B, $\xi$ Oph, 58 Oph, and 70 Oph A+B

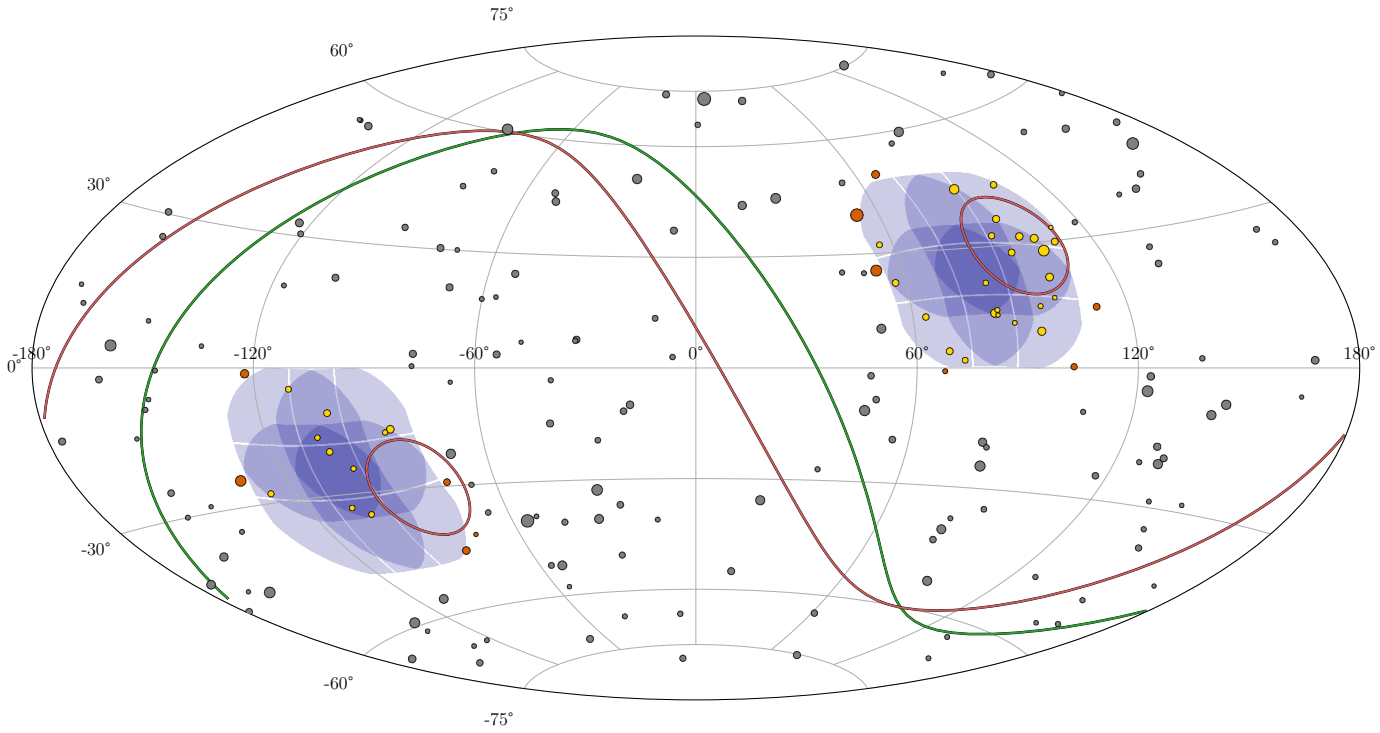


**Fig. 9.** Aitoff sky projection in galactic coordinates showing (circular markers) the TLS, with the marker size corresponding to the star's visual magnitude. The PLATO long-stare (LOP) fields are shown in blue (with shade corresponding to the number of either 24, 18, 12, or 6 overlapping cameras). Yellow markers indicate targets identified as being within current PLATO LOP field definitions (see text), while orange markers indicate targets within 5° of the LOP field boundaries. The TESS CVZs are given by the red circles that partly overlap the PLATO fields. The red line indicates the sky's equatorial plane, while the green line gives the ecliptic plane.

also in the HWO target list (Sect. 5.4). We identify 12 systems that were not previously known to have seismic hosts, including one brown dwarf host (HD 46588/HIP 32439), one (HD 184960/HIP 96258) that is positioned within the current definition of the PLATO LOPN1 field (Sect. 5.3), and several notable multiplanet systems, such as $\upsilon$ And (HIP 7513/Titawin), 47 UMa (HIP 53721/Chalawan), 61 Vir (HIP 64924), and 82 Eri (e Eri/HIP 15510) which Nari et al. (2025) recently found to also host a super-Earth orbiting in the star's habitable zone.

In Table 3 we provide an overview of the known exoplanet systems, which may benefit from the information obtained by an asteroseismic analysis. In addition to exoplanets, the table also lists any sub-stellar companions (such as brown dwarfs), and information on binarity (see also Table 5). The planetary data provided in Table 3 was primarily obtained from the "Planetary Systems" of the NASA Exoplanet Archive[9], and supplemented by information from the Extrasolar Planets Encyclopedia[10].

Worth mentioning is also $\psi^1$ Dra B (HIP 86620) which is known to host a long-period giant exoplanet ($\psi^1$ Dra Bb) with a minimum mass of 1.5 $M_{\rm Jup}$ and an orbital semi-major axis of 4.4 AU (Endl et al. 2016). Though we did not identify oscillations in $\psi^1$ Dra B, we did in its companion $\psi^1$ Dra A (see Table 5 and Fig. 2) and asteroseismology can therefore help constrain the age of the system. We note also that $\psi^1$ Dra A/B are within the current definition of the PLATO LOPN1 field.

Finally, several of our identified asteroseismic stars are known to host debris disks (Hughes et al. 2018; Pearce 2024). Notable examples include binary systems (Table 5) such as 99 Her (b Her/HIP 88745), which hosts a nearly polar-aligned circumbinary debris disk (Kennedy et al. 2012; Smallwood et al. 2020), and HD 121384 (HIP 68101) (Rhee et al. 2007; Rodriguez & Zuckerman 2012); HD 132254 (HIP 73100) and 110 Her (HIP 92043) have been identified as hosts of cold debris disks (Krivov et al. 2013; Marshall et al. 2013); and known exoplanet hosts, such as, e.g., 82 Eri (e Eri/HIP 15510) (Pepe et al. 2011; Montesinos et al. 2016) and 61 Vir (HIP 64924) (Wyatt et al. 2012) also exhibit debris disks.

Access to well-characterised stellar parameters from asteroseismology, particularly stellar ages, is crucial for understanding the evolution of debris disks. These parameters provide a critical context for interpreting the current state of the disks, including their composition, structure, and dynamical processes, while also constraining the history of planet formation and interactions within these systems (Trilling et al. 2008; Montesinos et al. 2016). Moreover, accurate stellar characterisation enables meaningful comparisons across different systems, thereby enhancing our ability to discern patterns and trends in the evolution of planetary systems.

### 5.6. Interferometry for angular stellar diameters

Long-baseline interferometric observations for the measurement of stellar angular diameters provide an essential ingredient for obtaining stellar fundamental parameters of the highest precision that are near model-independent (mainly with a dependence on the adopted limb-darkening). Most importantly, an independent estimate is provided for the stellar linear radius by incorporating the distance (e.g. from Gaia). Similarly, combining an estimate of the stellar bolometric flux with the measured angular diameter provides an independent $T_{\rm eff}$, which, when combined with the

[9] https://exoplanetarchive.ipac.caltech.edu
[10] https://exoplanet.eu/

**Table 2.** TLS stars in the PLATO fields

| Name | TIC | HIP | RA (deg) | DEC (deg) | $V$ (mag) | Sep (deg) | SpT |
|---|---|---|---|---|---|---|---|
| | | | Inside PLATO LOPS 2 | | | | |
| B Car | 308844962 | 39903 | 122.253 | -61.302 | 4.74 | 20.3 | F6VFe-0.8CH-0.4 |
| HD 62644 | 123699670 | 37606 | 115.738 | -45.173 | 5.04 | 14.3 | G8IV-V |
| X Pup | 170225363 | 32765 | 102.478 | -46.615 | 5.14 | 5.0 | F5.5V |
| $\nu^2$ Col | 32500750 | 26460 | 84.436 | -28.69 | 5.28 | 21.0 | F5V |
| 171 Pup | 149672905 | 37853 | 116.396 | -34.173 | 5.36 | 20.9 | F9V |
| $\zeta$ Pic | 219420836 | 24829 | 79.842 | -50.606 | 5.44 | 10.4 | F6IV |
| HD 36553 | 354552931 | 25768 | 82.539 | -47.078 | 5.46 | 8.7 | F8/G2 |
| HD 53705 | 130645536 | 34065 | 105.989 | -43.608 | 5.56 | 8.6 | G1.5V |
| HD 46569 | 255630992 | 31079 | 97.826 | -51.826 | 5.58 | 4.3 | F8VFe-0.4 |
| HD 65907 | 372914091 | 38908 | 119.445 | -60.303 | 5.59 | 18.6 | F9.5V |
| | | | Near PLATO LOPS 2 | | | | |
| $\gamma$ Lep | 93280676 | 27072 | 86.116 | -22.448 | 3.59 | 26.5 | F6V |
| HD 60532 | 456871289 | 36795 | 113.513 | -22.296 | 4.44 | 29.4 | F6IV-V |
| $\kappa$ Ret | 262843771 | 16245 | 52.344 | -62.938 | 4.71 | 27.9 | F3IV/V |
| $\alpha$ Men | 141810080 | 29271 | 92.56 | -74.753 | 5.08 | 26.9 | G7V |
| HD 21722 | 31799975 | 15968 | 51.401 | -69.336 | 5.96 | 30.2 | F5V |
| | | | Inside PLATO LOPN 1 | | | | |
| $\chi$ Dra | 341873045 | 89937 | 275.264 | 72.733 | 3.55 | 19.9 | F7V |
| $\theta$ Dra | 161825882 | 78527 | 240.472 | 58.565 | 4.01 | 21.2 | F9V |
| $\theta$ Cyg | 27014182 | 96441 | 294.111 | 50.221 | 4.49 | 10.8 | F3+V |
| $\upsilon$ Cep | 421444084 | 102431 | 311.338 | 57.58 | 4.52 | 19.8 | F8IV-V+F9IV-V |
| $\psi^1$ Dra A | 441804568 | 86614 | 265.484 | 72.149 | 4.57 | 19.9 | F5IV-V |
| $\sigma$ Dra | 259237827 | 96100 | 293.09 | 69.661 | 4.67 | 18.3 | K0V |
| $\omega$ Dra | 233195546 | 86201 | 264.238 | 68.758 | 4.77 | 17.0 | F4V |
| 19 Dra | 289622310 | 82860 | 254.007 | 65.135 | 4.88 | 16.9 | F8V |
| 36 Dra | 233121747 | 89348 | 273.474 | 64.397 | 4.99 | 11.7 | F5V |
| 17 Cyg | 58445695 | 97295 | 296.607 | 33.728 | 5.0 | 23.6 | F5.5IV-V |
| 35 Dra | 441813918 | 87234 | 267.363 | 76.963 | 5.02 | 24.4 | F6IV-Vs |
| 99 Her | 22516402 | 88745 | 271.757 | 30.562 | 5.05 | 22.6 | F6V |
| HD 136064 | 232563914 | 74605 | 228.66 | 67.347 | 5.15 | 27.2 | F8V |
| HD 176051 | 20601206 | 93017 | 284.257 | 32.901 | 5.2 | 20.6 | F9V+K1V |
| 26 Dra | 219777482 | 86036 | 263.748 | 61.875 | 5.23 | 11.5 | G0IV-V |
| 27 Cyg | 41195655 | 99031 | 301.591 | 35.972 | 5.38 | 24.0 | G8.5IVa |
| 72 Her | 9728611 | 84862 | 260.165 | 32.468 | 5.38 | 23.8 | G0V |
| HD 175225 | 48194330 | 92549 | 282.896 | 52.975 | 5.51 | 3.4 | G9IVa |
| 68 Dra | 236871353 | 99500 | 302.895 | 62.079 | 5.7 | 16.4 | F5V |
| HD 184960 | 26884478 | 96258 | 293.582 | 51.237 | 5.71 | 10.2 | F7V |
| HD 191195 | 405902259 | 99026 | 301.558 | 53.166 | 5.81 | 14.6 | F5V |
| HD 193664 | 403585118 | 100017 | 304.381 | 66.854 | 5.91 | 19.3 | G3V |
| 16 Cyg A | 27533341 | 96895 | 295.454 | 50.525 | 5.99 | 11.5 | G1.5Vb |
| HD 152303 | 233503400 | 81854 | 250.776 | 77.514 | 5.99 | 26.5 | F4V |
| | | | Near PLATO LOPN 1 | | | | |
| $\zeta$ Her | 43255143 | 81693 | 250.322 | 31.603 | 2.81 | 28.8 | G0IV |
| $\mu^1$ Her | 460067868 | 86974 | 266.615 | 27.721 | 3.42 | 26.3 | G5IV |
| $\chi$ Her | 157364190 | 77760 | 238.169 | 42.452 | 4.6 | 27.8 | F8VFe-2Hdel-1 |
| 16 Cep | 366412503 | 108535 | 329.812 | 73.18 | 5.04 | 29.6 | F5V |
| HD 210855 | 329759640 | 109572 | 332.953 | 56.839 | 5.24 | 31.5 | F8V |
| HD 190360 | 105999792 | 98767 | 300.906 | 29.897 | 5.73 | 28.8 | G7IV-V |

**Notes.** The table provides the stars identified within or near (within 5 deg of the field edge) the PLATO northern (LOPN1) and southern (LOPS2) long stare fields, with stars within each grouping sorted according to their visual magnitude ("$V$"). The first three columns provide identifiers for the stars in the form of their Bayer/Flamsteed designation (or primary name according to `Simbad`) in addition to their TESS ("TIC") and Hipparcos ("HIP") IDs. "Sep" gives the separation in degrees between the stars and the fields centres, while "SpT" gives the spectral type of the stars according to `Simbad`.

independent radius and $\nu_{\rm max}$ provides an estimate of the stellar mass (Pijpers et al. 2003; Cunha et al. 2007; Creevey et al. 2007; Bruntt et al. 2010; Bazot et al. 2011; Huber et al. 2012; White et al. 2013, 2018).

Identifying stars with both interferometric and asteroseismic measurements is therefore essential for calibrating asteroseismology, both in terms of the application of scaling relations and the fine details of model physics. In our search for existing interferometric stellar diameter measurements, we cross-referenced our sample against the compilation of Baines et al. (2023) (their Table 9), the Jean-Marie Mariotti Center (JMMC; Bourgés et al. 2014) Measured Stellar Diameters Catalog (JMDC, Cat II/345/jmdc; Duvert 2016, introduced as part of Chelli et al. (2016)) (updated last 13 Sep. 2021), the list of CHARA published interferometric diameters[11], and the samples of Rains et al. (2020), Karovicova et al. (2022), and North et al. (2007).

In Table 4 we list the 54 stars for which a published measurement could be found from the adopted compilations. We identify

[11] https://www.chara.gsu.edu/tables/interferometric-diameters

**Table 3.** TLS exoplanets and sub-stellar objects

| Name | HIP | $V$ (mag) | $\nu_{max}$ ($\mu$Hz) | Known Seismic (X/O) | Binary (X/O) | HWO (tier) | Planets (No.) | Reference (discovery) |
|---|---|---|---|---|---|---|---|---|
| $\upsilon$ And | 7513 | 4.1 | 1528 | O | X$^{\dagger}$ | C | 3 | 1, 2 |
| 82 Eri | 15510 | 4.26 | 3180 | O | O | B | 4 | 3, 4, 5 |
| $\lambda$ Ser | 77257 | 4.42 | 1856 | X | O | A | 1 | 6 |
| HD 60532$^{(PS)}$ | 36795 | 4.44 | 618 | O | O | - | 2 | 7 |
| 61 Vir | 64924 | 4.74 | 3099 | O | O | B | 3 | 8 |
| HD 102365 | 57443 | 4.89 | 3148 | X | X$^{(a)}$ | A | 1 | 9 |
| 70 Vir | 65721 | 4.97 | 940 | X | O | - | 1 | 10 |
| 47 UMa | 53721 | 5.03 | 2327 | O | O | A | 3 | 11, 12, 13 |
| 94 Cet | 14954 | 5.07 | 1267 | X | X$^{*\dagger}$ | - | 1 | 14 |
| HD 33564 | 25110 | 5.08 | 1736 | O | O | C | 1 | 15 |
| $\mu$ Ara | 86796 | 5.12 | 1936 | X | O | B | 4 | 16, 17, 18, 19 |
| $\rho$ CrB | 78459 | 5.39 | 1664 | X | O$^{\dagger}$ | B | 4 | 20, 21, 22 |
| HD 46588 | 32439 | 5.44 | 2416 | O | X$^{(b)}$ | B | 1 | 23 |
| 51 Peg | 113357 | 5.45 | 2485 | X | O | - | 1 | 24 |
| $\nu^2$ Lup | 75181 | 5.65 | 2689 | X | O | B | 3 | 25 |
| $\pi$ Men | 26394 | 5.65 | 2621 | X | O | B | 3 | 26, 27, 28 |
| HD 142 | 522 | 5.7 | 1890 | O | X$^{(c)}$ | - | 3 | 29, 30, 31 |
| HD 184960$^{PN}$ | 96258 | 5.71 | 1870 | O | O | - | 1 | 32 |
| HD 190360$^{(PN)}$ | 98767 | 5.73 | 2358 | O | X$^{(d)}$ | B | 2$^{(e)}$ | 33, 34 |
| HD 89744 | 50786 | 5.73 | 1028 | O | X$^{(f)}$ | - | 1$^{(g)}$ | 35 |
| HD 30562 | 22336 | 5.77 | 1447 | X | O | - | 1 | 36 |
| $\lambda^2$ For | 12186 | 5.78 | 1374 | X | X$^{(h)}$ | - | 1 | 37 |
| HD 221420 | 116250 | 5.82 | 1042 | O | X$^{(i)}$ | - | 1 | 38 |
| HD 38529 | 27253 | 5.95 | 622 | X | X$^{(j)}$ | - | 2$^{(k)}$ | 39, 40 |

**Notes.** The table provides an identification of the exoplanets and their hosts for the seismic stars in the sample. The stars are ordered according to their $V$-band brightness. The first two columns provide identifiers for the stars in the form of their Bayer/Flamsteed designation (or primary name according to `Simbad`) and their "'HIP" IDs. Super-scripts of *PN* or *PS* on the star's name refer to their position within (or near when in parenthesis) the northern (*N*) or southern (*S*) PLATO fields (see Table 2). "$V$" gives the $V$-band magnitude, "$\nu_{max}$" (central value only) is adopted from Table 1. "Known Seismic" denotes with an X (otherwise an O) if the star is a know asteroseismic target (see Table 1); "Binary" denotes with an X (otherwise an O) if the star is identified as being part of a binary or multiple star system, and here an asterics (*) indicates that orbital information is available in Table 5; "HWO" indicates if the star is part of the Mamajek & Stapelfeldt (2024) HWO target list, and if so provides its tier; "Planets" gives the number of identified exoplanets; "Reference" provides the reference(s) for the identified exoplanet(s).
$^{(\dagger)}$ see Appendix D; $^{(a)}$ A faint M4 dwarf companion star (GJ 442 B) at a distance of ~212 AU (Raghavan et al. 2010); $^{(b)}$ Loutrel et al. (2011) identified a brown dwarf companion (HD 46588 B; spT L9), one of the few known brown at the L/T transition for which both age and distance estimates are available; $^{(c)}$ A low-mass K-M dwarf companion star (LHS 1021 / HD 142 B) (Eggenberger et al. 2007; Mugrauer 2019); $^{(d)}$ A faint M4.5V dwarf companion star (G 125-55 / GJ 777 B) at a distance of ~2849 AU, which in turn could be an unresolved binary with a similar companion (Mason et al. 2014); $^{(e)}$ A potential third planet was identified by Hirsch et al. (2021); $^{(f)}$ A wide-separation ($a$~2460 AU) L-type companion (Wilson et al. 2001; Mugrauer et al. 2004), and another ($a$~219 AU) proposed candidate companion (Roberts et al. 2011; Fontanive et al. 2019); $^{(g)}$ Wittenmyer et al. (2019) finds indications of another Jupiter-mass exoplanet (HD 89744 c) at a separation of 8.3 ± 1.8 AU and with an orbital period of 6974 ± 2161 days; $^{(h)}$ A co-moving mid-M-dwarf companion (HD 16417 B) detected by Mugrauer et al. (2004); $^{(i)}$ A wide-separation ($a$~21,756 AU) companion candidate (likely a mid-M-dwarf) was identified by Venner et al. (2021) (see also El-Badry et al. 2021); $^{(j)}$ A wide-separation ($a$~11,000 AU) M2.5V companion (Raghavan et al. 2006; Montes et al. 2018); $^{(k)}$ Benedict et al. (2010) finds indications in the RV residuals of a possible third planetary companion at a period of ~194 days and an inferred $a$~0.75 AU.

**References.** (1) Butler et al. (1997); (2) Butler et al. (1999); (3) Pepe et al. (2011); (4) Feng et al. (2017); (5) Nari et al. (2025); (6) Rosenthal et al. (2021); (7) Desort et al. (2008); (8) Vogt et al. (2010); (9) Tinney et al. (2011); (10) Marcy & Butler (1996); (11) Butler & Marcy (1996); (12) Fischer et al. (2002); (13) Gregory & Fischer (2010); (14) Mayor et al. (2004); (15) Galland et al. (2005); (16) Butler et al. (2001); (17) McCarthy et al. (2004); (18) Santos et al. (2004); (19) Pepe et al. (2007); (20) Noyes et al. (1997); (21) Fulton et al. (2016); (22) Brewer et al. (2023); (23) Šubjak et al. (2023); (24) Mayor & Queloz (1995); (25) Udry et al. (2019); (26) Gandolfi et al. (2018); (27) Jones et al. (2002); (28) Hatzes et al. (2022); (29) Feng et al. (2022); (30) Tinney et al. (2002); (31) Wittenmyer et al. (2012); (32) Barnes et al. (2023); (33) Naef et al. (2003); (34) Vogt et al. (2005); (35) Korzennik et al. (2000); (36) Fischer et al. (2009); (37) O'Toole et al. (2009); (38) Kane et al. (2019); (39) Fischer et al. (2001); (40) Fischer et al. (2003).

31 of these as being new oscillators, hence significantly expanding the cohort of MS/SG stars suitable for testing asteroseismology with interferometry. In Fig. 11 we provide an overview of the TLS in terms of visual magnitude and declination and indicate the stars with existing interferometric measurements for stellar diameter determination. Brighter than $V = 4.5$, we identify only 6 targets (82 Eri, $\zeta$ Tuc, $\alpha$ Cha, $\gamma$ Pav, $\psi$ Cap, and HD 60532) where we could not identify an interferometric measurement in the literature. For each star Fig. 11 also provides a simple estimate of the expected angular diameter from combining distance (from TIC) with a seismic radius obtained from scaling relations using our measured $\nu_{max}$ and $\Delta\nu$ in combination with a $T_{eff}$ from (Casagrande et al. 2011) (or TIC if not available).

We note that all stars have a predicted angular diameter above ~0.38 mas. Combined with the brightness of the sample, all stars in the TLS (except some binaries) should be accessible for interferometric observations with instruments at either CHARA (Centre for High Angular Resolution Array; ten Brummelaar et al. 2005) or NPOI (Navy Precision Optical Interferometer; Armstrong et al. 1998) for the more northern targets, and VLTI (Very Large Telescope Interferometer Glindemann et al. 2001) for the more southern targets.

### 5.7. Binarity

Stars exhibiting solar-like oscillations whilst also being members of binary systems are particularly important if they can be characterised spectroscopically (preferably with solutions for both components) in addition to either being eclipsing or having their orbit traced on the sky (either from resolved or interferometric observations for visual binaries or from astrometric observations). The constraint offered by the binarity in providing near model-independent estimates for the stellar mass (individual masses in the best cases and minimum masses in the worst) is of paramount importance for testing the masses provided by asteroseismology (Serenelli et al. 2021).

**Table 4.** TLS long-baseline interferometry overview

| Name | TIC | HIP | $V$ (mag) | RA (deg) | DEC (deg) | $\nu_{\rm max}$ ($\mu$Hz) | References |
|---|---|---|---|---|---|---|---|
| $\eta$ Boo | 367758676 | 67927 | 2.68 | 208.7 | 18.4 | 697.9 ± 17.8 | 1, 2, 3, 4 |
| $\zeta$ Her | 43255143 | 81693 | 2.81 | 250.3 | 31.6 | 718.5 ± 24.4 | 1, 2, 4 |
| $\beta$ Hyi | 267211065 | 2021 | 2.82 | 6.4 | −77.3 | 1038.1 ± 14.9 | 5 |
| $\theta$ UMa | 150226696 | 46853 | 3.17 | 143.2 | 51.7 | 779.3 ± 17.8 | 6, 7 |
| $\xi$ Gem | 372480991 | 32362 | 3.35 | 101.3 | 12.9 | 2871.0 ± 111.3 | 6 |
| $\mu^1$ Her | 460067868 | 86974 | 3.42 | 266.6 | 27.7 | 1192.5 ± 17.5 | 2, 4, 7 |
| $\eta$ Cas | 445258206 | 3821 | 3.46 | 12.3 | 57.8 | 2840.0 ± 80.7 | 6, 8 |
| $\delta$ Eri | 38511251 | 17378 | 3.52 | 55.8 | −9.8 | 677.6 ± 8.3 | 3, 9 |
| $\delta$ Pav | 409891396 | 99240 | 3.55 | 302.2 | −66.2 | 2269.8 ± 64.4 | 9 |
| $\beta$ Vir | 366661076 | 57757 | 3.59 | 177.7 | 1.8 | 1446.3 ± 75.9 | 6, 8, 10 |
| $\gamma$ Lep | 93280676 | 27072 | 3.59 | 86.1 | −22.4 | 2257.5 ± 50.9 | 8 |
| $\beta$ Aql | 375621179 | 98036 | 3.71 | 298.8 | 6.4 | 414.7 ± 6.8 | 11, 4, 9 |
| $\iota$ Peg | 357336603 | 109176 | 3.77 | 331.8 | 25.3 | 2101.8 ± 126.6 | 8 |
| $\gamma$ Ser | 377415363 | 78072 | 3.85 | 239.1 | 15.7 | 1744.6 ± 38.2 | 6, 8 |
| $\theta$ Boo | 441709021 | 70497 | 4.04 | 216.3 | 51.9 | 1354.0 ± 108.4 | 6, 10 |
| $\iota$ Per | 116988032 | 14632 | 4.05 | 47.3 | 49.6 | 1855.3 ± 33.9 | 6, 8, 12 |
| $\iota$ Vir | 6029884 | 69701 | 4.07 | 214.0 | −6.0 | 644.8 ± 24.0 | 10 |
| $\upsilon$ And | 189576919 | 7513 | 4.1 | 24.2 | 41.4 | 1528.0 ± 50.6 | 13, 14, 15, 8, 16, 12 |
| $\theta$ Per | 302158903 | 12777 | 4.1 | 41.0 | 49.2 | 2314.2 ± 166.2 | 6, 8 |
| $\iota$ Psc | 419919445 | 116771 | 4.13 | 355.0 | 5.6 | 1416.4 ± 53.6 | 6, 8 |
| 110 Her | 282038438 | 92043 | 4.19 | 281.4 | 20.5 | 1061.9 ± 28.0 | 6, 10 |
| $\xi$ Peg | 60716322 | 112447 | 4.2 | 341.7 | 12.2 | 986.8 ± 16.7 | 6 |
| $\beta$ CVn | 458445966 | 61317 | 4.24 | 188.4 | 41.4 | 2385.4 ± 136.0 | 6, 7 |
| 10 Tau | 311092847 | 16852 | 4.29 | 54.2 | 0.4 | 1284.1 ± 63.1 | 6, 8 |
| $\lambda$ Ser | 296740796 | 77257 | 4.42 | 236.6 | 7.4 | 1856.6 ± 46.4 | 10 |
| $o^2$ Eri | 67772871 | 19849 | 4.43 | 63.8 | −7.7 | 3433.1 ± 368.6 | 17, 18, 9 |
| $\theta$ Cyg | 27014182 | 96441 | 4.49 | 294.1 | 50.2 | 1759.1 ± 67.1 | 6, 15, 19, 16, 20 |
| $\psi^1$ Dra A | 441804568 | 86614 | 4.57 | 265.5 | 72.1 | 1232.4 ± 19.8 | 6 |
| $\chi$ Her | 157364190 | 77760 | 4.6 | 238.2 | 42.5 | 1045.6 ± 17.7 | 10 |
| $\sigma$ Dra | 259237827 | 96100 | 4.67 | 293.1 | 69.7 | 4217.9 ± 122.6 | 21, 6 |
| $\lambda$ Aur | 409104974 | 24813 | 4.69 | 79.8 | 40.1 | 2152.0 ± 54.2 | 6, 8 |
| 61 Vir | 422478973 | 64924 | 4.74 | 199.6 | −18.3 | 3099.8 ± 101.0 | 8, 22 |
| 40 Leo | 95431211 | 50564 | 4.78 | 154.9 | 19.5 | 1405.8 ± 57.9 | 23 |
| HD 5015 | 285544488 | 4151 | 4.8 | 13.3 | 61.1 | 1399.3 ± 52.9 | 6 |
| 36 UMa | 416519065 | 51459 | 4.82 | 157.7 | 56.0 | 2319.5 ± 96.8 | 6 |
| 70 Vir | 95473936 | 65721 | 4.97 | 202.1 | 13.8 | 940.6 ± 12.9 | 13, 8, 24 |
| 36 Dra | 233121747 | 89348 | 4.99 | 273.5 | 64.4 | 1312.0 ± 16.9 | 25, 16 |
| 47 UMa | 21535479 | 53721 | 5.03 | 164.9 | 40.4 | 2327.9 ± 55.1 | 8 |
| 16 Cep | 366412503 | 108535 | 5.04 | 329.8 | 73.2 | 643.4 ± 11.2 | 16 |
| 94 Cet | 49845357 | 14954 | 5.07 | 48.2 | −1.2 | 1267.2 ± 99.6 | 13, 16 |
| HD 33564 | 142103211 | 25110 | 5.08 | 80.6 | 79.2 | 1736.0 ± 61.1 | 22 |
| $\chi$ Cnc | 302188141 | 40843 | 5.13 | 125.0 | 27.2 | 1991.8 ± 78.8 | 25 |
| $\rho$ And | 288294358 | 1686 | 5.16 | 5.3 | 38.0 | 390.3 ± 11.4 | 16 |
| 31 Aql | 359981217 | 95447 | 5.17 | 291.2 | 11.9 | 1791.8 ± 225.2 | 6 |
| 72 Her | 9728611 | 84862 | 5.38 | 260.2 | 32.5 | 2241.4 ± 85.1 | 25 |
| $\rho$ CrB | 458494003 | 78459 | 5.39 | 240.3 | 33.3 | 1664.7 ± 99.9 | 13, 22 |
| 51 Peg | 139298196 | 113357 | 5.45 | 344.4 | 20.8 | 2485.0 ± 97.8 | 13, 25, 16 |
| 15 Peg | 326202925 | 107975 | 5.52 | 328.1 | 28.8 | 1389.9 ± 70.7 | 20 |
| HD 195564 | 205591703 | 101345 | 5.66 | 308.1 | −9.9 | 1167.3 ± 46.9 | 25 |
| HD 190360 | 105999792 | 98767 | 5.73 | 300.9 | 29.9 | 2358.2 ± 74.1 | 13, 16, 20 |
| HD 89744 | 8154501 | 50786 | 5.73 | 155.5 | 41.2 | 1028.4 ± 108.5 | 26 |
| HD 49933 | 281812116 | 32851 | 5.78 | 102.7 | −0.5 | 1997.7 ± 117.8 | 27 |
| HD 38529 | 200093173 | 27253 | 5.95 | 86.6 | 1.2 | 622.5 ± 27.9 | 13 |
| 16 Cyg A | 27533341 | 96895 | 5.99 | 295.5 | 50.5 | 2236.5 ± 97.9 | 25, 19, 20 |

**Notes.** The table provides an overview of the stars with published measurements of the stellar diameter from long-baseline interferometry, with stars sorted according to their visual magnitude ("$V$"). The first three columns provide identifiers for the stars in the form of their Bayer/Flamsteed designation (or primary name according to `Simbad`) in addition to their TESS ("TIC") and Hipparcos ("HIP") IDs. The last column provides references to the interferometric sources.

**References.** (1) Nordgren et al. (2001); (2) Mozurkewich et al. (2003); (3) Thévenin et al. (2005); (4) Baines et al. (2014); (5) North et al. (2007); (6) Boyajian et al. (2012a); (7) Baines et al. (2018); (8) Mennesson et al. (2014); (9) Rains et al. (2020); (10) Baines et al. (2023); (11) Nordgren et al. (1999); (12) Baines et al. (2021); (13) Baines et al. (2008); (14) Zhao et al. (2011); (15) Ligi et al. (2012); (16) Ligi et al. (2016); (17) Kervella et al. (2004); (18) Boyajian et al. (2012b); (19) White et al. (2013); (20) Karovicova et al. (2022); (21) Boyajian et al. (2008); (22) von Braun et al. (2014); (23) Maestro et al. (2013); (24) Kane et al. (2015); (25) Boyajian et al. (2013); (26) Schaefer et al. (2018); (27) Bigot et al. (2011).

To date, when focusing on constraining the asteroseismology of solar-like oscillators, the effort has mainly been on eclipsing spectroscopic binary systems typically containing one or two evolved red giants (e.g., Gaulme et al. 2016; Brogaard et al. 2018, 2022; Benbakoura et al. 2021; Thomsen et al. 2022). In cases where oscillations are detectable in both components of a binary system containing MS and/or SG stars (Miglio et al. 2014), the binary period is often too long or the orbital configuration cannot be constrained to a degree that allows independent constraints to be placed on the masses (Metcalfe et al. 2015; White et al. 2017; Li et al. 2018; Joyce & Chaboyer 2018), whereby only the asteroseismic ages can be tested against the assumed coevality of the stars. This lack of added constraint on the stellar mass is also, in general, the case for the known binary systems with one well-characterised MS/SG oscillating component (Kjeldsen et al. 1995; Deal et al. 2017; Grundahl et al. 2017; Metcalfe et al. 2021; Ball et al. 2022). Given these challenges, only very few asteroseismic analyses of MS/SG stars have currently benefited from the added constraints of binarity in the stellar modelling (Appourchaux et al. 2015; Metcalfe et al. 2020), or have been able to serve as benchmarks of asteroseismology.

Given the brightness of the stars in our sample, many have been subjected to extensive studies and are generally well-characterised. To identify known binary stars in our sample that potentially could become important benchmarks of asteroseismology we cross-referenced against the Washington Double Star catalog (WDS; Mason et al. 2014), the Ninth Catalogue of Spectroscopic Binary Orbits (SB9; Pourbaix et al. 2004), the Sixth Catalog of Orbits of Visual Binary Stars (ORB6; Hartkopf et al. 2001a), and the Observatorio Astronómico Ramón María Aller Catalog of Orbits and Ephemerides of Visual Double Stars (OARMAC; Docobo et al. 2001, 2012). We note that many stars in the sample have a WDS designation. Still, we are interested in systems where constraints can be placed on the orbits rather than

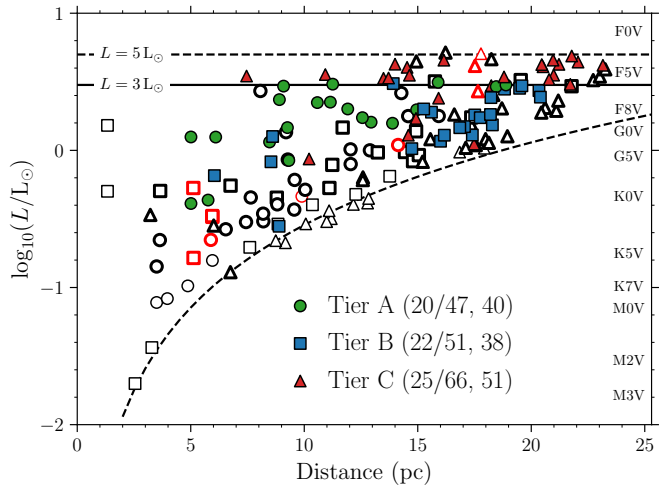


**Fig. 10.** HWO target stars in terms of their luminosity and distance, with values adopted from the tables of Mamajek & Stapelfeldt (2024). Filled markers indicate stars with detected oscillations, with the colour and shape indicating the star's tier (see legend). Stars with unfilled black thick-edged markers were considered for analysis, while black thin-edged ones did not conform to the selection criteria for our sample. Stars with red thick-edged markers were considered but did not have data available before S77, as considered in this analysis (but will later in Cycle 7), while red thin-edged ones are not scheduled for observations with TESS. The legend showing the different tiers gives in parentheses the number of detections out of the total number of stars in the tier, and lastly the number of stars from the tier that have been analysed.

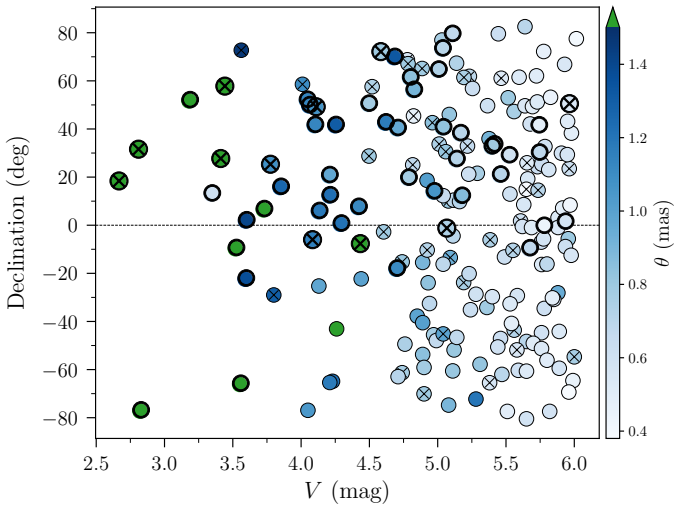


**Fig. 11.** TLS stars plotted in terms of visual magnitude against declination, with the colour indicating the expected angular diameter (see colourbar). Stars with a thick outline indicate the ones where an interferometric diameter could be found from the literature (Table 4), and stars with a cross (×) indicate the ones identified as binaries and listed in Table 5.

simply having information on the existence of companions and require as a minimum an estimate of the orbital period. In addition to consulting the above catalogues, we conducted an extensive literature search of all the asteroseismic targets. The result of our search is given in Table 5. As an additional check, we match our sample against the *Gaia* DR3 non-single star (NNS) catalogue `gaiadr3.nss_two_body_orbit` (Halbwachs et al. 2023; Holl et al. 2023) – seven stars[12] can be found in the NNS catalogue, but with no new additions beyond the ones already identified from the other catalogues. Of the seven stars all but two (HIPs 86036 and 5081) have orbital periods from the *Gaia* NNS catalogue in agreement with the values listed in Table 5, and both poorly matching stars have `goodness_of_fit` and/or `significance` values indicating a poor NNS solution. Only in the case of 35 Leo (HIP 50319) can the *Gaia* solution bring to bear information on the orbit (in the form of Campbell elements[13]) not available from existing observations.

In addition to catalogue identifiers, period measurements and semi-amplitudes (for spectroscopic systems), we also indicate which of the stars are located within or near the PLATO LOP fields (Sect. 5.3), and provide literature estimates of $v \sin i$ as this can influence the quality of ground-based spectroscopic follow-up efforts. Unless otherwise stated in Table 5, notes via a letter reference to the spectroscopic periods ("$P$ (Spec)") and semi-amplitudes ("$K_1$(/$K_2$)") are obtained from SB9, adopting the latest entry if multiple exist (a numerical reference to this entry is provided in the table). The visual/astrometric period ("$P$ (Orb)") is generally obtained from ORB6, if not otherwise indicated with a letter reference, and uncertainties in parentheses provide any non-zero root-mean-square-deviation between multiple entries in ORB6 and/or OARMAC. The table is meant to give an overview of the feasibility of follow-up observations of the stars and their potential use as benchmarks. Therefore, we have generally omitted uncertainty estimates on the parameters (see table notes).

Of the 48 asteroseismic stars with available binary orbital information listed in Table 5, a significant fraction could yield valuable benchmark systems for asteroseismology, and several are likely to be observed by PLATO (Sect. 5.3). Seven stars are listed as SB2 systems with orbital constraints also from being visual/astrometric binaries – for these individual components, masses can be directly determined and compared to the asteroseismic values. With additional follow-up observations, more systems could potentially be identified as SB2, and later *Gaia* releases will likely provide orbital constraints for more of the spectroscopically characterised systems. One facility that is well-suited to provide follow-up spectroscopic observations of the binary orbits for bright stars, and in many cases also for asteroseismology, is the Stellar Observations Network Group (SONG; Grundahl et al. 2017). In Table 5 we provide an overview of the current observations conducted for these stars using SONG[14] and note that most of the stars with periods below ~7 yr have already been scheduled for long-term monitoring. Some of the stars with high numbers of existing data from SONG will be the subject of future dedicated analysis of both the binary and asteroseismic data – this includes, e.g., stars like $\omega$ Dra (HIP 86201), $\iota$ Peg (HIP 109176), and $\chi$ Dra (Rudrasingam et al., in prep.). In Appendix D we provide notes concerning binarity for several individual stars, in some cases to elaborate on the information in Table 5 and in some to clarify why stars identified as binaries, e.g. on `SimBad`, have been excluded.

[12] HIPs 39903, 69226, 80686, 37606, 86036, 5081, and 50319

[13] from the conversion of the provided Thiele-Innes elements (see Halbwachs et al. 2023, Appendix A).

[14] We note that upon joining the SONG community (`https://soda.phys.au.dk/`), the spectra in the SONG database are free for members to use.

### 5.8. Solar analogues with seismic detections

Identifying and characterising stars resembling the Sun is important because they provide an essential context for understanding the Sun in terms of evolution, activity, and chemistry, and they are naturally of interest in the search for exoplanets. Sun-like stars come in different categories depending on their resemblance to the Sun, where "solar twins" are restricted to having near-solar parameters on all fronts, "solar analogues" are more loosely defined as having parameters "similar" to the Sun (Hardorp 1982; Cayrel de Strobel 1996). The definition of a solar analogue is not very stringent, and the criteria used in the literature for their identification vary. However, to give an overview of the subsample of (potential) interest for solar-analogue studies we apply the criteria of $T_{\rm eff}$ within ±500 K of the Sun, [Fe/H] within ±0.3 dex (corresponding to a metallicity within a factor of two of solar), an $M_V$ within ±1 magnitude of the solar at $M_{V,\odot} = 4.83$ (Soderblom & King 1998)[15]. We have not restricted the subsample to be without close companions, but refer to Sect. 5.7 (Table 5) for information on binarity.

To have a homogeneous source for the stellar $T_{\rm eff}$ and [Fe/H] we adopt values from the Geneva-Copenhagen Survey (Nordström et al. 2004) in the revised version by Casagrande et al. (2011). Distances and magnitudes were adopted from the TESS Input Catalog (TICv8.2; Paegert et al. 2021). In Fig. 12 we show the subsample that meets the above criteria (though we have still included stars with [Fe/H] beyond the limits). As seen, our sample contains a significant number of potential solar analogues that can now be characterised asteroseismically, and many of these are well-known from several spectroscopic compilations of solar analogues (e.g., Cayrel de Strobel 1996; Ramírez et al. 2009; Porto de Mello et al. 2014; Datson et al. 2015).

If we tighten the required resemblance to the Sun, nearing us the definition by some of a solar-twin (e.g., Adibekyan et al. 2017), to $T_{\rm eff} = 5772 \pm 100$ K and $\log g = 4.44 \pm 0.1$ dex (calculated from $T_{\rm eff}$ and $\nu_{\rm max}$, see Lund et al. 2024) we can identify four stars, namely: $\nu^2$ Lup (HIP 75181; a known multi-planet asteroseismic host, see Udry et al. 2019; Kane et al. 2020; Delrez et al. 2021), 51 Peg (HIP 113357; a known exoplanet host, Mayor & Queloz 1995), 26 Dra (HIP 86036; a known long-period visual and spectroscopic binary, see Table 5), and HD 102365 (HIP 57443; a known exoplanet host, see Tinney et al. 2011). Of these 51 Peg is already a known asteroseismic star (Metcalfe et al. 2024). As suggested by the Casagrande et al. (2011) [Fe/H]-values for these stars (Fig. 12) they are all outside the limit of [Fe/H] ± 0.1 dex corresponding to the tightened limits on $T_{\rm eff}$ and $\log g$ (but all within [Fe/H] ± 0.3 dex). In general, we find a broad consensus between the [Fe/H]-values from Casagrande et al. (2011) with those found from the literature, except for 26 Dra which in many other studies are found to have a near-solar metallicity (see, e.g., Ramírez et al. 2013; Tautvaišienė et al. 2020; Fuhrmann 2008; Soubiran et al. 2022). Of interest for future studies 26 Dra is also inside the current northern PLATO long-stare field (see Sect. 5.3).

### 5.9. Notes on individual targets

In the following, we list a few targets of potentially high interest that have not been discussed in detail in the previous sections. These targets are not necessarily mentioned because of the quality of their seismology, but for the potentially improved understanding, we may gain from these stars/systems through the information offered by an asteroseismic analysis.

$\theta$ UMa (HIP 46853): A very bright ($V = 3.17$) sub-giant solar-like oscillator (i.e., comparable in brightness to $\beta$ Hyi, $\zeta$ Her, and $\mu$ Her, see Fig. 3). While predicted by Bedding et al. (1996) to show oscillations it has until now escaped a detailed observational investment for an asteroseismic characterisation. $\theta$ UMa has independent interferometric measurements of its diameter (Table 4), and is currently being closely monitored in RV with SONG for asteroseismic analysis.

$\chi$ Dra (HIP 89937): A bright ($V = 3.55$) newly discovered solar-like oscillator (F7V; see Fig. 3) that is a member of a double-lined spectroscopic (SB2) and visual binary system (see Table 5), with a K1V companion. The binary orbit ($P = 280.5$ d) is extremely well-determined from RV observations, including many observations from SONG, from which individual component spectra can be disentangled for abundance analysis. In addition to the SB2 characterisation the visual orbit is well constrained from astrometric observations (e.g., Hartkopf et al. 2001b), allowing individual masses to be measured, and interferometric observations have been obtained using CHARA for independent constraint on the stellar radius. Importantly, $\chi$ Dra is included in PLATO's current northern LOP field and promises to become a key benchmark star for asteroseismology. A detailed system analysis will be presented in Rudrasingam et al. (in prep.).

B Car (HIP 39903): A known single-lined spectroscopic (Murdoch & Hearnshaw 1991, 1993) and visual binary (Goldin & Makarov 2006, 2007) with an orbital period of $P \sim 900$ d (see Table 5 and Fig. 3). Fuhrmann et al. (2011a) identifies B Car as a field blue straggler with a white dwarf companion. This is based on a match between the estimated secondary mass and the Rappaport et al. (1995) white dwarf mass-period relationship, and that the measured [Fe/Mg] = −0.27 abundance (and metallicity of [Fe/H] = −0.27) suggests an old ($\tau \sim 8 - 10$ Gyr) star (e.g., Nissen et al. 2020). We note that Brown et al. (2000) indicate the potential existence of a substellar companion based on IR-excess observed with the Hubble Near-Infrared Camera and Multi-Object Spectrometer (NICMOS) Camera 2 coronagraph (see also Schultz et al. (n.d.), who suggests that the companion is a rare brown T-type dwarf, which is very uncommon to find around an F-star like B Car). Finally, we note that B Car is within the PLATO LOPS2 field (Table 2).

$\iota$ Peg (HIP 109176) and $\omega$ Dra (HIP 86201): Both of these stars are members of well-characterised visual and SB2 systems (Table 5) with short orbital periods (e.g., Boden et al. 1999; Morel et al. 2000; Fekel et al. 2009; Konacki et al. 2010; Behr et al. 2011). Similar to $\chi$ Dra, it should therefore be readily possible to provide dynamical mass estimates to test the results from asteroseismology (with the caution that the assumption of isolated stellar evolution in an asteroseismic modelling effort could be questionable). $\omega$ Dra is furthermore within the current PLATO LOPN1 field (Table 2).

171 Pup (HIP 37853): This star is the primary of a wide binary system containing the common proper motion companion star

[15] http://www2.lowell.edu/users/jch/workshop/drs/drs-p1.html

[16] using the `isochrones` Python module (https://github.com/timothydmorton/isochrones).

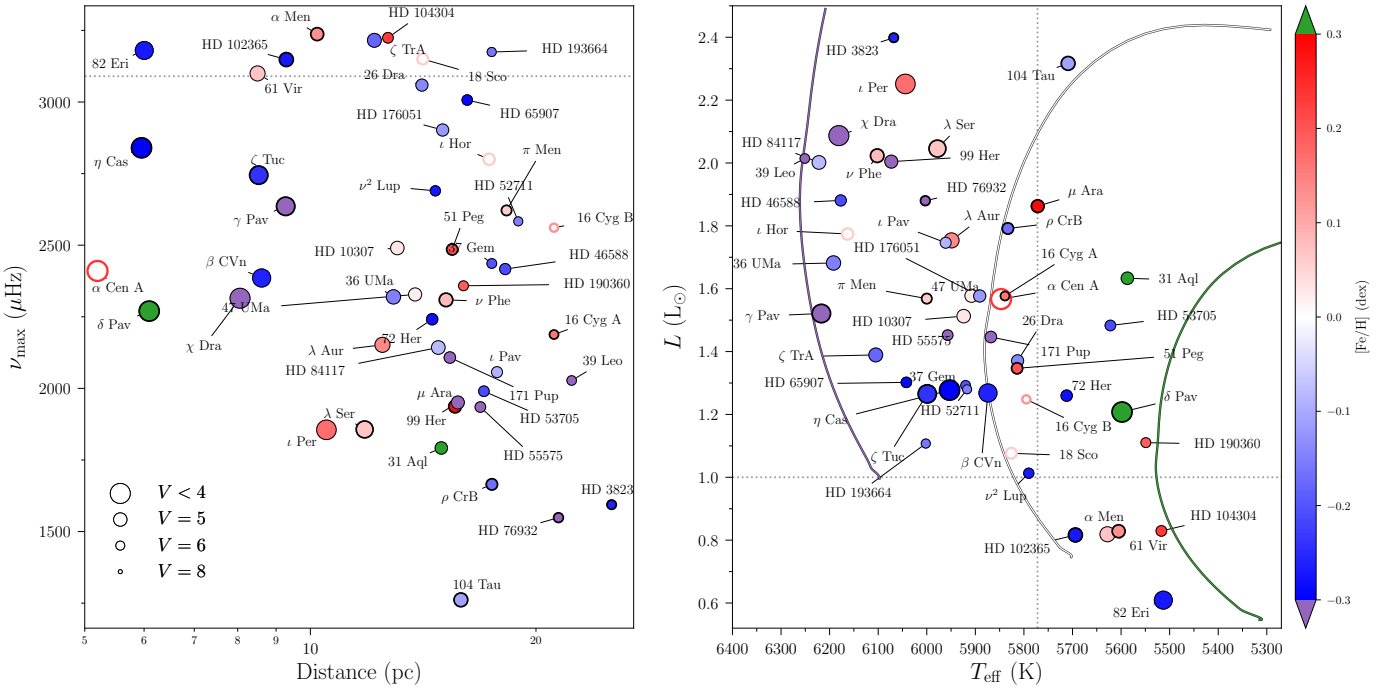


**Fig. 12.** Stars identified to match our solar-analogue criteria (see Sect. 5.8). The marker size indicates the visual magnitude (see legend), while the colour gives the [Fe/H]-value from Casagrande et al. (2011). Empty markers indicate known bright oscillators from ground-based surveys (and 16 Cyg B from *Kepler*) that match the solar-analogue criteria, but where no detection was obtained in this study. Markers with a thick black edge indicate the stars that are already known oscillators (see Table 1). Left: identified (potential) solar analogues in terms of distance and $\nu_{max}$ ($\alpha$ Cen A at a distance of ~1.35 pc is moved to a higher distance for a better display of the sample). The horizontal dotted line gives the solar $\nu_{max}$-value for reference. Right: identified (potential) solar analogues in terms of $T_{eff}$ and luminosity, using magnitudes and distances from the TESS Input Catalog (TICv8.2; Paegert et al. 2021). The dotted lines provide the solar values for reference. For reference, we also show 1 $M_\odot$ MIST[16]evolutionary tracks (Dotter 2016; Choi et al. 2016) with [Fe/H]-values of −0.3, 0, and +0.3 dex (increasing with tracks from left to right; also see colorbar).

VB3 (van Biesbroeck 1961), identified by Kunkel et al. (1984) to be a low luminosity white dwarf of spectral type DC9-11 (Wesemael et al. 1993). VB3 is often identified as WD 0743-336 (and sometimes WD 0743-340, GJ 288B or NLTT 18414B) and is one of the coolest WD stars and widest binaries known amongst Sirius-like-systems with a WD in a binary with a star of spectral type K or later (Holberg et al. 2013) (see also Bergeron et al. 2001; Holberg et al. 2008; McCook & Sion 2016). Holberg et al. (2013) provides a period for the system of 1.38 Myr, a separation of 14682.4 AU, and masses of 1.08 and 0.59$M_\odot$ for the components. The MS A-component is found to consist of a close pair (WDS discoverer designation *TOK 193 Aa,Ab*; resolved in speckle interferometry by Hartkopf et al. (2012) and Tokovinin (2012)) for which Tokovinin (2014) gives a period of 8.258 yr (the ORB6 database provides a period of 23.10 yr based on later observations by Tokovinin). We find that this star/system would be very interesting to study in relation to comparing the asteroseismic age of the MS star 171 Pup A with the estimated cooling age of VB3, which could help to empirically constrain the age determination for the oldest WDs. From the age difference, the pre-WD lifetime could be estimated, which could provide the WD progenitor mass and thereby help to constrain the initial-final mass relation. To date, only very few binary systems containing a WD and an oscillating companion have been identified, and these often tight systems contain an early-type MS primary star that does not readily allow an age to be determined using asteroseismology. Examples are the EL CVn binaries consisting of an A- or F-type primary and a low-mass helium white dwarf (WD) secondary, where the primary occasionally is found to oscillate as a $\delta$ Scuti pulsator (e.g., Maxted et al. 2014; Guo et al. 2017).

$o^2$ Eri (HIP 19849/40 Eridani A[17]) This star is part of a triple-star system, orbited ($P$~8000 yr, Table 5) by a binary (B and C components) consisting of a WD ($o^2$ Eri B/WD 0413-077; type DA2.9 and the first ever recognized WD) and an M-dwarf ($o^2$ Eri C) in a 230-year-long orbit (Bond et al. 2017; Mason et al. 2017). As for 171 Pup, an asteroseismic age determination could help constrain the WD age otherwise obtained from cooling tracks and initial-final mass relations.

31 Aql (HIP 95447/b Aql): With a metallicity of [Fe/H]~0.35 dex this star is analysed by Mishenina (1996) and Feltzing & Gonzalez (2001) (among others) in the context of being a "super-metal-rich" (SMR) star.

HD 76932 (HIP 44075): This star is listed by Nissen & Schuster (2011) as a thick-disk star and Fuhrmann et al. (2017) finds it to be discrepant in [Ba/Fe] vs. [Fe/H], suggesting it to have a WD companion.

HD 65907 (HIP 38908): Fuhrmann et al. (2012) analyzed this star in the context of being an old Pop II star based on its abundance but finds this to conflict with the age derived from evolu-

[17] To trekkies potentially better known as the planet *Vulcan's* host star in the *Star Trek* universe.

tionary tracks and explains discrepancy to be caused by a former mass transfer. An asteroseismic age could potentially help resolve the issue.

HD 81809 (HIP 46404): This star is well-studied in the context of stellar activity, and long-term X-ray monitoring has shown a well-defined chromospheric activity cycle with a period of 7.3 ± 1.5 yr (Orlando et al. 2017; Egeland 2018). Moreover, the star is a member of a well-defined visual and spectroscopic (SB2) binary system (see Table 5).

HD 156098 (HIP 84551): Analysis by Feng et al. (2022) list this star as being the host of two potential exoplanets with periods of respectively 21.85 ± 0.01 and $7841^{+247}_{-517}$ days. The star is also commonly used as a comparison star in the analysis of the GRO J1655-40 system (Foellmi 2009), where the companion was found to be a black hole (Orosz & Bailyn 1997; Mirabel et al. 2002).

HD 186155 (HIP 96825; HR 7495; KIC 9163520): This star was included in our initial selection and is identified as a so-called "Hump-and-Spike" (H+S) star by Pope et al. (2019) based on long-cadence (30-min) smear data from *Kepler* and has been analysed recently in this context by Henriksen et al. (2023) and Antoci et al. (2025). Based on the star's H+S classification and its location in the HR diagram (positioned in a region where solar-like oscillations are not expected), this star is not included in the final sample. However, we note that clear excess power akin to solar-like oscillations was identified at $\nu \sim 250\,\mu$Hz in addition to the low-frequency peaks associated with the H+S characteristics. The origin of this excess power remains to be understood.

## 6. Conclusions

We have with the TLS provided detections of asteroseismic signals for a total of 196 MS/SG stars, visible to the naked eye ($V \leq 6$), and of these, 128 are to the best of our knowledge new detections. Given the brightness of this sample, as opposed to many asteroseismic stars from *Kepler*, it is possible to obtain a high-quality characterisation of the stars from ground-based efforts, and many of the stars already have extensive literature from decades of scrutiny. Our goal with this analysis has been to report on the asteroseismic detections, to ensure continued observations from TESS, and to highlight the many potential uses of the sample in future in-depth analyses.

In processing the TESS data, we used the products produced by SPOC (Jenkins et al. 2016) and the light curves extracted from the TPF using custom apertures (Sect. 3, Appendix B). While we find neither data product to be superior in general, we consider them highly complementary and the custom apertures allowed us in several cases (see, e.g., Fig. 2) to make detections of oscillations (or improve upon these) where the SPOC apertures were ill-defined. From our processed light curves, we confirm the apparent superior quality of 20-s over 120-s cadence data identified by Huber et al. (2022) and see that this extends to the brighter stars covered with the TLS (Sect. 5.2).

We have provided values for the global asteroseismic parameters $\Delta\nu$ and $\nu_{\rm max}$ from the `PySYD` pipeline for all stars with identified oscillations (Sect. 5.1, Table 1), and all reported detections have been confirmed by three independent pipelines. We find an overall excellent agreement with values from the literature for the stars with previous detections (Sect. 5.1.1), and with only two exceptions, we were able to confirm all previous detections based on TESS data (Sect. 5.2). In our comparison of measured $\nu_{\rm max}$ values to those expected from the ATL3, we have identified an apparent underestimation of $\nu_{\rm max}$ from the latter, leading to too optimistic detection probabilities (Sect. 5.1.1 and Fig. 6). The bias in $\nu_{\rm max}$ estimates from ATL3 is likely caused by biases in the Gaia DR3 estimates of $T_{\rm eff}$ and $\log g$ (especially clear for the brightness range covered by our sample) used in the $\nu_{\rm max}$ calculation (Appendix C).

In our assessment of the properties of the stars in the sample we have identified a total of 34 stars overlapping the current LOPN1 or LOPS2 field definitions of PLATO (Garcia et al., in prep.), and thereby of interest for the calibration or validation of the asteroseismic parameters returned from this upcoming mission (Sect. 5.3); several stars of potential interest to studies of solar-analogues (Sect. 5.8); we identify 54 stars as having long-baseline interferometric observations (Sect. 5.6, Table 4), providing independent measurements of their radii, and 48 stars to be members of stellar binaries where an orbital characterisation has been possible – of these 23 (with 9 being SB2 systems) have both spectroscopic and visual/astrometric constraints providing independent constraints on the stellar masses (Sect. 5.7, Table 5); and 24 exoplanet-host stars (Table 3), 12 of which are without previous detections of oscillation (Sect. 5.5), and all except 11 systems are also included in HWO target list. In addition to these interesting sub-samples, we identify several individual stars/systems where the detection of oscillations could be of particular interest for dedicated in-depth studies (Sect. 5.9), including, i.a., the bright ($V = 3.17$) sub-giant $\theta$ UMa and the well-characterised SB2 system $\chi$ Dra (Rudrasingam et al., in prep.).

In addition to the global asteroseismic parameters, we estimate that of the order ~63% of the stars are amenable to peak-bagging for the analysis of individual mode parameters – this analysis and stellar modelling of the sample will be the subject of a future analysis. In future work, we will also extend our analysis to the correspondingly bright evolved stars observed by TESS (Fig. 4), and we will provide updates and extensions to the TLS following the continued collection of data from TESS.

*Acknowledgements.* The authors acknowledge the dedicated team behind the TESS mission, without whom this work would not have been possible. We acknowledge the PIs of the TESS Guest Investigator proposals that over the years have ensured the 120- and 20-s cadence observations of the stars analysed here (see `https://heasarc.gsfc.nasa.gov/docs/tess/approved-programs.html`). We are grateful to Daniel Hey for discussions on the ATL, to Pierre Maxted, Hugh Osborn, Valerio Nascimbeni, and Juan Cabrera for discussions on the PLATO LOP fields, and to Vichi L. Antoci for discussions on individual classical pulsators in the sample. M.N.L. acknowledges support from the ESA PRODEX programme. S.M. acknowledges support from the Spanish Ministry of Science and Innovation with the grants number PID2019-107061GB-C66 and PID2023-149439NB-C41, and through AEI under the Severo Ochoa Centres of Excellence Programme 2020–2023 (CEX2019-000920-S). R.A.G. acknowledges the support from the GOLF and PLATO Centre National D'Études Spatiales grants. T.R.B. acknowledges support from the Australian Research Council (FL220100117). D.H. acknowledges support from the Alfred P. Sloan Foundation, the National Aeronautics and Space Administration (80NSSC22K0303, 80NSSC23K0434, 80NSSC23K0435, 80NSSC21K0652) and the Australian Research Council (FT200100871). This research has made use of the Washington Double Star Catalog maintained at the U.S. Naval Observatory. This research has made use of the SIMBAD database (Wenger et al. 2000), operated at CDS, Strasbourg, France. This research has made use of the Jean-Marie Mariotti Center (JMMC) Measured Stellar Diameters Catalogue (available at `http://www.jmmc.fr/jsdc`) and the `OiDB` service (available at `http://oidb.jmmc.fr`). This research has made use of the NASA Exoplanet Archive, which is operated by the California Institute of Technology, under contract with the National Aeronautics and Space Administration under the Exoplanet Exploration Program. This research has made use of data obtained from or tools provided by the portal exoplanet.eu of The Extrasolar Planets Encyclopaedia. This work presents results from the

European Space Agency (ESA) space mission Gaia. Gaia data are being processed by the Gaia Data Processing and Analysis Consortium (DPAC). Funding for the DPAC is provided by national institutions, in particular the institutions participating in the Gaia MultiLateral Agreement (MLA). The Gaia mission website is https://www.cosmos.esa.int/gaia. The Gaia archive website is https://archives.esac.esa.int/gaia. This research made use of the SONG database SODA (https://soda.phys.au.dk/), operated and maintained at Aarhus University, DK. We acknowledge the use of the following Python-based software modules: `Astropy` (Astropy Collaboration et al. 2013), `PyAstronomy` (Czesla et al. 2019), `Lightkurve` (Vinícius et al. 2018), `KDEpy` (Odland 2018), `scikit-image` (van der Walt et al. 2014), `platopoint`, `tess-atl` (Hey et al. 2024), `tpfi` (Xing et al. 2024), and `pySYD` (Chontos et al. 2022).

**Table 5.** TLS and binarity

| Name | HIP | WDS | SB9 | $V$ (mag) | $\nu_{max}$ ($\mu$Hz) | $P$ (Spec) (year/day) | $P$ (Orb) (year/day) | $K_1(/K_2)$ km/s | $v \sin i$ km/s | SONG (# spectra) |
|---|---|---|---|---|---|---|---|---|---|---|
| $\eta$ Boo | 67927 | 13547+1824A | 794 | 2.68 | 697 | 494.2 d[(1)] | 494.2 d | 8.4 | 11.3[(2)] | 2075 |
| $\zeta$ Her$^{(PN)}$ | 81693 | 16413+3136AB | 915 | 2.81 | 718 | 34.4 yr[(3)] | 34.5 yr | 4.0 | 6.2[(4)] | 377 |
| $\mu^1$ Her$^{(PN)}$ | 86974 | 17465+2743Aa,Ab | - | 3.42 | 1192 | (*m*) | 98.9±22.7 yr[(m)] | 1.12[(m)] | 5.2[(4)] | >106000 |
| $\chi$ Dra$^{PN}$ | 89937 | 18211+7244Aa,Ab | 1058 | 3.55 | 2314 | 280.5 d[(5)] | 280.5 d | 17.3/24.3 | 5.5[(4)] | 1079 |
| $\iota$ Peg | 109176 | 22070+2521A | 1354 | 3.77 | 2101 | 10.2 d[(6)] | 10.2 d | 48.4/77.6 | 9.3[(4)] | 95 |
| $\upsilon$ Cep$^{PN}$ | 102431 | 20454+5735Aa,Ab | 1489 | 4.52 | 958 | 523.4 d[(7)] | 523.4 d | 8.3/8.5 | 8.7[(4)] | 3 |
| B Car$^{PS}$ | 39903 | 08090-6118A | 3654 | 4.74 | 1386 | 899.3 d[(8)] | 925.0(±10.6) d | 3.2 | 8.8[(9)] | - |
| $\omega$ Dra$^{PN}$ | 86201 | 17370+6845A | 981 | 4.77 | 1999 | 5.3 d[(6)] | 5.3 d | 36.3/44.7 | 5.9[(10)] | 248 |
| 12 Boo | 69226 | 14104+2506AB | 804 | 4.82 | 694 | 9.6 d[(6)] | 9.6 d | 67.1/69.1 | 17.0[(10)] | 391 |
| $\omega$ And | 6813 | 01277+4524A | 3863 | 4.83 | 1899 | 254.8 d[(11)] | 254.9 d | 17.8/18.9 | 57.1[(10)] | 3 |
| 19 Dra$^{PN}$ | 82860 | 16564+6502C | 938 | 4.88 | 2313 | 52.1 d[(12)] | (*d*) | 17.2/(*e*) | 13.0[(13)] | 4 |
| $\zeta$ TrA | 80686 | 16285-7005A | 898 | 4.9 | 3215 | 13.0 d[(a)] | 12.9 d | 7.4 | 3.23[(26)] | - |
| $\epsilon$ Lib | 75379 | - | 841 | 4.92 | 775 | 226.9 d[(12)] | (*b*) | 14.2 | 10.0[(13)] | 5 |
| HD 10307 | 7918 | 01418+4237AB | 2546 | 4.96 | 2490 | 19.7 yr[(14)] | 19.5 yr | 3.0 | 4.9[(4)] | 6 |
| 99 Her$^{PN}$ | 88745 | 18070+3034Aa,Ab | 3658 | 5.05 | 1950 | 56.4 yr[(3)] | 56.4(±0.2) yr | 3.2 | 4.5[(4)] | 4 |
| $\kappa$ For | 11072 | 02225-2349A | - | 5.19 | 1160 | 26.54 ± 0.05 yr[(f)] | 26.5 yr | 5.45 ± 0.04[(f)] | 6.25[(15)] | - |
| 94 Aqr | 115126 | 23191-1328Aa,Ab | 1438 | 5.2 | 886 | 6.3 yr[(12)] | 6.3 yr | 6.0 | 4.9[(4)] | 4 |
| HD 176051$^{PN}$ | 93017 | 18570+3254AB | 2559 | 5.2 | 2902 | 61.4 yr[(16)] | 61.4(±0.1) yr | 3.5 | 5.7[(4)] | 5 |
| 26 Dra$^{PN}$ | 86036 | 17350+6153AB | 2557 | 5.23 | 3058 | 74.2 yr[(16)] | 76.1 yr | 3.8 | 6.0[(4)] | 5 |
| HD 81809 | 46404 | 09278-0604AB | 1474 | 5.38 | 691 | 34.5 yr[(5)] | 32.0 yr | 4.8/8.2 | 5.5[(4)] | 2 |
| HD 14214 | 10723 | - | 118 | 5.6 | 1667 | 93.3 d[(12)] | (*g*) | 19.3 | 5.6[(4)] | 4 |
| HD 214850 | 111974 | 22409+1433AB | 1395 | 5.72 | 637 | 20.9 yr[(17)] | 20.8 yr | 13.6 | 5.3[(4)] | 4 |
| 35 Leo | 50319 | 10167+2325B | - | 5.95 | 985 | 531 d[(h)] | (*h*) | NA | 5.5[(4)] | - |
| $\theta$ Dra$^{PN}$ | 78527 | - | 882 | 4.01 | 722 | 3.1 d[(18)] | - | 25.1/66.0 | 30.7[(4)] | 2 |
| $\tau^1$ Hya | 46509 | 09291-0246A | 2549 | 4.59 | 1572 | 7.7 yr[(19)] | - | 2.8 | 32.2[(4)] | 3 |
| $\sigma$ Cet | 11783 | 02321-1515Aa,Ab | - | 4.74 | 913 | 3.2 yr[(j)] | - | 27/19.5[(j)] | - | 3 |
| 16 UMa | 45333 | - | 558 | 5.18 | 1514 | 16.2 d[(20)] | - | 35.3/65.0 | 6.5[(4)] | 3 |
| $\rho$ Tuc | 3330 | - | 40 | 5.38 | 724 | 4.8 d[(21)] | - | 26.1 | 23.2[(9)] | - |
| HD 104304 | 58576 | 12007-1028A | - | 5.54 | 3224 | 48.5 yr[(n)] | - | NA | 2.87[(22)] | - |
| HD 46569$^{PS}$ | 31079 | - | - | 5.58 | 932 | 25.6 ± 1.5 yr[(i)] | - | 1.7 ± 0.08[(i)] | 5.6[(9)] | - |
| 72 Psc | 5081 | 01051+1457A | 1654 | 5.64 | 946 | 50.4 d[(23)] | - | 36.0/39.9 | 5.0[(24)] | 6 |
| HD 121384 | 68101 | 13565-5442A | - | 6.0 | 425 | 178.7 ± 0.1 d[(o)] | - | 10.9 ± 2.2[(o)] | NA | - |
| $\eta$ Cas | 3821 | 00491+5749A | - | 3.46 | 2839 | - | 480.0 yr | NA | 5.4[(4)] | 6058 |
| $\alpha$ For | 14879 | 03121-2859A | - | 3.8 | 1128 | - | 269.0(±22.5) yr | NA | 6.24[(15)] | 3 |
| $\iota$ Vir | 69701 | 14190-0636C | - | 4.07 | 644 | - | 55 yr[(k)] | NA | - | 1 |
| $\theta$ Per | 12777 | 02442+4914A | - | 4.1 | 2314 | - | 2720 yr | NA | 10.2[(4)] | 4 |
| o$^2$ Eri | 19849 | 04153-0739A | - | 4.43 | 3433 | - | 8000 yr[(p)] | NA | 1.23[(25)] | 3 |
| $\mu$ Cyg | 107310 | 21441+2845AB | - | 4.49 | 1213 | - | 789.0(±37.9) yr | NA | 5.45[(26)] | 2 |
| $\psi^1$ Dra A$^{PN}$ | 86614 | 17419+7209A | - | 4.57 | 1232 | - | 10000 yr | NA | 12.5[(27)] | 6 |
| | | | | | | 18.5 yr[(c)] | - | 5.2/11.1[(c)] | | |
| $\sigma^2$ UMa | 45038 | 09104+6708AB | - | 4.8 | 1354 | - | 921.0 yr | NA | 7.55[(26)] | 3 |
| 17 Cyg$^{PN}$ | 97295 | 19464+3344A | - | 5.0 | 1484 | - | 232.0(±3.4) yr | NA | 9.0[(13)] | 1 |
| HD 62644$^{PS}$ | 37606 | 07430-4511AB | - | 5.04 | 708 | - | 380.0(±1.5) d | NA | 2.49[(22)] | - |
| $\kappa$ Del | 101916 | 20391+1005A | - | 5.07 | 622 | - | 45.0 yr | NA | 4.42[(22)] | 3 |
| 94 Cet | 14954 | 03128-0112A | - | 5.07 | 1267 | - | 2029[(l)] (±304.5) yr | NA | 10.3[(4)] | 149 |
| HD 100203 | 56290 | 11323+6105AB | - | 5.46 | 1532 | - | 72.7(±0.2) yr | NA | 6.1[(10)] | - |
| HD 53705$^{PS}$ | 34065 | 07040-4337A | - | 5.56 | 1989 | - | 4.1 yr | NA | 4.3[(9)] | - |
| 10 Ari | 9621 | 02037+2556AB | - | 5.64 | 574 | - | 325.0(±8.0) yr | NA | 7.482[(28)] | 1 |
| 16 Cyg A$^{PN}$ | 96895 | 19418+5032Aa | - | 5.99 | 2236 | - | 13513 yr | NA | - | - |

**Notes.** The table provides an identification of the binarity for the seismic stars in the sample. The first four columns provide identifiers for the stars in the form of their Bayer/Flamsteed designation (or primary name according to `Simbad`) and their "HIP", "WDS", and "SB9" IDs. Super-scripts of *PN* or *PS* on the star's name refer to their position within (or near when in parenthesis) the northern (*N*) or southern (*S*) PLATO fields (see Table 2). "*V*" gives the *V*-band magnitude, "$\nu_{max}$" (central value only) is adopted from Table 1. "*P*" refers to the binary period, where spectroscopic ("Spec") periods are obtained from SB9 (unless otherwise stated with a letter reference), with reference to the adopted most recent period determination. Orbital ("Orb") binary periods are obtained from ORB6 (unless otherwise stated with a letter reference), with non-zero RMSDs between ORB6 and OARMAC entries in parenthesis. "$K_1(/K_2)$" gives the semi-amplitude(s) corresponding to the *P* (Spec) reference. "SONG" gives the number of spectra available for the target in the SONG database SODA (`https://soda.phys.au.dk/`).
[(a)] Included in SB9 with reference to Spencer Jones (1928), but more recent spectroscopic analysis is provided by Skuljan et al. (2004); [(b)] Adopting the spectroscopic orbital information Castelaz (1989) provides astrometric binary orbit solution; [(c)] $\psi^1$ Dra is a hierarchical multiple system where the AB system is determined astrometrically (in ORB6), while the AC system is determined spectroscopically by Gullikson et al. (2015); [(d)] Adopting the spectroscopic orbital information Ren & Fu (2013) provides astrometric binary orbit solution; [(e)] Found to be SB2 by Katoh et al. (2013), but $K_2$ is not provided due to weakness of lines; [(f)] Fekel et al. (2018) (see also Tokovinin 2013) provides a joint analysis of spectroscopic, astrometric, and visual orbit data; [(g)] Adopting the spectroscopic orbital information Fekel et al. (2007) provides astrometric binary orbit solution; [(h)] Tokovinin (2014) provides an orbital period for this SB1 binary (but no semi-amplitude), in agreement with the Gaia DR3 Non-single-star (NNS) period of 524 ± 6 days (Halbwachs et al. 2023); [(i)] Zechmeister et al. (2013); [(j)] McLaughlin (1962); [(k)] Gontcharov & Kiyaeva (2010); [(l)] Adopting the value in OARMAC from Roberts et al. (2011); [(m)] Roberts et al. (2016) provides a combined astrometric ans spectroscopic analysis; [(n)] Preliminary period by Schnupp et al. (2010) from 9 yr RV data (no semi-amplitude provided); [(o)] Jenkins et al. (2015) provides spectroscopic solution and finds indications of a high eccentricity (*ecc*~0.84) low-mass companion; [(p)] Estimate by Heintz (1974), ORB6 only lists period for BC component of this triple system.

**References.** (1) Bertiau (1957); (2) Hourihane et al. (2023); (3) Agati et al. (2015); (4) Luck (2017); (5) Pourbaix (2000); (6) Behr et al. (2011); (7) Griffin (1999); (8) Murdoch & Hearnshaw (1993); (9) Ammler-von Eiff & Reiners (2012); (10) Schröder et al. (2009); (11) Griffin (2011); (12) Katoh et al. (2013); (13) Takeda et al. (2005); (14) Halbwachs et al. (2018a); (15) Borisov et al. (2023); (16) Duquennoy & Mayor (1991); (17) Batten et al. (1985); (18) Mazeh et al. (2002); (19) Halbwachs et al. (2012); (20) Fekel et al. (2015); (21) Neubauer (1929); (22) Hojjatpanah et al. (2019); (23) Griffin (2001); (24) Bernacca & Perinotto (1970); (25) Díaz et al. (2018); (26) Martínez-Arnáiz et al. (2010); (27) Strassmeier et al. (2023); (28) Jönsson et al. (2020);

## Appendix A: Stars without observations from TESS

Table A.1 provides an overview of the stars that met our selection criteria in terms of $M_V$ and $B-V$, but did not have TESS observations up to and including Sector 77 as considered in this analysis. Table A.1 lists both the 69 stars that will be observed during Cycle 7 and the 19 stars that are not scheduled for observations.

## Appendix B: Comparing SPOC and custom apertures

As mentioned in Sect. 3, we use, in addition to data from SPOC light curves extracted from the TESS TPFs using custom apertures made from the combination of SPOC and K2P$^2$ apertures (Lund et al. 2015). In Fig. B.1 we compare the joint apertures and those from SPOC based on 120-s cadence data, and as seen the aperture sizes follow the expected trend against magnitude[18]. Per definition, the joint apertures will always be equal to or larger than the one from SPOC alone, but we can see that from a TESS magnitude ($T_{\rm mag}$) of ~4.7 and below the aperture from SPOC contributes an increasing fraction of pixels to the joint aperture – this is the magnitude region where the blooming trails from saturation become significant. Above $T_{\rm mag}$~4.7, the aperture from K2P$^2$ will typically fully contain the SPOC aperture. As expected, we see (not shown) little ($\pm1-2$ pixels) to no difference between the apertures defined for 120-s vs. 20-s cadence data.

The aperture sizes in the left and middle panels of Fig. B.1 are median values if stars are observed in multiple sectors. For a given star, there is some scatter in the aperture sizes defined for different sectors. There can be many causes for such scatter, e.g., from the variation in TESS PSFs across the focal plane which could add to the scatter for a given star from varying boresight distances (Vanderspek et al. 2018), and this effect would also add to the width of the aperture size distribution of the given $T_{\rm mag}$. From the right panel of Fig. B.1 we see that at least part of the scatter in aperture sizes for a given star is related to the observing sector. The plot shows for a given star the difference in aperture sizes between SPOC and K2P$^2$ for a given sector ($i$) compared to the median of the SPOC and K2P$^2$ apertures across all observing sectors for the star. We see that on this scale (and with the adopted settings for the threshold for selecting pixels of interest), the K2P$^2$ apertures are in median ~40% larger than the SPOC ones across all magnitudes and sectors. There are, however, clear variations between different sectors, or rather between different pointings/cycles – in Cycle 1 (southern ecliptic hemisphere; sectors 1-13) the K2P$^2$ apertures are relatively larger than SPOC as compared to Cycle 2 (northern ecliptic hemisphere; sectors 14-26), and the largest effect is seen for the fainter stars in the sample. One might speculate that this relates to different observing conditions in the different sectors/pointings, and indeed variations in scattered light or pointing stability could and might have an effect, but an important aspect also seems to be the TPF stamp sizes (Fig. B.2).

In Fig. B.2 we show the variation in TPF stamp widths and heights as a function of magnitude and observing sector. As expected, a strong dependence on the stamp height (direction of potential blooming trails) on magnitude is seen, while the width has a value of 11 or 25 pixels. In the early cycles (1-3, sectors 1-39) there is a general tendency for brighter targets observed in 120-s cadence to have widths of 25 pixels while fainter targets adopt widths of 11 pixels. For 20-s cadence observations (introduced from Cycle 3, starting with Sector 27), this tendency is mainly observed for Cycle 3 (sectors 27-39) – later sectors almost exclusively adopt widths of 11 pixels. Concerning the stamp heights, we see that a value of 25 pixels is representative in median across cycles and cadences.

[18] The SPOC outlier near $T_{\rm mag}$~4.75 is TIC 20601206 (HIP 93017) which for several sectors in 120-s cadence data have an aperture defined by a few disjoint pixels. For the corresponding 20-s cadence data, the apertures look as expected.

## Appendix C: Comparison to the ATL

The apparent underestimation of $\nu_{\rm max}$ in the ATL (Fig. 6) means that the calculated detection probability will generally be overestimated, as oscillation amplitudes correlate inversely with $\nu_{\rm max}$. The ATL was built to guide the target selection process for the TESS Asteroseismic Science Consortium (TASC). Though certainly not intentional, the slightly optimistic detection probabilities ensure that a minimal number of targets showing oscillations, if observed, are overlooked in the observing proposals. Conversely, this could explain the generally low fraction of positive seismic detections obtained from TESS, at least early in the mission.

The ATL in its different versions is built on the methodology laid out by Chaplin et al. (2011b), and the ATL3 version (Hey et al. 2024) relies primarily on the Gaia DR3 (Gaia Collaboration et al. 2023) estimates of $T_{\rm eff}$ and $\log g$ to calculate $\nu_{\rm max}$ following:

$$\nu_{\rm max} = \frac{g}{g_\odot}\sqrt{\frac{T_{\rm eff,\odot}}{T_{\rm eff}}}\,\nu_{\rm max,\odot}\,. \tag{C.1}$$

The $T_{\rm eff}$ ($\log g$) in ATL3 is first and foremost taken as Gaia's `teff_gspphot` (`logg_gspphot`), followed by the $T_{\rm eff}$ ($\log g$) in the TIC (which can originate from a variety of sources; see Stassun et al. 2019) and finally Gaia's `teff_gspspec` (`logg_gspspec`), depending on availability. We note that the detection probability calculation adopted by Lund et al. (2016, 2024) for K2 targets follows the same overall methodology, but here adopting principally 2MASS ($J-K_S$) colours and the relation of Casagrande et al. (2010) to estimate $T_{\rm eff}$, combined with a luminosity (from Hipparcos) and the stellar mass from a simple mass-luminosity relation to estimate $\nu_{\rm max}$ following $\nu_{\rm max} = M/L\,(T_{\rm eff}/T_{\rm eff,\odot})^{3.5} \times \nu_{\rm max,\odot}$. However, in this case, no systematic offset is seen between predicted and measured $\nu_{\rm max}$ values (see their Figure 11 and F.1, respectively), suggesting that the Gaia inputs used to calculate $\nu_{\rm max}$ are somehow biased.

To assess the $\nu_{\rm max}$ underestimation from the current ATL3 we made a comparison of ATL3 $\nu_{\rm max}$ against values from the catalogues of Hatt et al. (2023), Zhou et al. (2024), Lund et al. (2024) (K2; Keystone), and the *Kepler* targets from Lund et al. (2017), Mathur et al. (2022), and Serenelli et al. (2017). For the K2 and *Kepler* samples, we have estimates of both $T_{\rm eff}$ and $\log g$ (from $T_{\rm eff}$ and $\nu_{\rm max}$) from the above publications, while we for the current TLS adopt the GCS values of Casagrande et al. (2011).

For all samples, we see a general underestimation of $\nu_{\rm max}$ from ATL3, ranging between 12 – 20%, and being the most significant for the TLS and K2 samples. For the samples where we have $T_{\rm eff}$ and $\log g$ (*Kepler*, K2, and TLS) in addition to $\nu_{\rm max}$, Fig. C.1 illustrates that a general median underestimation of ~1.2% and ~1.6% is obtained for the $T_{\rm eff}$ and $\log g$ values adopted in ATL3 (primarily from Gaia DR3's `gspphot`) – this was also noted in the analysis of $\sigma$ Dra by Hon et al. (2024).

**Table A.1.** Stars fulfilling TLS selection criteria, but with no data before Sector 78

| Name | TIC | HIP | $V$ (mag) | Constellation | RA (deg) | DEC (deg) | HWO (tier) | Seis. ref. | Sectors |
|---|---|---|---|---|---|---|---|---|---|
| $\alpha$ Oph | 289643770 | 86032 | 2.08 | Ophiucus | 263.7 | 12.6 | - | [a] | 79 |
| $\delta$ Cap | 155842257 | 107556 | 2.85 | Capricornus | 326.8 | −16.1 | - | - | 92 |
| 72 Oph | 24592444 | 88771 | 3.71 | Ophiucus | 271.8 | 9.6 | - | - | 80 |
| $\gamma$ Oph | 324016035 | 87108 | 3.75 | Ophiucus | 267.0 | 2.7 | - | - | 80 |
| $\rho^1$ Sgr | 334177803 | 95168 | 3.92 | Sagittarius | 290.4 | −17.8 | - | [b] | 92 |
| 70 Oph | 398120047 | 88601 | 4.03 | Ophiucus | 271.4 | 2.5 | B | 1 | 80 |
| b Oph | 87238691 | 85340 | 4.16 | Ophiucus | 261.6 | −24.2 | - | - | 91, 92 |
| 36 Oph[c] | 79454735 | 84405 | 4.33 | Ophiucus | 258.8 | −26.6 | B | - | 91 |
| $\xi$ Oph | 75899957 | 84893 | 4.39 | Ophiucus | 260.3 | −21.1 | C | - | 91 |
| $\zeta$ Ser | 104572330 | 88175 | 4.62 | Serpens | 270.1 | −3.7 | - | - | 80 |
| $\theta^1$ Ser | 227271980 | 92946 | 4.62 | Serpens | 284.1 | 4.2 | - | - | 80 |
| 20 Oph | 181290095 | 82369 | 4.64 | Ophiucus | 252.5 | −10.8 | - | - | 91 |
| $\omega$ Sgr | 209188615 | 98066 | 4.7 | Sagittarius | 299.0 | −26.3 | - | - | 92 |
| $\mu$ Aqr | 23913506 | 103045 | 4.73 | Aquarius | 313.2 | −9.0 | - | - | 81, 92 |
| $\rho$ Cap | 429135124 | 101027 | 4.77 | Capricornus | 307.2 | −17.8 | - | - | 92 |
| $\tau$ Oph | 204010915 | 88404 | 4.77 | Ophiucus | 270.8 | −8.2 | - | - | 80 |
| $\eta$ Cap | 418824772 | 104019 | 4.82 | Capricornus | 316.1 | −19.9 | - | - | 92 |
| 58 Oph | 238115675 | 86736 | 4.86 | Ophiucus | 265.9 | −21.7 | C | - | 91, 92 |
| $\psi$ Sco | 420895269 | 79375 | 4.93 | Scorpius | 243.0 | −10.1 | - | - | 91 |
| $\theta^2$ Ser | 227271997 | 92951 | 4.98 | Serpens | 284.1 | 4.2 | - | - | 80 |
| e02 Sgr | 422736099 | 96950 | 5.06 | Sagittarius | 295.6 | −16.1 | - | - | 92 |
| $\mu$ Cap | 206238826 | 108036 | 5.08 | Capricornus | 328.3 | −13.6 | - | - | 92 |
| HD 170680 | 186642657 | 90806 | 5.12 | Sagittarius | 277.9 | −18.4 | - | - | 92 |
| 42 Cap | 155706950 | 107095 | 5.16 | Capricornus | 325.4 | −14.0 | - | - | 92 |
| 15 Sgr | 243895751 | 89439 | 5.29 | Sagittarius | 273.8 | −20.7 | - | - | 91 |
| $\chi$ Cap | 99389357 | 104365 | 5.3 | Capricornus | 317.1 | −21.2 | - | - | 92 |
| $\mu$ Lib | 386858986 | 72489 | 5.32 | Libra | 222.3 | −14.1 | - | - | 91 |
| HD 171802 | 371026327 | 91217 | 5.38 | Ophiucus | 279.1 | 9.1 | - | - | 80 |
| $\eta$ Lib | 71859994 | 77060 | 5.41 | Libra | 236.0 | −15.7 | - | - | 91 |
| HD 155078 | 145740988 | 83962 | 5.43 | Ophiucus | 257.4 | −10.5 | - | - | 91 |
| HD 171834 | 371127111 | 91237 | 5.43 | Ophiucus | 279.2 | 6.7 | - | [d] | 80 |
| 16 Sco | 420896293 | 79387 | 5.43 | Scorpius | 243.0 | −8.5 | - | - | 91 |
| 95 Vir | 19924794 | 68940 | 5.46 | Virgo | 211.7 | −9.3 | - | [e] | 91 |
| 18 Aqr | 288404080 | 105668 | 5.48 | Aquarius | 321.0 | −12.9 | - | - | 92 |
| 18 Sco | 135656809 | 79672 | 5.49 | Scorpius | 243.9 | −8.4 | A | 2 | 91 |
| HD 186185 | 422856892 | 97063 | 5.49 | Sagittarius | 295.9 | −15.5 | - | - | 92 |
| HD 138413 | 73852746 | 76106 | 5.5 | Libra | 233.2 | −19.7 | - | - | 91 |
| HD 124683 | 428790951 | 69658 | 5.53 | Virgo | 213.8 | −18.2 | - | - | 91 |
| HD 150453 | 287619474 | 81754 | 5.55 | Ophiucus | 250.5 | −19.9 | - | - | 91 |
| HD 175317 | 352487147 | 92882 | 5.56 | Sagittarius | 283.9 | −16.4 | - | - | 92 |
| HD 181240 | 12056898 | 95077 | 5.59 | Sagittarius | 290.2 | −22.4 | - | - | 92 |
| HD 166285 | 338412799 | 89000 | 5.67 | Ophiucus | 272.5 | 3.1 | - | - | 80 |
| HD 173638 | 145429390 | 92136 | 5.69 | Scutum | 281.7 | −10.1 | - | - | 80 |
| 37 Cap | 441018038 | 106559 | 5.7 | Capricornus | 323.7 | −20.1 | - | - | 92 |
| 19 Aqr | 187064019 | 105761 | 5.71 | Aquarius | 321.3 | −9.7 | - | - | 92 |
| 73 Oph | 18517778 | 88964 | 5.71 | Ophiucus | 272.4 | 4.0 | - | - | 80 |
| HD 131977[f] | 287157634 | 73184 | 5.72 | Libra | 224.4 | −21.4 | A | - | 91 |
| 26 Oph | 18809756 | 83196 | 5.74 | Ophiucus | 255.0 | −25.0 | - | - | 91 |
| HD 171130 | 433218066 | 90991 | 5.74 | Scutum | 278.4 | −14.9 | - | - | 80, 92 |
| 34 Peg | 265917815 | 110785 | 5.76 | Pegasus | 336.7 | 4.4 | - | - | 82 |
| HD 163318 | 135485021 | 87836 | 5.76 | Sagittarius | 269.2 | −28.1 | - | - | 91, 92 |
| HD 162917 | 277303601 | 87558 | 5.77 | Ophiucus | 268.3 | 6.1 | - | - | 80 |
| HD 172051 | 1544160 | 91438 | 5.85 | Sagittarius | 279.7 | −21.1 | - | - | 92 |
| HD 152311[g] | 220765386 | 82621 | 5.86 | Ophiucus | 253.4 | −20.4 | - | - | 91 |
| V CS Vir | 46095850 | 69929 | 5.86 | Virgo | 214.7 | −18.7 | - | - | 91 |
| HD 124425 | 147755337 | 69493 | 5.89 | Virgo | 213.4 | −0.8 | - | - | 91 |
| HD 199443 | 442481598 | 103460 | 5.89 | Capricornus | 314.4 | −16.0 | - | - | 92 |
| 5 Aql A | 225849715 | 92117 | 5.89 | Aquila | 281.6 | −1.0 | - | - | 80 |
| 17 Cap | 422364664 | 102487 | 5.91 | Capricornus | 311.5 | −21.5 | - | - | 92 |
| 33 Oph | 142696134 | 83478 | 5.91 | Hercules | 255.9 | 13.6 | - | - | 79 |
| HD 151862 | 147752950 | 82350 | 5.91 | Hercules | 252.4 | 13.3 | - | - | 79 |
| HD 171856 | 842202 | 91347 | 5.93 | Sagittarius | 279.5 | −21.4 | - | - | 92 |
| HD 163336 | 210131774 | 87813 | 5.93 | Serpens | 269.1 | −15.8 | - | - | 80, 91, 92 |
| V DV Aqr | 442508593 | 103545 | 5.95 | Aquarius | 314.7 | −14.5 | - | - | 92 |
| HD 163624 | 62916034 | 87875 | 5.95 | Ophiucus | 269.3 | 0.1 | - | - | 80 |
| 45 Cap | 155772218 | 107302 | 5.96 | Capricornus | 326.0 | −14.7 | - | - | 92 |
| 16 Sgr | 243891646 | 89440 | 5.96 | Sagittarius | 273.8 | −20.4 | - | - | 91 |
| $\xi$ Sco | 49725171 | 78727 | 4.16 | Scorpius | 241.1 | −11.4 | - | - | - |
| $\tau^6$ Eri | 121078878 | 17651 | 4.22 | Eridanus | 56.7 | −23.2 | C | - | - |
| 47 Oph | 125165048 | 85365 | 4.53 | Ophiucus | 261.7 | −5.1 | - | - | - |
| $\upsilon$ Oph | 163938779 | 80628 | 4.62 | Ophiucus | 247.0 | −8.4 | - | - | - |
| $\sigma$ Ser | 270639162 | 80179 | 4.82 | Serpens | 245.5 | 1.0 | - | - | - |
| 60 Her | 263798437 | 83613 | 4.89 | Hercules | 256.3 | 12.7 | - | - | - |
| $\alpha^1$ Lib | 386886976 | 72603 | 5.15 | Libra | 222.7 | −16.0 | - | - | - |
| HD 158614 | 164139204 | 85667 | 5.31 | Ophiucus | 262.6 | −1.1 | - | - | - |
| HD 158352 | 348108914 | 85537 | 5.41 | Ophiucus | 262.2 | 0.3 | - | - | - |
| 49 Lib | 410696277 | 78400 | 5.47 | Libra | 240.1 | −16.5 | - | - | - |
| 47 Her | 276880793 | 82402 | 5.48 | Hercules | 252.6 | 7.2 | - | - | - |
| HD 159170 | 164542749 | 85922 | 5.61 | Ophiucus | 263.4 | −5.7 | - | - | - |
| 4 Ser | 461273024 | 74689 | 5.62 | Serpens | 229.0 | 0.4 | - | - | - |
| HD 164402 | 110325484 | 88298 | 5.72 | Sagittarius | 270.5 | −22.8 | - | - | - |
| 14 Oph | 282056074 | 81734 | 5.74 | Ophiucus | 250.4 | 1.2 | - | - | - |
| 12 Oph | 58092025 | 81300 | 5.77 | Ophiucus | 249.1 | −2.3 | A | - | - |
| HD 145148 | 277548101 | 79137 | 5.93 | Serpens | 242.3 | 6.4 | - | - | - |
| o Cap A | 72429235 | 101123 | 5.94 | Capricornus | 307.5 | −18.6 | - | - | - |
| V V2213 Oph | 297236135 | 83601 | 6.0 | Ophiucus | 256.3 | 0.7 | - | - | - |

**Notes.** The table provides an overview of the stars matching the selection criteria for the TLS, but without observations up until and including Sector 77, inluding at the bottom stars without any scheduled observations in Cycle 7. Stars are sorted according to their visual magnitude ("$V$"). The first three columns provide identifiers for the stars in the form of their Bayer/Flamsteed designation (or primary name according to `Simbad`) in addition to their TESS ("TIC") and Hipparcos ("HIP") IDs. The "HWO" column indicates if the star is found in the HWO target list and provides the tier (A, B, or C). The last two columns provide references to the primary sources of previous seismic detections if they exits, and lists the Sectors with scheduled TESS observations.

[a] Fast-rotating A-star with oscillations measured by Monnier et al. (2010) and Mirouh et al. (2014); [b] Listed as a $\delta$ Sct variable in the GCVS (Samus' et al. 2017) based on observations by Baglin et al. (1973); [c] Triple-star system of K-dwarfs (Cayrel de Strobel et al. 1989); [d] Identified as a potential $\gamma$ Dor pulsator by Uytterhoeven et al. (2011); [e] Identified as a $\delta$ Sct variable by Paunzen et al. (2017); [f] A quaternary star system with the B and C components forming their own binary system, and with component D being a T-type brown-dwarf (Gl 570 D) in a 1500 au wide orbit (Burgasser et al. 2000; Geballe et al. 2001); [g] Long period ($P$~2713 d) visual and spectroscopic binary (Tokovinin 2012; Fekel et al. 2018).

**References.** (1) Carrier & Eggenberger (2006b); (2) Bazot et al. (2011).

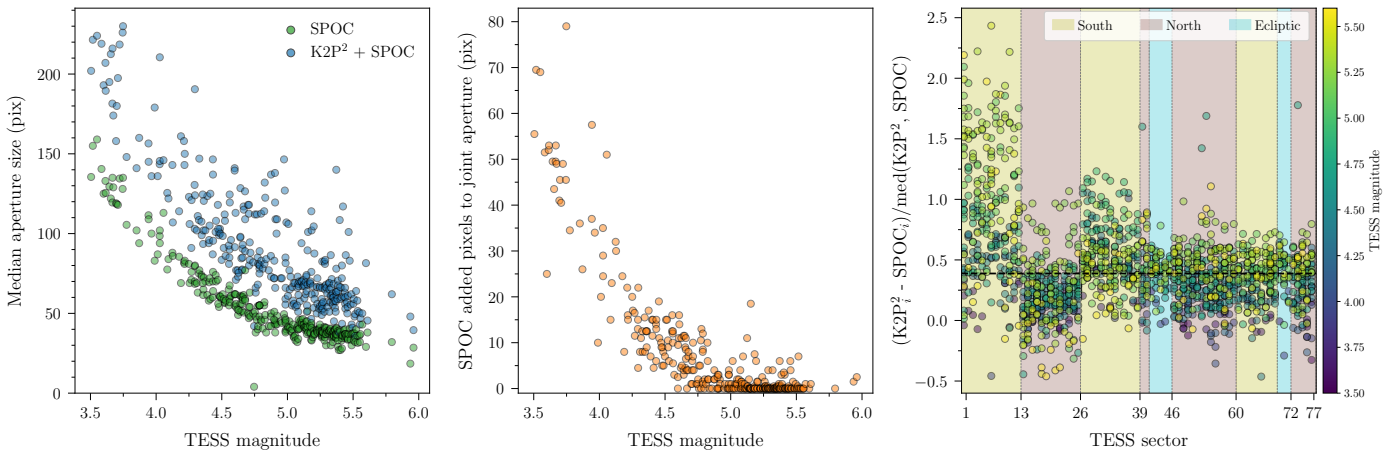


**Fig. B.1.** Comparison between SPOC and K2P$^2$ apertures. Left: Median (across sectors) aperture size in pixels against TESS magnitude for stars observed in 120-s cadence for apertures defined by SPOC and the adopted joint custom K2P$^2$ + SPOC apertures (see legend). Middle: Number of pixels contributed to the custom apertures by SPOC (i.e., number of pixels not contained in the K2P$^2$ aperture) as a function of TESS magnitude. Right: Difference in K2P$^2$ and SPOC aperture size relative to the median, with points colour-coded according to TESS magnitude. The dashed horizontal line provides the median level across sectors, while vertical lines indicate shifts in pointing (see legend), typically coinciding with different sectors.

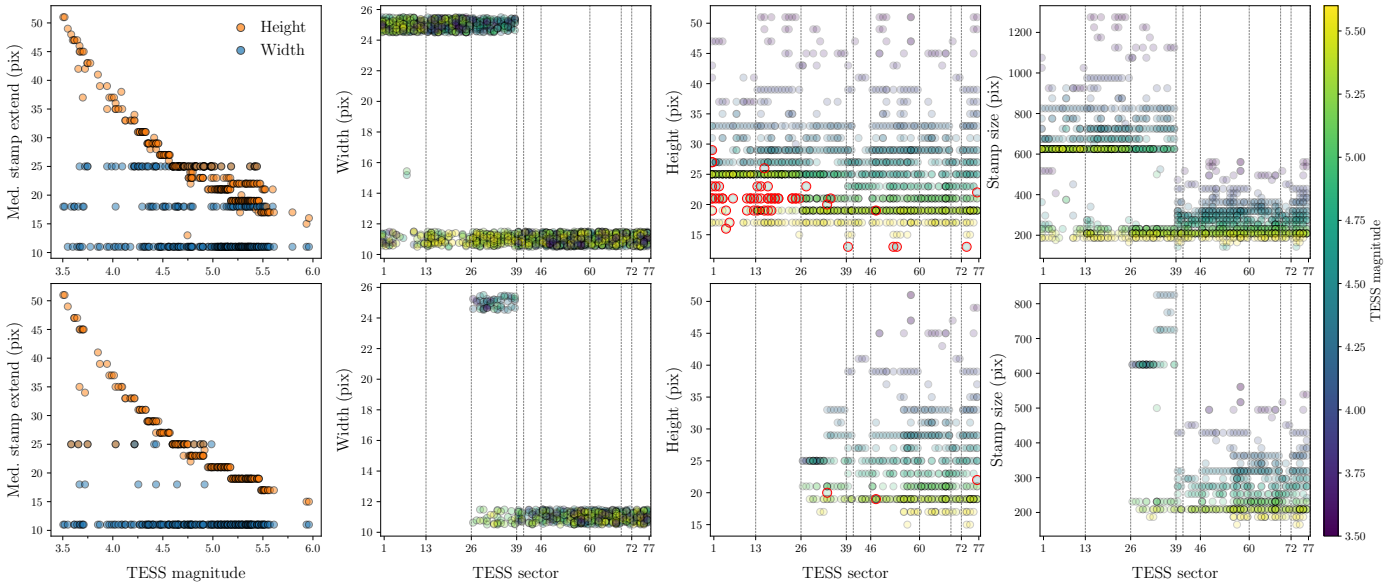


**Fig. B.2.** Properties of TESS pixel stamps for 120-s (top row) and 20-s (bottom row) cadence observations. First column: Median pixel stamp width and height across sectors for individual stars as a function of their TESS magnitude. Second (third) column: Stamp width (height) as a function of sector, coloured by TESS magnitude. Width values have been dithered by up to ±0.5 pixels to better show any dependence on magnitude. Vertical lines indicate changes in pointings (see Fig. B.1, right panel). For the heights, red markers indicate stars that are found to have a pixel stamp height that is smaller than 2 or more fainter stars, i.e., breaking with the general monotonic increase in stamp height with decreasing TESS magnitude seen on the first column. Fourth column: Total stamp size as a function of sector, colour-coded according to TESS magnitude.

For both parameters, especially $T_{\rm eff}$, we see a tendency for the underestimation to increase with the stellar brightness.

We also compared the offset in $\nu_{\rm max}$ for the different possible sources of $T_{\rm eff}$ and $\log g$ used in ATL3. Our analysis suggests that for the brighter stars given by the TLS and K2 samples with TESS magnitudes in the approximate range 2.7 – 8.5 a significantly better agreement is obtained by preferentially adopting inputs from TIC (followed by `teff_gspphot`/`logg_gspphot` and lastly `teff_gspspec`/`logg_gspspec`) – this order of preferred inputs reduced the $\nu_{\rm max}$ underestimation from ∼16 – 17% to ∼6 – 8% in median. However, for the fainter *Kepler* sample, typically with TESS magnitudes >8, the current order adopted by the ATL3 does provide the smallest $\nu_{\rm max}$ underestimation at ∼9% in median.

## Appendix D: Notes on binarity for individual stars

In addition to the stars listed in Table 5 we identified 8 stars ($\theta$ UMa, $\eta$ Cas, $\lambda$ Ser, HD 5015, 14 Boo, $\upsilon$ And, HD 46588, and $\beta$ CVn) that are labeled as spectroscopic binaries on `SimBad` from appearing in the Seventh Catalogue of Spectroscopic Binary Orbits (SBC7; Batten et al. 1978). In all cases, the discovery reference in SBC7 is to Abt & Levy (1976) where the stars are given as new (first orbit) binary detections. However, nearly all new detections in Abt & Levy (1976) were effectively refuted

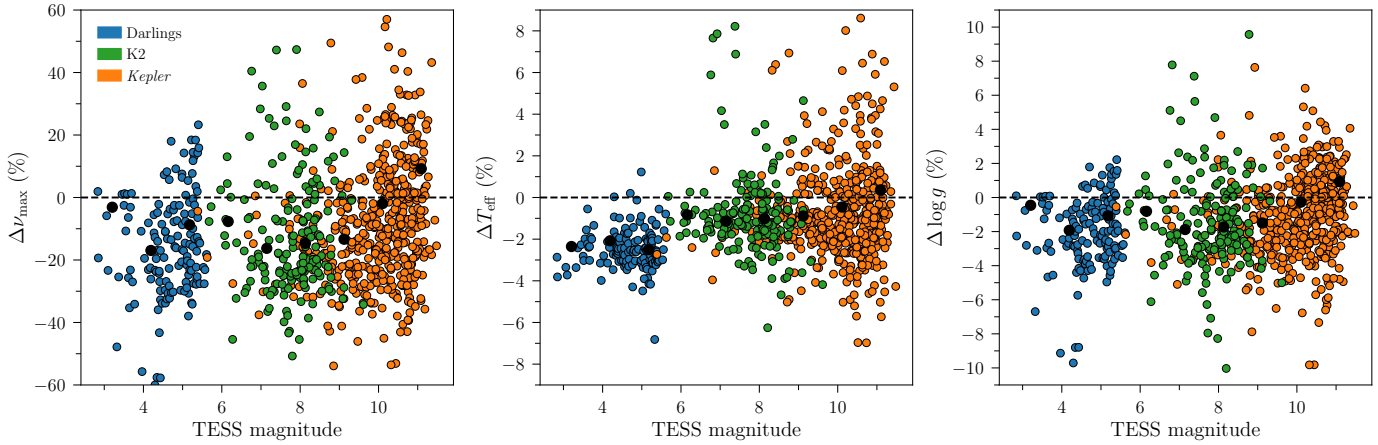


**Fig. C.1.** Comparison between ATL3 input/output and measured values for the TLS and literature values for the K2 (Lund et al. 2016, 2024) and *Kepler* (Lund et al. 2017; Mathur et al. 2022; Serenelli et al. 2017) samples. Left: relative difference (measured-predicted) between measured and predicted values of $\nu_{\rm max}$ from ATL3 with its standard priority of inputs on $T_{\rm eff}$ and $\log g$ (primarily from Gaia DR3's `gspphot`) against TESS magnitude. Middle (Right): relative difference on $T_{\rm eff}$ ($\log g$) for the three samples. For the K2 and *Kepler* samples, the measured values are obtained from the literature and adopted from Casagrande et al. (2011) for the TLS. The black markers indicate median binned values of the combined samples.

by Morbey & Griffin (1987) (and acknowledged by Abt (1987)), including all the above cases identified in our sample.

Below, we provide notes on the binarity of individual stars in our sample.

104 Tau (HIP 23835/m Tau) has been intensely studied for binarity and is included in ORB6 with reference to Eggen (1956) who finds two possible period solutions of 1.19 yr and 2.38 yr for the system. However, as discussed in Tokovinin (2012) (see also Heintz & Borgman 1984) the system has remained unresolved in many speckle interferometric studies and found, e.g., by Nidever et al. (2002) to be RV stable over a baseline ruling out the previously published period(s).

$\upsilon$ And (HIP 7513; Titawin) appears in WDS and is listed in Tokovinin (2014) (see also Lowrance et al. 2002; Raghavan et al. 2010) as a multiple hierarchical system with a wide common proper motion companion (WDS component D) in a > 16.000 yr orbit. $\upsilon$ And is the host of at least three confirmed exoplanets (Butler et al. 1997, 1999).

$\rho$ CrB (HIP 78459) is listed in ORB6 with reference to Gatewood et al. (2001) who argued, based on an analysis of Hipparcos and their astrometric data, that the first claimed planetary companion by Noyes et al. (1997) at a period of 39.6 days must instead be a stellar-mass object. However, the significance of this claim was questioned by Zucker & Mazeh (2001) and later refuted by Bender et al. (2005), who was unable to detect the alleged M dwarf companion from high-resolution infrared spectroscopy. Later RV follow-up studies (of which there are many) have currently identified four exoplanets (e.g., Brewer et al. 2023).

$\kappa$ For (HIP 11072) is a triple star system consisting of a tight binary (radio emitting) M-dwarf pair in a 3.7 day orbit, which orbits the main star with a period of 26.54 ± 0.05 years (Fekel et al. 2018; Tokovinin 2013, and references therein). It is listed on `SimBad` as being part of the young moving group IC 2391 (Nakajima & Morino 2012), but according to Tokovinin (2013), the calculation of the kinematic parameters leading to this conclusion were biased in that they overlooked the companion.

$\sigma$ Cet (HIP 11783) is given by McLaughlin (1947) and McLaughlin (1962) as a triple spectroscopic binary, consisting of an A-star pair in a 3.76 day orbit ($K_1 = K_2 = 110$ km/s), which orbits the main G-type star at a period of 3.3 yr. We note that the above references are short notes with limited information, and no later or follow-up studies have been identified.

$\iota$ Vir (HIP 69701) appears to be part of a hierarchical quadruple system, consisting of two binary pairs in orbit around a common centre of mass. $\iota$ Vir (WDS C component) is an astrometric binary with a low-mass companion in an orbit with a preliminary period of ~55 yr (Gontcharov & Kiyaeva 2010). The binary system HIP 69962 (the WDS AB component listed in ORB6 with reference to Videla et al. (2022), and also included in SB9 with a period of ~18.7 yr (Halbwachs et al. 2018b)) is a likely wide ($\rho$ = 57.1 arcmin (0.37 pc)) binary component to $\iota$ Vir (Shaya & Olling 2011). Fuhrmann & Chini (2015) discuss $\iota$ Vir as a possible blue straggler given its higher X-ray luminosity compared to the wide companion.

$\mu$ Her (HIP 86974) is a quadruple system consisting of an M-dwarf Ab component orbiting the primary G5IV star at a period of ~99 yr (Roberts et al. 2016), and a faint BC binary component consisting of an M-dwarfs pair with a period of ~43.5 yr (Prieur et al. 2014; Mann et al. 2019). We note that currently, the SONG project has observed $\mu$ Her for more than ten years for a detailed asteroseismic characterisation (Grundahl et al. 2017), and these observations can also greatly help to improve the Aa-Ab orbital solution and yield an independent mass constraint (Marcussen et al., in prep.).

94 Cet (HIP 14954) is a triple-star system (Wiegert et al. 2016) consisting of an M-dwarf binary pair with a period of ~1 yr (Roell et al. 2012) in a wide 2029-year-long orbit around 94 Cet

A (Roberts et al. 2011). 94 Cet is furthermore a known asteroseismic target (Deal et al. 2017) and an exoplanet host (Mayor et al. 2004) (see also Table 3).

$\lambda$ Ara (HIP 86486) is speculated by Fuhrmann et al. (2011b) to be an equal mass binary from the discrepancy between a spectroscopic $\log g$ with that of astrometry from Hipparcos. Only vague lower limits on period are provided, and $\lambda$ Ara has not been included in Table 5. We note, however, that if we use Eq. C.1 with our measured $\nu_{\rm max}$ of $1476 \pm 43\,\mu$Hz and the $T_{\rm eff}$ of $6532 \pm 80$ K from Fuhrmann et al. (2011b) we obtain $\log g = 4.15 \pm 0.01$ dex, which is fully consistent with the Hipparcos $\log g$ of 4.1 ± 0.1 dex.

## References


1997, ESA Special Publication, Vol. 1200, The HIPPARCOS and TYCHO catalogues. Astrometric and photometric star catalogues derived from the ESA HIPPARCOS Space Astrometry Mission
Abt, H. A. 1987, ApJ, 317, 353
Abt, H. A. & Levy, S. G. 1976, ApJS, 30, 273
Adibekyan, V., Delgado-Mena, E., Feltzing, S., et al. 2017, Astronomische Nachrichten, 338, 442
Agati, J. L., Bonneau, D., Jorissen, A., et al. 2015, A&A, 574, A6
Ammler-von Eiff, M. & Reiners, A. 2012, A&A, 542, A116
Antoci, V., Cantiello, M., Khalack, V., et al. 2025, arXiv e-prints, arXiv:2502.11879
Appourchaux, T., Antia, H. M., Ball, W., et al. 2015, A&A, 582, A25
Appourchaux, T., Michel, E., Auvergne, M., et al. 2008, A&A, 488, 705
Arentoft, T., Kjeldsen, H., Bedding, T. R., et al. 2008, ApJ, 687, 1180
Armstrong, J. T., Mozurkewich, D., Rickard, L. J., et al. 1998, ApJ, 496, 550
Astropy Collaboration, Robitaille, T. P., Tollerud, E. J., et al. 2013, A&A, 558, A33
Baglin, A., Auvergne, M., Boisnard, L., et al. 2006, in 36th COSPAR Scientific Assembly, Vol. 36, 3749
Baglin, A., Breger, M., Chevalier, C., et al. 1973, A&A, 23, 221
Baines, E. K., Armstrong, J. T., Schmitt, H. R., et al. 2014, ApJ, 781, 90
Baines, E. K., Armstrong, J. T., Schmitt, H. R., et al. 2018, AJ, 155, 30
Baines, E. K., Clark, James H., I., Schmitt, H. R., Stone, J. M., & von Braun, K. 2023, AJ, 166, 268
Baines, E. K., McAlister, H. A., ten Brummelaar, T. A., et al. 2008, ApJ, 680, 728
Baines, E. K., Thomas Armstrong, J., Clark, J. H., et al. 2021, AJ, 162, 198
Ball, W. H., Chaplin, W. J., Nielsen, M. B., et al. 2020, MNRAS, 499, 6084
Ball, W. H., Miglio, A., Chaplin, W. J., et al. 2022, MNRAS, 516, 3709
Ballot, J., Gizon, L., Samadi, R., et al. 2011, A&A, 530, A97
Barban, C., Deheuvels, S., Baudin, F., et al. 2009, A&A, 506, 51
Barban, C., Deheuvels, S., Goupil, M. J., et al. 2013, in Journal of Physics Conference Series, Vol. 440, Journal of Physics Conference Series (IOP), 012030
Barnes, J. R., Standing, M. R., Haswell, C. A., et al. 2023, MNRAS, 524, 5196
Batten, A. H., Fletcher, J. M., & Mann, P. J. 1978, Publications of the Dominion Astrophysical Observatory Victoria, 15, 121
Batten, A. H., Lu, W., & Scarfe, C. D. 1985, JRASC, 79, 167
Bazot, M., Ireland, M. J., Huber, D., et al. 2011, A&A, 526, L4
Bedding, T. R., Butler, R. P., Carrier, F., et al. 2006, ApJ, 647, 558
Bedding, T. R., Butler, R. P., Kjeldsen, H., et al. 2001, ApJ, 549, L105
Bedding, T. R., Kjeldsen, H., Reetz, J., & Barbuy, B. 1996, Monthly Notices of the Royal Astronomical Society, 280, 1155
Behr, B. B., Cenko, A. T., Hajian, A. R., et al. 2011, AJ, 142, 6
Benbakoura, M., Gaulme, P., McKeever, J., et al. 2021, A&A, 648, A113
Bender, C., Simon, M., Prato, L., Mazeh, T., & Zucker, S. 2005, AJ, 129, 402
Benedict, G. F., McArthur, B. E., Bean, J. L., et al. 2010, AJ, 139, 1844
Bergeron, P., Leggett, S. K., & Ruiz, M. T. 2001, ApJS, 133, 413
Bernacca, P. L. & Perinotto, M. 1970, Contributi dell'Osservatorio Astrofisica dell'Universita di Padova in Asiago, 239, 1
Bertiau, F. C. 1957, ApJ, 125, 696
Bigot, L., Mourard, D., Berio, P., et al. 2011, A&A, 534, L3
Bixel, A. & Apai, D. 2020, ApJ, 896, 131
Boden, A. F., Koresko, C. D., van Belle, G. T., et al. 1999, ApJ, 515, 356
Boettner, C., Viswanathan, A., & Dayal, P. 2024, arXiv e-prints, arXiv:2407.15917
Bonanno, A., Benatti, S., Claudi, R., et al. 2008, ApJ, 676, 1248
Bond, H. E., Bergeron, P., & Bédard, A. 2017, ApJ, 848, 16
Borisov, S. B., Chilingarian, I. V., Rubtsov, E. V., et al. 2023, ApJS, 266, 11
Borsa, F., Scandariato, G., Rainer, M., et al. 2015, A&A, 578, A64
Borucki, W. J., Koch, D., Basri, G., et al. 2010, Science, 327, 977
Bouchy, F., Bazot, M., Santos, N. C., Vauclair, S., & Sosnowska, D. 2005, A&A, 440, 609
Bouchy, F. & Carrier, F. 2001, A&A, 374, L5
Bouchy, F. & Carrier, F. 2002, A&A, 390, 205
Boumier, P., Benomar, O., Baudin, F., et al. 2014, A&A, 564, A34
Bourgés, L., Lafrasse, S., Mella, G., et al. 2014, in Astronomical Society of the Pacific Conference Series, Vol. 485, Astronomical Data Analysis Software and Systems XXIII, ed. N. Manset & P. Forshay, 223
Boyajian, T. S., McAlister, H. A., Baines, E. K., et al. 2008, ApJ, 683, 424
Boyajian, T. S., McAlister, H. A., van Belle, G., et al. 2012a, ApJ, 746, 101
Boyajian, T. S., von Braun, K., van Belle, G., et al. 2013, ApJ, 771, 40
Boyajian, T. S., von Braun, K., van Belle, G., et al. 2012b, ApJ, 757, 112
Brewer, J. M., Zhao, L. L., Fischer, D. A., et al. 2023, AJ, 166, 46
Brogaard, K., Arentoft, T., Slumstrup, D., et al. 2022, A&A, 668, A82
Brogaard, K., Hansen, C. J., Miglio, A., et al. 2018, MNRAS, 476, 3729
Brown, J., Bennum, D., Rodrigue, M., et al. 2000, in American Astronomical Society Meeting Abstracts, Vol. 197, American Astronomical Society Meeting Abstracts, 11.03
Brown, T. M., Gilliland, R. L., Noyes, R. W., & Ramsey, L. W. 1991, ApJ, 368, 599
Bruntt, H., Bedding, T. R., Quirion, P. O., et al. 2010, MNRAS, 405, 1907
Burgasser, A. J., Kirkpatrick, J. D., Cutri, R. M., et al. 2000, ApJ, 531, L57
Butler, R. P. & Marcy, G. W. 1996, ApJ, 464, L153
Butler, R. P., Marcy, G. W., Fischer, D. A., et al. 1999, ApJ, 526, 916
Butler, R. P., Marcy, G. W., Williams, E., Hauser, H., & Shirts, P. 1997, ApJ, 474, L115
Butler, R. P., Tinney, C. G., Marcy, G. W., et al. 2001, ApJ, 555, 410
Campante, T. L., Barclay, T., Swift, J. J., et al. 2015, ApJ, 799, 170
Campante, T. L., Kjeldsen, H., Li, Y., et al. 2024, A&A, 683, L16
Campante, T. L., Schofield, M., Kuszlewicz, J. S., et al. 2016, ApJ, 830, 138
Carrier, F., Bouchy, F., Kienzle, F., et al. 2001, A&A, 378, 142
Carrier, F. & Bourban, G. 2003, A&A, 406, L23
Carrier, F. & Eggenberger, P. 2006a, Mem. Soc. Astron. Italiana, 77, 326
Carrier, F. & Eggenberger, P. 2006b, A&A, 450, 695
Carrier, F., Eggenberger, P., D'Alessandro, A., & Weber, L. 2005, New A, 10, 315
Carrier, F., Kjeldsen, H., Bedding, T. R., et al. 2007, A&A, 470, 1059
Casagrande, L., Ramírez, I., Meléndez, J., Bessell, M., & Asplund, M. 2010, A&A, 512, A54
Casagrande, L., Schönrich, R., Asplund, M., et al. 2011, A&A, 530, A138
Castelaz, M. W. 1989, AJ, 97, 1184
Castro, M., Baudin, F., Benomar, O., et al. 2021, MNRAS, 505, 2151
Cayrel de Strobel, G. 1996, A&A Rev., 7, 243
Cayrel de Strobel, G., Perrin, M. N., Cayrel, R., & Lebreton, Y. 1989, A&A, 225, 369
Chaplin, W. J., Bedding, T. R., Bonanno, A., et al. 2011a, ApJ, 732, L5
Chaplin, W. J., Kjeldsen, H., Bedding, T. R., et al. 2011b, ApJ, 732, 54
Chaplin, W. J. & Miglio, A. 2013, ARA&A, 51, 353
Chelli, A., Duvert, G., Bourgès, L., et al. 2016, A&A, 589, A112
Choi, J., Dotter, A., Conroy, C., et al. 2016, ApJ, 823, 102
Chontos, A., Huber, D., Berger, T. A., et al. 2021, ApJ, 922, 229
Chontos, A., Huber, D., Sayeed, M., & Yamsiri, P. 2022, The Journal of Open Source Software, 7, 3331
Corsaro, E., Bonanno, A., Kayhan, C., et al. 2024, A&A, 683, A161
Creevey, O. L., Monteiro, M. J. P. F. G., Metcalfe, T. S., et al. 2007, ApJ, 659, 616
Cunha, M. S., Aerts, C., Christensen-Dalsgaard, J., et al. 2007, A&A Rev., 14, 217
Cutri, R. M., Skrutskie, M. F., van Dyk, S., et al. 2003, VizieR Online Data Catalog: 2MASS All-Sky Catalog of Point Sources (Cutri+ 2003), VizieR On-line Data Catalog: II/246. Originally published in: 2003yCat.2246....0C
Czesla, S., Schröter, S., Schneider, C. P., et al. 2019, PyA: Python astronomy-related packages
Datson, J., Flynn, C., & Portinari, L. 2015, A&A, 574, A124
Davies, G. R., Silva Aguirre, V., Bedding, T. R., et al. 2016, MNRAS, 456, 2183
Deal, M., Escobar, M. E., Vauclair, S., et al. 2017, A&A, 601, A127
Delrez, L., Ehrenreich, D., Alibert, Y., et al. 2021, Nature Astronomy, 5, 775
Desort, M., Lagrange, A. M., Galland, F., et al. 2008, A&A, 491, 883
Díaz, M. R., Jenkins, J. S., Tuomi, M., et al. 2018, AJ, 155, 126
Docobo, J. A., Ling, J. F., & Campo, P. P. 2012, Catalog of Orbits and Ephemerids of Visual Double Stars, version On-Line (www.usc.es/astro/catalog.htm)
Docobo, J. A., Ling, J. F., Prieto, C., et al. 2001, Acta Astron., 51, 353
Dotter, A. 2016, ApJS, 222, 8
Duquennoy, A. & Mayor, M. 1991, A&A, 248, 485
Duvert, G. 2016, VizieR Online Data Catalog: JMDC : JMMC Measured Stellar Diameters Catalogue (Duvert, 2016), VizieR On-line Data Catalog: II/345. Originally published in: JMMC center (2016)
Egeland, R. 2018, ApJ, 866, 80

Eggen, O. J. 1956, AJ, 61, 405
Eggenberger, A., Udry, S., Chauvin, G., et al. 2007, A&A, 474, 273
El-Badry, K., Rix, H.-W., & Heintz, T. M. 2021, MNRAS, 506, 2269
Endl, M., Brugamyer, E. J., Cochran, W. D., et al. 2016, ApJ, 818, 34
Epanechnikov, V. A. 1969, Theory of Probability & Its Applications, 14, 153
Eschen, Y. N. E., Bayliss, D., Wilson, T. G., et al. 2024, MNRAS, 535, 1778
Fekel, F. C., Tomkin, J., & Williamson, M. H. 2009, AJ, 137, 3900
Fekel, F. C., Williamson, M., & Pourbaix, D. 2007, AJ, 133, 2431
Fekel, F. C., Williamson, M. H., Muterspaugh, M. W., et al. 2015, AJ, 149, 63
Fekel, F. C., Willmarth, D. W., Abt, H. A., & Pourbaix, D. 2018, AJ, 156, 117
Feltzing, S. & Gonzalez, G. 2001, A&A, 367, 253
Feng, F., Butler, R. P., Vogt, S. S., et al. 2022, ApJS, 262, 21
Feng, F., Tuomi, M., & Jones, H. R. A. 2017, A&A, 605, A103
Fischer, D., Driscoll, P., Isaacson, H., et al. 2009, ApJ, 703, 1545
Fischer, D. A., Marcy, G. W., Butler, R. P., Laughlin, G., & Vogt, S. S. 2002, ApJ, 564, 1028
Fischer, D. A., Marcy, G. W., Butler, R. P., et al. 2001, ApJ, 551, 1107
Fischer, D. A., Marcy, G. W., Butler, R. P., et al. 2003, ApJ, 586, 1394
Foellmi, C. 2009, New A, 14, 674
Fontanive, C., Rice, K., Bonavita, M., et al. 2019, MNRAS, 485, 4967
Fuhrmann, K. 2008, MNRAS, 384, 173
Fuhrmann, K. & Chini, R. 2015, ApJ, 809, 107
Fuhrmann, K., Chini, R., Haas, M., et al. 2012, ApJ, 761, 159
Fuhrmann, K., Chini, R., Hoffmeister, V. H., & Stahl, O. 2011a, MNRAS, 416, 391
Fuhrmann, K., Chini, R., Hoffmeister, V. H., & Stahl, O. 2011b, MNRAS, 415, 1240
Fuhrmann, K., Chini, R., Kaderhandt, L., Chen, Z., & Lachaume, R. 2017, MNRAS, 471, 3768
Fulton, B. J., Howard, A. W., Weiss, L. M., et al. 2016, ApJ, 830, 46
Gaia Collaboration, Babusiaux, C., van Leeuwen, F., et al. 2018, A&A, 616, A10
Gaia Collaboration, Vallenari, A., Brown, A. G. A., et al. 2023, A&A, 674, A1
Galland, F., Lagrange, A. M., Udry, S., et al. 2005, A&A, 444, L21
Gandolfi, D., Barragán, O., Livingston, J. H., et al. 2018, A&A, 619, L10
García, R. A. & Ballot, J. 2019, Living Reviews in Solar Physics, 16, 4
García, R. A., Mathur, S., Salabert, D., et al. 2010, Science, 329, 1032
Gatewood, G., Han, I., & Black, D. C. 2001, ApJ, 548, L61
Gaulme, P. 2023, PLATO Science Calibration and Validation Input Catalog
Gaulme, P., McKeever, J., Jackiewicz, J., et al. 2016, ApJ, 832, 121
Geballe, T. R., Saumon, D., Leggett, S. K., et al. 2001, ApJ, 556, 373
Ginsburg, A., Sipőcz, B. M., Brasseur, C. E., et al. 2019, AJ, 157, 98
Gliese, W. & Jahreiß, H. 1991, Preliminary Version of the Third Catalogue of Nearby Stars, On: The Astronomical Data Center CD-ROM: Selected Astronomical Catalogs, Vol. I; L.E. Brotzmann, S.E. Gesser (eds.), NASA/Astronomical Data Center, Goddard Space Flight Center, Greenbelt, MD
Glindemann, A., Bauvir, B., Delplancke, F., et al. 2001, The Messenger, 104, 2
Goldin, A. & Makarov, V. V. 2006, ApJS, 166, 341
Goldin, A. & Makarov, V. V. 2007, ApJS, 173, 137
Gontcharov, G. A. & Kiyaeva, O. V. 2010, New A, 15, 324
Goupil, M. J., Catala, C., Samadi, R., et al. 2024, A&A, 683, A78
Gregory, P. C. & Fischer, D. A. 2010, MNRAS, 403, 731
Griffin, R. F. 1999, The Observatory, 119, 272
Griffin, R. F. 2001, The Observatory, 121, 162
Griffin, R. F. 2011, The Observatory, 131, 225
Grundahl, F., Fredslund Andersen, M., Christensen-Dalsgaard, J., et al. 2017, ApJ, 836, 142
Gullikson, K., Endl, M., Cochran, W. D., & MacQueen, P. J. 2015, ApJ, 815, 62
Guo, Z., Gies, D. R., Matson, R. A., et al. 2017, ApJ, 837, 114
Guzik, J. A., Houdek, G., Chaplin, W. J., et al. 2016, ApJ, 831, 17
Halbwachs, J. L., Mayor, M., & Udry, S. 2012, MNRAS, 422, 14
Halbwachs, J. L., Mayor, M., & Udry, S. 2018a, A&A, 619, A81
Halbwachs, J. L., Mayor, M., & Udry, S. 2018b, A&A, 619, A81
Halbwachs, J.-L., Pourbaix, D., Arenou, F., et al. 2023, A&A, 674, A9
Handberg, R. & Campante, T. L. 2011, A&A, 527, A56
Handberg, R. & Lund, M. N. 2014, MNRAS, 445, 2698
Hardorp, J. 1982, A&A, 105, 120
Hartkopf, W. I., Mason, B. D., & Worley, C. E. 2001a, Sixth Catalog of Orbits of Visual Binary Stars, http://www.ad.usno.navy.mil/wds/orb6/orb6.html
Hartkopf, W. I., McAlister, H. A., & Mason, B. D. 2001b, A&A, 122, 3480
Hartkopf, W. I., Tokovinin, A., & Mason, B. D. 2012, AJ, 143, 42
Harvey, J. 1985, in ESA Special Publication, Vol. 235, Future Missions in Solar, Heliospheric & Space Plasma Physics, ed. E. Rolfe & B. Battrick, 199
Hatt, E., Nielsen, M. B., Chaplin, W. J., et al. 2023, A&A, 669, A67
Hatzes, A. P., Gandolfi, D., Korth, J., et al. 2022, AJ, 163, 223
Heintz, W. D. 1974, AJ, 79, 819
Heintz, W. D. & Borgman, E. R. 1984, AJ, 89, 1068
Hekker, S., Kallinger, T., Baudin, F., et al. 2009, A&A, 506, 465
Henriksen, A. I., Antoci, V., Saio, H., et al. 2023, MNRAS, 524, 4196
Hey, D., Huber, D., Ong, J., Stello, D., & Foreman-Mackey, D. 2024, arXiv e-prints, arXiv:2403.02489
Hirsch, L. A., Rosenthal, L., Fulton, B. J., et al. 2021, AJ, 161, 134
Hoeg, E., Bässgen, G., Bastian, U., et al. 1997, A&A, 323, L57
Hoffleit, D. & Warren, W. H., J. 1995, VizieR Online Data Catalog: Bright Star Catalogue, 5th Revised Ed. (Hoffleit+, 1991), VizieR On-line Data Catalog: V/50. Originally published in: 1964BS....C.....0H; 1991bsc..book.....H
Hojjatpanah, S., Figueira, P., Santos, N. C., et al. 2019, A&A, 629, A80
Holberg, J. B., Oswalt, T. D., Sion, E. M., Barstow, M. A., & Burleigh, M. R. 2013, MNRAS, 435, 2077
Holberg, J. B., Sion, E. M., Oswalt, T., et al. 2008, AJ, 135, 1225
Holl, B., Sozzetti, A., Sahlmann, J., et al. 2023, A&A, 674, A10
Hon, M., Huber, D., Li, Y., et al. 2024, arXiv e-prints, arXiv:2407.21234
Hon, M., Kuszlewicz, J. S., Huber, D., Stello, D., & Reyes, C. 2022, AJ, 164, 135
Hourihane, A., François, P., Worley, C. C., et al. 2023, A&A, 676, A129
Howell, S. B., Sobeck, C., Haas, M., et al. 2014, PASP, 126, 398
Huber, D. 2018, in Astrophysics and Space Science Proceedings, Vol. 49, Asteroseismology and Exoplanets: Listening to the Stars and Searching for New Worlds, ed. T. L. Campante, N. C. Santos, & M. J. P. F. G. Monteiro, 119
Huber, D., Bedding, T. R., Stello, D., et al. 2011, ApJ, 743, 143
Huber, D., Ireland, M. J., Bedding, T. R., et al. 2012, ApJ, 760, 32
Huber, D., Stello, D., Bedding, T. R., et al. 2009, Communications in Asteroseismology, 160, 74
Huber, D., White, T. R., Metcalfe, T. S., et al. 2022, AJ, 163, 79
Hughes, A. M., Duchêne, G., & Matthews, B. C. 2018, ARA&A, 56, 541
Jannsen, N., De Ridder, J., Seynaeve, D., et al. 2024, A&A, 681, A18
Jenkins, J. M., Twicken, J. D., McCauliff, S., et al. 2016, in Society of Photo-Optical Instrumentation Engineers (SPIE) Conference Series, Vol. 9913, Software and Cyberinfrastructure for Astronomy IV, ed. G. Chiozzi & J. C. Guzman, 99133E
Jenkins, J. S., Díaz, M., Jones, H. R. A., et al. 2015, MNRAS, 453, 1439
Jones, H. R. A., Paul Butler, R., Tinney, C. G., et al. 2002, MNRAS, 333, 871
Jönsson, H., Holtzman, J. A., Allende Prieto, C., et al. 2020, AJ, 160, 120
Joyce, M. & Chaboyer, B. 2018, ApJ, 864, 99
Kane, S. R., Boyajian, T. S., Henry, G. W., et al. 2015, ApJ, 806, 60
Kane, S. R., Dalba, P. A., Li, Z., et al. 2019, AJ, 157, 252
Kane, S. R., Yalçınkaya, S., Osborn, H. P., et al. 2020, AJ, 160, 129
Karovicova, I., White, T. R., Nordlander, T., et al. 2022, A&A, 658, A47
Katoh, N., Itoh, Y., Toyota, E., & Sato, B. 2013, AJ, 145, 41
Kennedy, G. M., Wyatt, M. C., Sibthorpe, B., et al. 2012, MNRAS, 421, 2264
Kervella, P., Thévenin, F., Di Folco, E., & Ségransan, D. 2004, A&A, 426, 297
Kjeldsen, H., Bedding, T. R., Arentoft, T., et al. 2008, ApJ, 682, 1370
Kjeldsen, H., Bedding, T. R., Butler, R. P., et al. 2005, ApJ, 635, 1281
Kjeldsen, H., Bedding, T. R., Viskum, M., & Frandsen, S. 1995, AJ, 109, 1313
Konacki, M., Muterspaugh, M. W., Kulkarni, S. R., & Hełminiak, K. G. 2010, ApJ, 719, 1293
Korzennik, S. G., Brown, T. M., Fischer, D. A., Nisenson, P., & Noyes, R. W. 2000, ApJ, 533, L147
Krivov, A. V., Eiroa, C., Löhne, T., et al. 2013, ApJ, 772, 32
Kunkel, W. E., Liebert, J., & Boroson, T. A. 1984, PASP, 96, 891
Li, Y., Bedding, T. R., Li, T., et al. 2018, MNRAS, 476, 470
Li, Y., Huber, D., Ong, J. M. J., et al. 2025, arXiv e-prints, arXiv:2502.00971
Lightkurve Collaboration, Cardoso, J. V. d. M., Hedges, C., et al. 2018, Lightkurve: Kepler and TESS time series analysis in Python, Astrophysics Source Code Library
Ligi, R., Creevey, O., Mourard, D., et al. 2016, A&A, 586, A94
Ligi, R., Mourard, D., Lagrange, A. M., et al. 2012, A&A, 545, A5
Loutrel, N. P., Luhman, K. L., Lowrance, P. J., & Bochanski, J. J. 2011, ApJ, 739, 81
Lowrance, P. J., Kirkpatrick, J. D., & Beichman, C. A. 2002, ApJ, 572, L79
Luck, R. E. 2017, AJ, 153, 21
Lund, M. N., Basu, S., Bieryla, A., et al. 2024, A&A, 688, A13
Lund, M. N., Chaplin, W. J., Casagrande, L., et al. 2016, PASP, 128, 124204
Lund, M. N., Handberg, R., Davies, G. R., Chaplin, W. J., & Jones, C. D. 2015, ApJ, 806, 30
Lund, M. N., Knudstrup, E., Silva Aguirre, V., et al. 2019, AJ, 158, 248
Lund, M. N., Silva Aguirre, V., Davies, G. R., et al. 2017, ApJ, 835, 172
Lundkvist, M. S., Huber, D., Silva Aguirre, V., & Chaplin, W. J. 2018, arXiv e-prints, arXiv:1804.02214
Lundkvist, M. S., Kjeldsen, H., Bedding, T. R., et al. 2024, ApJ, 964, 110
Maestro, V., Che, X., Huber, D., et al. 2013, MNRAS, 434, 1321
Malla, S. P., Stello, D., Montet, B. T., et al. 2024, MNRAS, 534, 1775
Mamajek, E. & Stapelfeldt, K. 2024, arXiv e-prints, arXiv:2402.12414
Mann, A. W., Dupuy, T., Kraus, A. L., et al. 2019, ApJ, 871, 63
Marcy, G. W. & Butler, R. P. 1996, ApJ, 464, L147
Marshall, J. P., Krivov, A. V., del Burgo, C., et al. 2013, A&A, 557, A58
Martić, M., Lebrun, J. C., Schmitt, J., Appourchaux, T., & Bertaux, J. L. 2001, in ESA Special Publication, Vol. 464, SOHO 10/GONG 2000 Workshop: Helio- and Asteroseismology at the Dawn of the Millennium, ed. A. Wilson & P. L. Pallé, 431–434
Martić, M., Schmitt, J., Lebrun, J. C., et al. 1999, A&A, 351, 993

Martínez-Arnáiz, R., Maldonado, J., Montes, D., Eiroa, C., & Montesinos, B. 2010, A&A, 520, A79
Mason, B. D., Hartkopf, W. I., & Miles, K. N. 2017, AJ, 154, 200
Mason, B. D., Wycoff, G. L., Hartkopf, W. I., Douglass, G. G., & Worley, C. E. 2014, VizieR Online Data Catalog: The Washington Visual Double Star Catalog (Mason+ 2001-2014), VizieR On-line Data Catalog: B/wds. Originally published in: 2001AJ....122.3466M
Mathur, S., Bruntt, H., Catala, C., et al. 2013, A&A, 549, A12
Mathur, S., García, R. A., Breton, S., et al. 2022, A&A, 657, A31
Mathur, S., García, R. A., Bugnet, L., et al. 2019, Frontiers in Astronomy and Space Sciences, 6, 46
Mathur, S., García, R. A., Catala, C., et al. 2010a, A&A, 518, A53
Mathur, S., García, R. A., Régulo, C., et al. 2010b, A&A, 511, A46
Maxted, P. F. L., Bloemen, S., Heber, U., et al. 2014, MNRAS, 437, 1681
Mayor, M. & Queloz, D. 1995, Nature, 378, 355
Mayor, M., Udry, S., Naef, D., et al. 2004, A&A, 415, 391
Mazeh, T., Prato, L., Simon, M., et al. 2002, ApJ, 564, 1007
McCarthy, C., Butler, R. P., Tinney, C. G., et al. 2004, ApJ, 617, 575
McCook, G. P. & Sion, E. M. 2016, VizieR Online Data Catalog: Spectroscopically identified white dwarfs (McCook+, 2014), VizieR On-line Data Catalog: B/wd. Originally published in: 1999ApJS..121....1M
McLaughlin, D. B. 1947, ApJ, 105, 497
McLaughlin, D. B. 1962, AJ, 67, 117
Mennesson, B., Millan-Gabet, R., Serabyn, E., et al. 2014, ApJ, 797, 119
Metcalfe, T. S., Buzasi, D., Huber, D., et al. 2023, AJ, 166, 167
Metcalfe, T. S., Chaplin, W. J., Appourchaux, T., et al. 2012, ApJ, 748, L10
Metcalfe, T. S., Creevey, O. L., & Davies, G. R. 2015, ApJ, 811, L37
Metcalfe, T. S., Strassmeier, K. G., Ilyin, I. V., et al. 2024, ApJ, 960, L6
Metcalfe, T. S., van Saders, J. L., Basu, S., et al. 2020, ApJ, 900, 154
Metcalfe, T. S., van Saders, J. L., Basu, S., et al. 2021, ApJ, 921, 122
Michel, E., Baglin, A., Auvergne, M., et al. 2008, Science, 322, 558
Miglio, A., Chaplin, W. J., Farmer, R., et al. 2014, ApJ, 784, L3
Mirabel, I. F., Mignani, R., Rodrigues, I., et al. 2002, A&A, 395, 595
Mirouh, G. M., Reese, D. R., Lara, F. E., Ballot, J., & Rieutord, M. 2014, in IAU Symposium, Vol. 301, Precision Asteroseismology, ed. J. A. Guzik, W. J. Chaplin, G. Handler, & A. Pigulski, 455–456
Mishenina, T. V. 1996, A&AS, 119, 321
Monnier, J. D., Townsend, R. H. D., Che, X., et al. 2010, ApJ, 725, 1192
Montalto, M., Piotto, G., Marrese, P. M., et al. 2021, A&A, 653, A98
Montes, D., González-Peinado, R., Tabernero, H. M., et al. 2018, MNRAS, 479, 1332
Montesinos, B., Eiroa, C., Krivov, A. V., et al. 2016, A&A, 593, A51
Morbey, C. L. & Griffin, R. F. 1987, ApJ, 317, 343
Morel, P., Morel, C., Provost, J., & Berthomieu, G. 2000, A&A, 354, 636
Mosser, B., Bouchy, F., Catala, C., et al. 2005, A&A, 431, L13
Mosser, B., Deheuvels, S., Michel, E., et al. 2008, A&A, 488, 635
Mosser, B., Michel, E., Appourchaux, T., et al. 2009, A&A, 506, 33
Mozurkewich, D., Armstrong, J. T., Hindsley, R. B., et al. 2003, AJ, 126, 2502
Mugrauer, M. 2019, MNRAS, 490, 5088
Mugrauer, M., Neuhäuser, R., Mazeh, T., Guenther, E., & Fernández, M. 2004, Astronomische Nachrichten, 325, 718
Murdoch, K. & Hearnshaw, J. B. 1991, Ap&SS, 186, 169
Murdoch, K. & Hearnshaw, J. B. 1993, The Observatory, 113, 126
Naef, D., Mayor, M., Korzennik, S. G., et al. 2003, A&A, 410, 1051
Nakajima, T. & Morino, J.-I. 2012, AJ, 143, 2
Nari, N., Dumusque, X., Hara, N. C., et al. 2025, A&A, 693, A297
Nascimbeni, V., Piotto, G., Börner, A., et al. 2022, A&A, 658, A31
Nascimbeni, V., Piotto, G., Cabrera, J., et al. 2025, arXiv e-prints, arXiv:2501.07687
Neubauer, F. J. 1929, PASP, 41, 371
Nidever, D. L., Marcy, G. W., Butler, R. P., Fischer, D. A., & Vogt, S. S. 2002, ApJS, 141, 503
Nielsen, M. B., Ball, W. H., Standing, M. R., et al. 2020, A&A, 641, A25
Nielsen, M. B., Davies, G. R., Ball, W. H., et al. 2021, AJ, 161, 62
Nissen, P. E., Christensen-Dalsgaard, J., Mosumgaard, J. R., et al. 2020, A&A, 640, A81
Nissen, P. E. & Schuster, W. J. 2011, A&A, 530, A15
Nordgren, T. E., Germain, M. E., Benson, J. A., et al. 1999, AJ, 118, 3032
Nordgren, T. E., Sudol, J. J., & Mozurkewich, D. 2001, AJ, 122, 2707
Nordström, B., Mayor, M., Andersen, J., et al. 2004, A&A, 418, 989
North, J. R., Davis, J., Bedding, T. R., et al. 2007, MNRAS, 380, L80
Noyes, R. W., Jha, S., Korzennik, S. G., et al. 1997, ApJ, 483, L111
Odland, T. 2018, tommyod/KDEpy: Kernel Density Estimation in Python
Orlando, S., Favata, F., Micela, G., et al. 2017, A&A, 605, A19
Orosz, J. A. & Bailyn, C. D. 1997, ApJ, 477, 876
O'Toole, S., Tinney, C. G., Butler, R. P., et al. 2009, ApJ, 697, 1263
Paegert, M., Stassun, K. G., Collins, K. A., et al. 2021, arXiv e-prints, arXiv:2108.04778
Paunzen, E., Hümmerich, S., Bernhard, K., & Walczak, P. 2017, MNRAS, 468, 2017
Pearce, T. D. 2024, arXiv e-prints, arXiv:2403.11804
Pepe, F., Correia, A. C. M., Mayor, M., et al. 2007, A&A, 462, 769
Pepe, F., Lovis, C., Ségransan, D., et al. 2011, A&A, 534, A58
Perryman, M. A. C., Lindegren, L., Kovalevsky, J., et al. 1997, A&A, 323, L49
Pijpers, F. P., Teixeira, T. C., Garcia, P. J., et al. 2003, A&A, 406, L15
Pope, B. J. S., White, T. R., Farr, W. M., et al. 2019, ApJS, 245, 8
Porto de Mello, G. F., da Silva, R., da Silva, L., & de Nader, R. V. 2014, A&A, 563, A52
Pourbaix, D. 2000, A&AS, 145, 215
Pourbaix, D., Tokovinin, A. A., Batten, A. H., et al. 2004, A&A, 424, 727
Prieur, J. L., Scardia, M., Pansecchi, L., et al. 2014, Astronomische Nachrichten, 335, 817
Raghavan, D., Henry, T. J., Mason, B. D., et al. 2006, ApJ, 646, 523
Raghavan, D., McAlister, H. A., Henry, T. J., et al. 2010, ApJS, 190, 1
Rains, A. D., Ireland, M. J., White, T. R., Casagrande, L., & Karovicova, I. 2020, MNRAS, 493, 2377
Ramírez, I., Allende Prieto, C., & Lambert, D. L. 2013, ApJ, 764, 78
Ramírez, I., Meléndez, J., & Asplund, M. 2009, A&A, 508, L17
Rappaport, S., Podsiadlowski, P., Joss, P. C., Di Stefano, R., & Han, Z. 1995, MNRAS, 273, 731
Rauer, H., Aerts, C., Cabrera, J., et al. 2024, arXiv e-prints, arXiv:2406.05447
Ren, S. & Fu, Y. 2013, AJ, 145, 81
Rhee, J. H., Song, I., Zuckerman, B., & McElwain, M. 2007, ApJ, 660, 1556
Ricker, G. R., Winn, J. N., Vanderspek, R., et al. 2014, in Society of Photo-Optical Instrumentation Engineers (SPIE) Conference Series, Vol. 9143, Space Telescopes and Instrumentation 2014: Optical, Infrared, and Millimeter Wave, ed. J. Oschmann, Jacobus M., M. Clampin, G. G. Fazio, & H. A. MacEwen, 914320
Roberts, Lewis C., J., Mason, B. D., Aguilar, J., et al. 2016, AJ, 151, 169
Roberts, Lewis C., J., Turner, N. H., ten Brummelaar, T. A., Mason, B. D., & Hartkopf, W. I. 2011, AJ, 142, 175
Rodriguez, D. R. & Zuckerman, B. 2012, ApJ, 745, 147
Roell, T., Neuhäuser, R., Seifahrt, A., & Mugrauer, M. 2012, A&A, 542, A92
Rosenthal, L. J., Fulton, B. J., Hirsch, L. A., et al. 2021, ApJS, 255, 8
Samus', N. N., Kazarovets, E. V., Durlevich, O. V., Kireeva, N. N., & Pastukhova, E. N. 2017, Astronomy Reports, 61, 80
Santos, N. C., Bouchy, F., Mayor, M., et al. 2004, A&A, 426, L19
Sayeed, M., Huber, D., Chontos, A., & Li, Y. 2025, arXiv e-prints, arXiv:2503.15599
Schaefer, G. H., White, R. J., Baines, E. K., et al. 2018, ApJ, 858, 71
Schnupp, C., Bergfors, C., Brandner, W., et al. 2010, A&A, 516, A21
Schofield, M., Chaplin, W. J., Huber, D., et al. 2019, ApJS, 241, 12
Schröder, C., Reiners, A., & Schmitt, J. H. M. M. 2009, A&A, 493, 1099
Schultz, A., Lisse, C., Brown, J., et al. n.d., unpublished manuscript. Available at: https://www.researchgate.net/publication/237119578_Discovery_of_Three_Faint_Brown_Dwarfs_with_HSTNICMOS
Serenelli, A., Johnson, J., Huber, D., et al. 2017, ApJS, 233, 23
Serenelli, A., Weiss, A., Aerts, C., et al. 2021, A&A Rev., 29, 4
Shaya, E. J. & Olling, R. P. 2011, ApJS, 192, 2
Skuljan, J., Ramm, D. J., & Hearnshaw, J. B. 2004, MNRAS, 352, 975
Smallwood, J. L., Franchini, A., Chen, C., et al. 2020, MNRAS, 494, 487
Soderblom, D. R. & King, J. R. 1998, in Solar Analogs: Characteristics and Optimum Candidates., ed. J. C. Hall, 41
Soubiran, C., Brouillet, N., & Casamiquela, L. 2022, A&A, 663, A4
Spencer Jones, H. 1928, Annals of the Cape Observatory, 10, 8
Stassun, K. G., Oelkers, R. J., Paegert, M., et al. 2019, AJ, 158, 138
Stello, D., Chaplin, W. J., Basu, S., Elsworth, Y., & Bedding, T. R. 2009, MNRAS, 400, L80
Strassmeier, K. G., Weber, M., Gruner, D., et al. 2023, A&A, 671, A7
Takeda, Y., Sato, B., Kambe, E., et al. 2005, PASJ, 57, 13
Tautvaišienė, G., Mikolaitis, Š., Drazdauskas, A., et al. 2020, ApJS, 248, 19
Tautvaišienė, G., Mikolaitis, Š., Drazdauskas, A., et al. 2022, ApJS, 259, 45
Teixeira, T. C., Kjeldsen, H., Bedding, T. R., et al. 2009, A&A, 494, 237
ten Brummelaar, T. A., McAlister, H. A., Ridgway, S. T., et al. 2005, ApJ, 628, 453
Thévenin, F., Kervella, P., Pichon, B., et al. 2005, A&A, 436, 253
Thomsen, J. S., Brogaard, K., Arentoft, T., et al. 2022, MNRAS, 517, 4187
Tinney, C. G., Butler, R. P., Jones, H. R. A., et al. 2011, ApJ, 727, 103
Tinney, C. G., Butler, R. P., Marcy, G. W., et al. 2002, ApJ, 571, 528
Tokovinin, A. 2012, AJ, 144, 56
Tokovinin, A. 2013, AJ, 145, 76
Tokovinin, A. 2014, AJ, 147, 86
Trilling, D. E., Bryden, G., Beichman, C. A., et al. 2008, ApJ, 674, 1086
Tuchow, N. W., Stark, C. C., & Mamajek, E. 2024, AJ, 167, 139
Udry, S., Dumusque, X., Lovis, C., et al. 2019, A&A, 622, A37
Uytterhoeven, K., Mathias, P., Baglin, A., et al. 2011, arXiv e-prints, arXiv:1111.1840
van Biesbroeck, G. 1961, AJ, 66, 528
van der Walt, S., Schönberger, J. L., Nunez-Iglesias, J., et al. 2014, PeerJ, 2, e453
Van Eylen, V., Lund, M. N., Silva Aguirre, V., et al. 2014, ApJ, 782, 14

van Leeuwen, F., Evans, D. W., Grenon, M., et al. 1997, A&A, 323, L61
Vanderspek, R., Doty, J. P., Fausnaugh, M., et al. 2018, TESS Instrument Handbook, version 0.1
Vauclair, S., Laymand, M., Bouchy, F., et al. 2008, A&A, 482, L5
Venner, A., Vanderburg, A., & Pearce, L. A. 2021, AJ, 162, 12
Verner, G. A., Elsworth, Y., Chaplin, W. J., et al. 2011, MNRAS, 415, 3539
Verner, G. A. & Roxburgh, I. W. 2011, arXiv e-prints, arXiv:1104.0631
Viani, L. S., Basu, S., Corsaro, E., Ball, W. H., & Chaplin, W. J. 2019, ApJ, 879, 33
Videla, M., Mendez, R. A., Clavería, R. M., Silva, J. F., & Orchard, M. E. 2022, AJ, 163, 220
Vinícius, Z., Barentsen, G., Hedges, C., Gully-Santiago, M., & Cody, A. M. 2018, KeplerGO/lightkurve
Vogt, S. S., Butler, R. P., Marcy, G. W., et al. 2005, ApJ, 632, 638
Vogt, S. S., Wittenmyer, R. A., Butler, R. P., et al. 2010, ApJ, 708, 1366
von Braun, K., Boyajian, T. S., van Belle, G. T., et al. 2014, MNRAS, 438, 2413
Vrard, M., Mourard, D., Creevey, O., et al. 2024, in 8th TESS/15th Kepler Asteroseismic Science Consortium Workshop, 12
Šubjak, J., Lodieu, N., Kabáth, P., et al. 2023, A&A, 671, A10
Wenger, M., Ochsenbein, F., Egret, D., et al. 2000, A&AS, 143, 9
Wesemael, F., Greenstein, J. L., Liebert, J., et al. 1993, PASP, 105, 761
White, T. R., Benomar, O., Silva Aguirre, V., et al. 2017, A&A, 601, A82
White, T. R., Huber, D., Maestro, V., et al. 2013, MNRAS, 433, 1262
White, T. R., Huber, D., Mann, A. W., et al. 2018, MNRAS, 477, 4403
Wiegert, J., Faramaz, V., & Cruz-Saenz de Miera, F. 2016, MNRAS, 462, 1735
Wilson, J. C., Kirkpatrick, J. D., Gizis, J. E., et al. 2001, AJ, 122, 1989
Wittenmyer, R. A., Clark, J. T., Zhao, J., et al. 2019, MNRAS, 484, 5859
Wittenmyer, R. A., Horner, J., Tuomi, M., et al. 2012, ApJ, 753, 169
Wyatt, M. C., Kennedy, G., Sibthorpe, B., et al. 2012, MNRAS, 424, 1206
Xing, K., Zong, W., Silvotti, R., et al. 2024, ApJS, 271, 57
Zechmeister, M., Kürster, M., Endl, M., et al. 2013, A&A, 552, A78
Zhao, M., Monnier, J. D., Che, X., et al. 2011, PASP, 123, 964
Zhou, J., Bi, S., Yu, J., et al. 2024, ApJS, 271, 17
Zucker, S. & Mazeh, T. 2001, arXiv e-prints, arXiv:0104098

**Table 1.** TLS global asteroseismic parameters

| Name | TIC | HIP | $V$ (mag) | Constellation | RA (deg) | DEC (deg) | $\nu_{\max}$ ($\mu$Hz) | $\Delta\nu$ ($\mu$Hz) | HWO (tier) | Seis. ref. | Also in Table |
|---|---|---|---|---|---|---|---|---|---|---|---|
| $\eta$ Boo | 367758676 | 67927 | 2.68 | Boötes | 208.7 | 18.4 | 697.9 ± 17.8 | 39.2 ± 0.9 | - | 1, 2, 3 | 4, 5 |
| $\zeta$ Her | 43255143 | 81693 | 2.81 | Hercules | 250.3 | 31.6 | 718.5 ± 24.4 | 40.0 ± 1.0 | - | 4 | 2, 4, 5 |
| $\beta$ Hyi | 267211065 | 2021 | 2.82 | Hydrus | 6.4 | −77.3 | 1038.1 ± 14.9 | 56.9 ± 0.4 | C | 5, 6, 2, 7 | 4 |
| $\theta$ UMa | 150226696 | 46853 | 3.17 | Ursa Major | 143.2 | 51.7 | 779.3 ± 17.8 | 44.6 ± 0.5 | - | - | 4 |
| $\xi$ Gem | 372480991 | 32362 | 3.35 | Gemini | 101.3 | 12.9 | 2871.0 ± 111.3 | 126.2 ± 2.5 | - | - | 4 |
| $\mu^1$ Her | 460067868 | 86974 | 3.42 | Hercules | 266.6 | 27.7 | 1192.5 ± 17.5 | 63.8 ± 0.2 | - | 8, 9, 2 | 2, 4, 5 |
| $\eta$ Cas | 445258206 | 3821 | 3.46 | Cassiopeia | 12.3 | 57.8 | 2840.0 ± 80.7 | 128.0 ± 0.4 | A | 4 | 4, 5 |
| $\delta$ Eri | 38511251 | 17378 | 3.52 | Eridanus | 55.8 | −9.8 | 677.6 ± 8.3 | 41.5 ± 0.8 | A | 10, 2, 7, 3 | 4 |
| $\delta$ Pav | 409891396 | 99240 | 3.55 | Pavo | 302.2 | −66.2 | 2269.8 ± 64.4 | 107.9 ± 0.2 | A | 11 | 4 |
| $\chi$ Dra | 341873045 | 89937 | 3.55 | Draco | 275.3 | 72.7 | 2314.7 ± 24.4 | 108.4 ± 0.1 | - | - | 2, 5 |
| $\beta$ Vir | 366661076 | 57757 | 3.59 | Virgo | 177.7 | 1.8 | 1446.3 ± 75.9 | 71.9 ± 0.5 | C | 12 | 4 |
| $\gamma$ Lep | 93280676 | 27072 | 3.59 | Lepus | 86.1 | −22.4 | 2257.5 ± 50.9 | 102.0 ± 0.9 | A | - | 2, 4 |
| $\beta$ Aql | 375621179 | 98036 | 3.71 | Aquila | 298.8 | 6.4 | 414.7 ± 6.8 | 26.8 ± 0.6 | - | 13, 7, 3 | 4 |
| $\iota$ Peg | 357336603 | 109176 | 3.77 | Pegasus | 331.8 | 25.3 | 2101.8 ± 126.6 | 100.7 ± 1.4 | - | - | 4, 5 |
| $\alpha$ For | 88523071 | 14879 | 3.8 | Fornax | 48.0 | −29.0 | 1128.3 ± 47.3 | 61.0 ± 0.9 | C | 13 | 5 |
| $\gamma$ Ser | 377415363 | 78072 | 3.85 | Serpens | 239.1 | 15.7 | 1744.6 ± 38.2 | 84.9 ± 0.9 | A | 13 | 4 |
| $\theta$ Dra | 161825882 | 78527 | 4.01 | Draco | 240.5 | 58.6 | 723.0 ± 15.8 | 40.2 ± 0.3 | - | - | 2, 5 |
| $\theta$ Boo | 441709021 | 70497 | 4.04 | Boötes | 216.3 | 51.9 | 1354.0 ± 108.4 | 68.9 ± 1.5 | C | - | 4 |
| $\iota$ Per | 116988032 | 14632 | 4.05 | Perseus | 47.3 | 49.6 | 1855.3 ± 33.9 | 89.7 ± 0.4 | A | - | 4 |
| $\alpha$ Cha | 287532010 | 40702 | 4.05 | Chamaleon | 124.6 | −76.9 | 1005.8 ± 65.4 | 54.8 ± 0.5 | - | - | - |
| $\iota$ Vir | 6029884 | 69701 | 4.07 | Virgo | 214.0 | −6.0 | 644.8 ± 24.0 | 36.2 ± 0.8 | - | - | 4, 5 |
| $\upsilon$ And | 189576919 | 7513 | 4.1 | Andromeda | 24.2 | 41.4 | 1528.0 ± 50.6 | 76.2 ± 0.6 | C | - | 3, 4 |
| $\theta$ Per | 302158903 | 12777 | 4.1 | Perseus | 41.0 | 49.2 | 2314.2 ± 166.2 | 104.1 ± 1.3 | A | - | 4, 5 |
| $\iota$ Psc | 419919445 | 116771 | 4.13 | Pisces | 355.0 | 5.6 | 1416.4 ± 53.6 | 75.3 ± 0.6 | C | - | 4 |
| $\psi$ Cap | 269995013 | 102485 | 4.13 | Capricornus | 311.5 | −25.3 | 1849.1 ± 34.5 | 89.1 ± 2.3 | C | - | - |
| 110 Her | 282038438 | 92043 | 4.19 | Hercules | 281.4 | 20.5 | 1061.9 ± 28.0 | 56.2 ± 1.6 | - | - | 4 |
| $\xi$ Peg | 60716322 | 112447 | 4.2 | Pegasus | 341.7 | 12.2 | 986.8 ± 16.7 | 57.3 ± 0.5 | C | 7 | 4 |
| $\gamma$ Pav | 265488188 | 105858 | 4.21 | Pavo | 321.6 | −65.4 | 2635.8 ± 60.9 | 119.6 ± 0.6 | A | 14, 15, 2 | - |
| $\zeta$ Tuc | 425935521 | 1599 | 4.23 | Tucana | 5.0 | −64.9 | 2744.6 ± 148.6 | 125.6 ± 0.5 | B | 15, 2 | - |
| $\beta$ CVn | 458445966 | 61317 | 4.24 | Canes Venatici | 188.4 | 41.4 | 2385.4 ± 136.0 | 117.4 ± 1.1 | A | - | 4 |
| 82 Eri | 301051051 | 15510 | 4.26 | Eridanus | 50.0 | −43.1 | 3180.0 ± 104.9 | 147.5 ± 1.5 | B | - | 3 |
| 10 Tau | 311092847 | 16852 | 4.29 | Taurus | 54.2 | 0.4 | 1284.1 ± 63.1 | 69.7 ± 1.2 | B | - | 4 |
| $\lambda$ Ser | 296740796 | 77257 | 4.42 | Serpens | 236.6 | 7.4 | 1856.6 ± 46.4 | 89.3 ± 0.6 | A | 16 | 3, 4 |
| o$^2$ Eri | 67772871 | 19849 | 4.43 | Eridanus | 63.8 | −7.7 | 3433.1 ± 368.6 | 131.9 ± 3.1 | A | - | 4, 5 |
| HD 60532 | 456871289 | 36795 | 4.44 | Puppis | 113.5 | −22.3 | 618.2 ± 28.0 | 33.5 ± 1.2 | - | 2, 7 | 2, 3 |
| $\theta$ Cyg | 27014182 | 96441 | 4.49 | Cygnus | 294.1 | 50.2 | 1759.1 ± 67.1 | 82.8 ± 1.2 | - | 17 | 2, 4 |
| $\mu$ Cyg | 452700589 | 107310 | 4.49 | Cygnus | 326.0 | 28.7 | 1213.9 ± 67.7 | 62.3 ± 1.8 | - | - | 5 |
| $\upsilon$ Cep | 421444084 | 102431 | 4.52 | Cepheus | 311.3 | 57.6 | 958.7 ± 22.3 | 53.6 ± 0.4 | - | 2 | 2, 5 |
| $\psi^1$ Dra A | 441804568 | 86614 | 4.57 | Draco | 265.5 | 72.1 | 1232.4 ± 19.8 | 61.8 ± 0.3 | - | - | 2, 4, 5 |
| $\tau^1$ Hya | 77549389 | 46509 | 4.59 | Hydra | 142.3 | −2.8 | 1572.0 ± 44.5 | 75.5 ± 1.4 | - | - | 5 |
| $\chi$ Her | 157364190 | 77760 | 4.6 | Hercules | 238.2 | 42.5 | 1045.6 ± 17.7 | 58.8 ± 0.7 | A | 2, 7, 3 | 2, 4 |
| $\sigma$ Dra | 259237827 | 96100 | 4.67 | Draco | 293.1 | 69.7 | 4217.9 ± 122.6 | 182.2 ± 0.5 | A | 18 | 2, 4 |
| $\lambda$ Aur | 409104974 | 24813 | 4.69 | Auriga | 79.8 | 40.1 | 2152.0 ± 54.2 | 100.6 ± 0.8 | A | - | 4 |
| $\kappa$ Ret | 262843771 | 16245 | 4.71 | Reticulum | 52.3 | −62.9 | 1552.1 ± 48.6 | 73.1 ± 1.3 | C | - | 2 |
| 61 Vir | 422478973 | 64924 | 4.74 | Virgo | 199.6 | −18.3 | 3099.8 ± 101.0 | 138.6 ± 1.3 | B | - | 3, 4 |
| B Car | 308844962 | 39903 | 4.74 | Carina | 122.3 | −61.3 | 1386.8 ± 27.0 | 71.6 ± 0.6 | - | - | 2, 5 |
| $\sigma$ Cet | 66604391 | 11783 | 4.74 | Cetus | 38.0 | −15.2 | 913.8 ± 40.1 | 50.9 ± 0.9 | - | 2 | 5 |
| $\lambda$ Ara | 96745915 | 86486 | 4.76 | Ara | 265.1 | −49.4 | 1476.1 ± 43.0 | 71.1 ± 1.7 | C | - | - |
| $\omega$ Dra | 233195546 | 86201 | 4.77 | Draco | 264.2 | 68.8 | 1999.5 ± 55.0 | 88.3 ± 2.0 | - | - | 2, 5 |
| 40 Leo | 95431211 | 50564 | 4.78 | Leo | 154.9 | 19.5 | 1405.8 ± 57.9 | 75.1 ± 2.3 | C | - | 4 |
| HD 5015 | 285544488 | 4151 | 4.8 | Cassiopeia | 13.3 | 61.1 | 1399.3 ± 52.9 | 70.8 ± 0.6 | C | - | 4 |
| $\sigma^2$ UMa | 219709102 | 45038 | 4.8 | Ursa Major | 137.6 | 67.1 | 1354.9 ± 64.6 | 72.1 ± 0.6 | C | - | 5 |
| 12 Boo | 418010485 | 69226 | 4.82 | Boötes | 212.6 | 25.1 | 694.7 ± 21.3 | 41.6 ± 1.2 | - | 19 | 5 |
| 36 UMa | 416519065 | 51459 | 4.82 | Ursa Major | 157.7 | 56.0 | 2319.5 ± 96.8 | 105.0 ± 2.1 | A | - | 4 |
| $\omega$ And | 191764184 | 6813 | 4.83 | Andromeda | 21.9 | 45.4 | 1899.2 ± 336.0 | 96.1 ± 1.8 | - | - | 5 |
| HD 114613 | 30293512 | 64408 | 4.85 | Centaurus | 198.0 | −37.8 | 875.7 ± 18.6 | 48.1 ± 0.9 | C | 2, 7 | - |
| 19 Dra | 289622310 | 82860 | 4.88 | Draco | 254.0 | 65.1 | 2313.1 ± 493.9 | 104.8 ± 3.5 | - | - | 2, 5 |
| 6 Cet | 289673491 | 910 | 4.89 | Cetus | 2.8 | −15.5 | 1369.8 ± 37.8 | 73.4 ± 0.6 | A | - | - |
| Y Vel | 447823435 | 51523 | 4.89 | Vela | 157.8 | −53.7 | 1080.5 ± 42.8 | 58.9 ± 0.4 | C | 2, 7 | - |
| HD 102365 | 454082369 | 57443 | 4.89 | Centaurus | 176.6 | −40.5 | 3148.2 ± 188.4 | 137.3 ± 1.5 | A | 2 | 3 |
| $\zeta$ TrA | 362747897 | 80686 | 4.9 | Triangulum Australe | 247.1 | −70.1 | 3215.4 ± 380.4 | 148.8 ± 1.4 | - | - | 5 |
| HD 114837 | 255854921 | 64583 | 4.9 | Centaurus | 198.6 | −59.1 | 1723.1 ± 49.8 | 84.8 ± 0.9 | C | - | - |
| 104 Tau | 27136704 | 23835 | 4.91 | Taurus | 76.9 | 18.6 | 1261.4 ± 46.5 | 69.2 ± 0.3 | C | 7 | - |
| $\epsilon$ Lib | 37018039 | 75379 | 4.92 | Libra | 231.1 | −10.3 | 775.9 ± 51.4 | 43.4 ± 1.6 | - | - | 5 |
| HD 84117 | 11310083 | 47592 | 4.93 | Hydra | 145.6 | −23.9 | 2142.6 ± 90.3 | 107.4 ± 1.8 | A | - | - |
| 17 Crt | 429149606 | 56280 | 4.93 | Hydra | 173.1 | −29.3 | 1413.4 ± 112.2 | 70.8 ± 1.4 | - | - | - |
| $\tau$ PsA | 97402436 | 109422 | 4.94 | Pisces Austrinus | 332.5 | −32.5 | 2112.0 ± 145.3 | 92.8 ± 1.8 | A | - | - |
| HD 10307 | 327507922 | 7918 | 4.96 | Andromeda | 25.4 | 42.6 | 2490.1 ± 96.0 | 115.3 ± 1.2 | - | - | 5 |
| 70 Vir | 95473936 | 65721 | 4.97 | Virgo | 202.1 | 13.8 | 940.6 ± 12.9 | 51.5 ± 1.0 | - | 2, 7, 3 | 3, 4 |
| $\nu$ Phe | 229092427 | 5862 | 4.97 | Phoenix | 18.8 | −45.5 | 2309.1 ± 107.3 | 106.9 ± 1.2 | B | 2 | - |
| 36 Dra | 233121747 | 89348 | 4.99 | Draco | 273.5 | 64.4 | 1312.0 ± 16.9 | 69.6 ± 0.2 | C | - | 2, 4 |
| $\nu^1$ Lup | 136915882 | 75206 | 4.99 | Lupus | 230.5 | −47.9 | 749.2 ± 25.2 | 41.0 ± 1.2 | - | 2 | - |
| 17 Cyg | 58445695 | 97295 | 5.0 | Cygnus | 296.6 | 33.7 | 1484.4 ± 36.1 | 78.6 ± 1.5 | C | - | 2, 5 |
| 35 Dra | 441813918 | 87234 | 5.02 | Draco | 267.4 | 77.0 | 705.3 ± 7.0 | 42.1 ± 0.1 | - | 2, 7 | 2 |
| 47 UMa | 21535479 | 53721 | 5.03 | Ursa Major | 164.9 | 40.4 | 2327.9 ± 55.1 | 106.1 ± 0.8 | A | - | 3, 4 |
| 53 Vir | 308210818 | 64407 | 5.04 | Virgo | 198.0 | −16.2 | 796.5 ± 13.3 | 43.7 ± 0.6 | - | - | - |
| HD 62644 | 123699670 | 37606 | 5.04 | Puppis | 115.7 | −45.2 | 708.4 ± 6.7 | 41.1 ± 0.3 | - | 2, 7 | 2, 5 |
| 74 Ori | 437886584 | 29800 | 5.04 | Orion | 94.1 | 12.3 | 2115.3 ± 156.2 | 99.6 ± 1.6 | B | - | - |
| 16 Cep | 366412503 | 108535 | 5.04 | Cepheus | 329.8 | 73.2 | 643.4 ± 11.2 | 39.4 ± 0.6 | - | - | 2, 4 |
| 99 Her | 22516402 | 88745 | 5.05 | Hercules | 271.8 | 30.6 | 1950.7 ± 41.0 | 96.2 ± 0.6 | - | - | 2, 5 |
| $\kappa$ Del | 282254078 | 101916 | 5.07 | Delphinus | 309.8 | 10.1 | 622.5 ± 9.8 | 36.2 ± 0.7 | - | - | 5 |
| 94 Cet | 49845357 | 14954 | 5.07 | Cetus | 48.2 | −1.2 | 1267.2 ± 99.6 | 69.5 ± 1.6 | - | 20 | 3, 4, 5 |
| $\alpha$ Men | 141810080 | 29271 | 5.08 | Mensa | 92.6 | −74.8 | 3237.0 ± 77.1 | 140.4 ± 0.1 | C | 21, 2 | 2 |
| HD 33564 | 142103211 | 25110 | 5.08 | Camelopardalis | 80.6 | 79.2 | 1736.0 ± 61.1 | 87.4 ± 1.4 | C | - | 3, 4 |
| 15 LMi | 23969522 | 48113 | 5.08 | Ursa Major | 147.1 | 46.0 | 1402.7 ± 90.1 | 74.9 ± 0.5 | B | - | - |
| $\phi^2$ Pav | 351604689 | 101983 | 5.11 | Pavo | 310.0 | −60.5 | 919.8 ± 17.0 | 51.3 ± 0.7 | - | 2, 7 | - |
| 68 Eri | 248411315 | 23941 | 5.11 | Eridanus | 77.2 | −4.5 | 1222.5 ± 28.5 | 65.9 ± 1.7 | - | - | - |
| o Aql | 408842743 | 97675 | 5.12 | Aquila | 297.8 | 10.4 | 1831.8 ± 304.5 | 89.2 ± 1.7 | B | 3 | - |
| $\mu$ Ara | 362661163 | 86796 | 5.12 | Ara | 266.0 | −51.8 | 1936.8 ± 75.6 | 89.9 ± 0.8 | B | 22, 2, 7 | 3 |
| $\chi$ Cnc | 302188141 | 40843 | 5.13 | Cancer | 125.0 | 27.2 | 1991.8 ± 78.8 | 96.4 ± 0.7 | B | - | 4 |
| X Pup | 170225363 | 32765 | 5.14 | Puppis | 102.5 | −46.6 | 1279.7 ± 66.0 | 69.0 ± 0.9 | - | 2 | 2 |
| HD 136064 | 232563914 | 74605 | 5.15 | Ursa Minor | 228.7 | 67.3 | 1081.9 ± 23.8 | 59.1 ± 0.2 | - | - | 2 |
| $\rho$ And | 288294358 | 1686 | 5.16 | Andromeda | 5.3 | 38.0 | 390.3 ± 11.4 | 27.2 ± 0.8 | - | - | 4 |
| $\sigma$ Peg | 318705095 | 112935 | 5.16 | Pegasus | 343.1 | 9.8 | 1039.8 ± 71.5 | 58.1 ± 0.9 | - | - | - |
| 31 Aql | 359981217 | 95447 | 5.17 | Aquila | 291.2 | 11.9 | 1791.8 ± 225.2 | 88.7 ± 0.8 | C | - | 4 |
| 16 UMa | 86177169 | 45333 | 5.18 | Ursa Major | 138.6 | 61.4 | 1514.7 ± 29.8 | 77.6 ± 0.6 | - | - | 5 |
| $\kappa$ For | 279342892 | 11072 | 5.19 | Fornax | 35.6 | −23.8 | 1160.4 ± 38.1 | 63.2 ± 0.4 | - | 2 | 5 |

**Table 1.** Continued.

| Name | TIC | HIP | $V$ | Constellation | RA | DEC | $\nu_{\rm max}$ | $\Delta\nu$ | HWO | Seis. ref. | Also in Table |
|---|---|---|---|---|---|---|---|---|---|---|---|
| HD 176051 | 20601206 | 93017 | 5.2 | Lyra | 284.3 | 32.9 | 2902.2 ± 132.1 | 127.4 ± 1.7 | - | - | 2, 5 |
| 94 Aqr | 214664574 | 115126 | 5.2 | Aquarius | 349.8 | −13.5 | 886.9 ± 12.0 | 48.4 ± 0.6 | - | 23, 2, 7, 3 | 5 |
| HD 94388 | 52160996 | 53252 | 5.23 | Hydra | 163.4 | −20.1 | 973.0 ± 29.0 | 57.4 ± 1.6 | - | - | - |
| $\eta$ Ari | 306484795 | 10306 | 5.23 | Aries | 33.2 | 21.2 | 1098.7 ± 37.8 | 56.6 ± 0.9 | - | - | - |
| 26 Dra | 219777482 | 86036 | 5.23 | Draco | 263.7 | 61.9 | 3059.0 ± 176.8 | 132.9 ± 0.9 | - | - | 2, 5 |
| $\theta$ Scl | 70847587 | 950 | 5.24 | Sculptor | 2.9 | −35.1 | 1871.3 ± 138.5 | 91.2 ± 2.0 | C | - | - |
| HD 210855 | 329759640 | 109572 | 5.24 | Cepheus | 333.0 | 56.8 | 711.4 ± 13.2 | 41.2 ± 0.5 | - | - | 2 |
| $\nu^2$ Col | 32500750 | 26460 | 5.28 | Columba | 84.4 | −28.7 | 691.3 ± 43.5 | 38.9 ± 1.3 | - | - | 2 |
| $\nu$ Ind | 317019578 | 110618 | 5.28 | Indus | 336.2 | −72.3 | 343.7 ± 4.2 | 25.6 ± 0.4 | - | 24, 25, 2, 7 | - |
| $\mu^2$ Cnc | 446006789 | 39780 | 5.3 | Cancer | 121.9 | 21.6 | 1075.5 ± 26.7 | 59.7 ± 0.6 | - | - | - |
| HD 212330 | 259291108 | 110649 | 5.31 | Tucana | 336.2 | −57.8 | 1181.2 ± 20.6 | 65.3 ± 0.3 | B | 2 | - |
| 22 Lyn | 328324648 | 36439 | 5.35 | Lynx | 112.5 | 49.7 | 2167.1 ± 147.6 | 102.8 ± 1.6 | B | - | - |
| 171 Pup | 149672905 | 37853 | 5.36 | Puppis | 116.4 | −34.2 | 2107.7 ± 59.8 | 104.4 ± 0.9 | - | - | 2 |
| HD 81809 | 46802551 | 46404 | 5.38 | Hydra | 141.9 | −6.1 | 691.0 ± 19.8 | 38.3 ± 1.5 | - | 2, 3 | 5 |
| 27 Cyg | 41195655 | 99031 | 5.38 | Cygnus | 301.6 | 36.0 | 702.8 ± 44.4 | 40.6 ± 1.2 | - | - | 2 |
| $\rho$ Tuc | 234498449 | 3330 | 5.38 | Tucana | 10.6 | −65.5 | 724.1 ± 28.7 | 39.2 ± 0.9 | - | - | 5 |
| 72 Her | 9728611 | 84862 | 5.38 | Hercules | 260.2 | 32.5 | 2241.4 ± 85.1 | 106.2 ± 1.0 | C | - | 2, 4 |
| $\rho$ CrB | 458494003 | 78459 | 5.39 | Corona Borealis | 240.3 | 33.3 | 1664.7 ± 99.9 | 87.4 ± 1.7 | B | 26 | 3, 4 |
| CD29 12513 | 392326236 | 80399 | 5.4 | Scorpius | 246.2 | −29.7 | 1051.4 ± 79.2 | 58.1 ± 1.6 | - | - | - |
| HD 46588 | 141523112 | 32439 | 5.44 | Camelopardalis | 101.6 | 79.6 | 2416.6 ± 128.7 | 113.9 ± 1.5 | B | - | 3 |
| $\zeta$ Pic | 219420836 | 24829 | 5.44 | Pictor | 79.8 | −50.6 | 853.0 ± 42.4 | 49.5 ± 0.4 | - | 2 | 2 |
| 51 Peg | 139298196 | 113357 | 5.45 | Pegasus | 344.4 | 20.8 | 2485.0 ± 97.8 | 114.9 ± 1.1 | - | 27 | 3, 4 |
| HD 36553 | 354552931 | 25768 | 5.46 | Pictor | 82.5 | −47.1 | 544.7 ± 16.1 | 33.7 ± 0.2 | - | 2, 7 | 2 |
| HD 100203 | 100011351 | 56290 | 5.46 | Ursa Major | 173.1 | 61.1 | 1532.7 ± 38.3 | 74.0 ± 2.1 | - | - | 5 |
| $\iota$ Pav | 303704858 | 89042 | 5.47 | Pavo | 272.6 | −62.0 | 2056.7 ± 153.0 | 101.3 ± 1.5 | B | - | - |
| $\iota$ Crt | 40535161 | 56802 | 5.48 | Crater | 174.7 | −13.2 | 1282.8 ± 51.3 | 67.4 ± 1.8 | - | - | - |
| HD 175225 | 48194330 | 92549 | 5.51 | Draco | 282.9 | 53.0 | 752.1 ± 11.3 | 43.5 ± 0.3 | - | - | 2 |
| $\iota$ Hyi | 431380163 | 15201 | 5.51 | Hydrus | 49.0 | −77.4 | 1685.4 ± 75.6 | 79.7 ± 1.7 | - | - | - |
| 15 Peg | 326202925 | 107975 | 5.52 | Pegasus | 328.1 | 28.8 | 1389.9 ± 70.7 | 73.0 ± 1.1 | - | 2 | 4 |
| HD 156098 | 152449405 | 84551 | 5.53 | Scorpius | 259.3 | −32.7 | 631.4 ± 42.9 | 34.7 ± 1.3 | - | - | - |
| 14 Boo | 459250741 | 69536 | 5.53 | Boötes | 213.5 | 13.0 | 929.6 ± 40.5 | 51.3 ± 1.4 | - | - | - |
| $\phi$ Gru | 175400332 | 115054 | 5.54 | Grus | 349.5 | −40.8 | 1330.9 ± 60.4 | 65.0 ± 1.6 | - | - | - |
| HD 55575 | 156890613 | 35136 | 5.54 | Lynx | 109.0 | 47.2 | 1934.9 ± 111.0 | 94.6 ± 1.7 | B | - | - |
| HD 104304 | 152738837 | 58576 | 5.54 | Virgo | 180.2 | −10.4 | 3224.3 ± 52.3 | 136.2 ± 0.7 | - | - | 5 |
| HD 53705 | 130645536 | 34065 | 5.56 | Puppis | 106.0 | −43.6 | 1989.9 ± 98.4 | 101.8 ± 0.7 | B | - | 2, 5 |
| HD 46569 | 255630992 | 31079 | 5.58 | Carina | 97.8 | −51.8 | 932.2 ± 20.5 | 49.7 ± 0.3 | - | - | 2, 5 |
| HD 17948 | 390733496 | 13665 | 5.59 | Cassiopeia | 44.0 | 61.5 | 1785.4 ± 51.4 | 86.0 ± 1.4 | - | - | - |
| HD 65907 | 372914091 | 38908 | 5.59 | Carina | 119.4 | −60.3 | 3006.9 ± 165.7 | 128.5 ± 1.2 | B | - | 2 |
| HD 14214 | 419994887 | 10723 | 5.6 | Cetus | 34.5 | 1.8 | 1667.2 ± 51.5 | 83.4 ± 0.9 | - | - | 5 |
| HD 43318 | 242250358 | 29716 | 5.62 | Orion | 93.9 | −0.5 | 863.0 ± 51.8 | 50.1 ± 1.8 | - | - | - |
| HD 132254 | 309765388 | 73100 | 5.63 | Boötes | 224.1 | 49.6 | 1764.3 ± 80.8 | 87.8 ± 2.2 | - | - | - |
| HD 133002 | 288183829 | 72573 | 5.63 | Ursa Minor | 222.6 | 82.5 | 424.7 ± 15.9 | 26.0 ± 0.5 | - | 7 | - |
| 10 Ari | 118247219 | 9621 | 5.64 | Aries | 30.9 | 25.9 | 574.7 ± 19.2 | 34.6 ± 1.2 | - | 2 | 5 |
| 72 Psc | 384881668 | 5081 | 5.64 | Pisces | 16.3 | 14.9 | 946.2 ± 77.0 | 52.0 ± 1.6 | - | - | 5 |
| 64 Cet | 337046898 | 10212 | 5.64 | Cetus | 32.8 | 8.6 | 760.9 ± 24.6 | 43.0 ± 0.6 | - | - | - |
| HD 159332 | 462666639 | 85912 | 5.65 | Hercules | 263.3 | 19.3 | 869.8 ± 28.2 | 49.2 ± 0.9 | - | 2 | - |
| $\pi$ Men | 261136679 | 26394 | 5.65 | Mensa | 84.3 | −80.5 | 2621.4 ± 59.7 | 116.6 ± 0.5 | B | 15, 2 | 3 |
| $\nu^2$ Lup | 136916387 | 75181 | 5.65 | Lupus | 230.5 | −48.3 | 2689.9 ± 138.1 | 123.0 ± 0.9 | B | 28 | 3 |
| HD 136359 | 456061659 | 75308 | 5.65 | Circinus | 230.8 | −60.7 | 843.2 ± 37.1 | 47.1 ± 1.9 | - | - | - |
| HD 195564 | 205591703 | 101345 | 5.66 | Capricornus | 308.1 | −9.9 | 1167.3 ± 46.9 | 59.3 ± 1.8 | - | - | 4 |
| 44 And | 196692178 | 5493 | 5.67 | Andromeda | 17.6 | 42.1 | 424.3 ± 24.7 | 27.4 ± 0.8 | - | - | - |
| 5 And | 252676979 | 114210 | 5.68 | Andromeda | 346.9 | 49.3 | 1291.0 ± 35.5 | 65.9 ± 1.5 | - | - | - |
| 38 Cet | 248383125 | 5833 | 5.7 | Cetus | 18.7 | −1.0 | 831.3 ± 34.9 | 45.6 ± 1.4 | - | - | - |
| HD 142 | 389757979 | 522 | 5.7 | Phoenix | 1.6 | −49.1 | 1890.9 ± 163.6 | 91.1 ± 2.0 | - | - | 3 |
| 68 Dra | 236871353 | 99500 | 5.7 | Draco | 302.9 | 62.1 | 716.2 ± 14.7 | 40.2 ± 0.6 | - | - | 2 |
| HD 184960 | 26884478 | 96258 | 5.71 | Cygnus | 293.6 | 51.2 | 1870.6 ± 73.9 | 91.9 ± 0.9 | - | - | 2, 3 |
| HD 214850 | 379660147 | 111974 | 5.72 | Pegasus | 340.2 | 14.5 | 637.9 ± 14.3 | 39.4 ± 1.5 | - | - | 5 |
| HD 190360 | 105999792 | 98767 | 5.73 | Cygnus | 300.9 | 29.9 | 2358.2 ± 74.1 | 112.2 ± 0.7 | B | - | 2, 3, 4 |
| HD 89744 | 8154501 | 50786 | 5.73 | Ursa Major | 155.5 | 41.2 | 1028.4 ± 108.5 | 55.2 ± 1.6 | - | - | 3, 4 |
| 84 Her | 460022840 | 86731 | 5.73 | Hercules | 265.8 | 24.3 | 631.4 ± 16.0 | 37.6 ± 1.5 | - | - | - |
| 37 Gem | 80226651 | 33277 | 5.74 | Gemini | 103.8 | 25.4 | 2436.1 ± 418.7 | 109.8 ± 1.3 | B | - | - |
| HD 9562 | 29845542 | 7276 | 5.75 | Cetus | 23.4 | −7.0 | 1030.5 ± 36.2 | 58.8 ± 0.9 | - | - | - |
| HD 199623 | 79015105 | 103673 | 5.76 | Indus | 315.1 | −51.3 | 1631.1 ± 59.9 | 81.1 ± 1.6 | - | - | - |
| 59 Eri | 118034753 | 22325 | 5.76 | Eridanus | 72.1 | −16.3 | 781.6 ± 24.0 | 46.6 ± 1.7 | - | - | - |
| HD 109409 | 72814920 | 61379 | 5.76 | Centaurus | 188.7 | −44.7 | 1172.3 ± 23.9 | 61.5 ± 0.3 | - | 2, 7 | - |
| 22 UMa | 358013866 | 47013 | 5.77 | Ursa Major | 143.7 | 72.2 | 744.5 ± 26.3 | 41.0 ± 0.9 | - | - | - |
| HD 30562 | 176379354 | 22336 | 5.77 | Eridanus | 72.2 | −5.7 | 1447.6 ± 216.6 | 74.1 ± 1.0 | - | 2 | 3 |
| HD 49933 | 281812116 | 32851 | 5.78 | Monoceros | 102.7 | −0.5 | 1997.7 ± 117.8 | 92.5 ± 1.5 | - | 29, 30 | 4 |
| $\lambda^2$ For | 122555698 | 12186 | 5.78 | Fornax | 39.2 | −34.6 | 1374.3 ± 28.0 | 69.7 ± 0.7 | - | 31, 2 | 3 |
| HD 11007 | 20931913 | 8433 | 5.78 | Triangulum | 27.2 | 32.7 | 1239.7 ± 75.9 | 67.0 ± 0.7 | - | - | - |
| HD 89569 | 463794734 | 50493 | 5.8 | Vela | 154.7 | −56.1 | 1143.8 ± 32.2 | 61.1 ± 1.8 | - | - | - |
| HD 76932 | 348837162 | 44075 | 5.8 | Hydra | 134.7 | −16.1 | 1548.6 ± 56.4 | 86.0 ± 0.8 | - | 2 | - |
| HD 191195 | 405902259 | 99026 | 5.81 | Cygnus | 301.6 | 53.2 | 1353.0 ± 146.7 | 69.2 ± 2.3 | - | - | 2 |
| 39 Leo | 95360514 | 50384 | 5.81 | Leo | 154.3 | 23.1 | 2027.5 ± 100.2 | 104.4 ± 1.4 | - | - | - |
| HD 221420 | 277890728 | 116250 | 5.82 | Octans | 353.3 | −77.4 | 1043.0 ± 17.5 | 56.1 ± 0.2 | - | 2, 7 | 3 |
| $\iota^2$ For | 122556844 | 12288 | 5.84 | Fornax | 39.6 | −30.2 | 1227.8 ± 37.5 | 63.2 ± 1.5 | - | - | - |
| HD 103026 | 141969034 | 57841 | 5.85 | Hydra | 177.9 | −30.8 | 1189.9 ± 86.2 | 66.1 ± 1.2 | - | - | - |
| $\epsilon$ For | 88405751 | 14086 | 5.88 | Fornax | 45.4 | −28.1 | 402.1 ± 7.2 | 27.8 ± 0.4 | - | 2, 7 | - |
| HD 45067 | 42334982 | 30545 | 5.88 | Monoceros | 96.3 | −0.9 | 1117.1 ± 116.1 | 59.9 ± 0.9 | - | 2 | - |
| HD 3823 | 281667171 | 3170 | 5.89 | Tucana | 10.1 | −59.5 | 1593.8 ± 44.7 | 82.6 ± 0.6 | - | 2 | - |
| 13 Tri | 286176467 | 11548 | 5.89 | Triangulum | 37.2 | 29.9 | 1049.1 ± 38.7 | 57.8 ± 0.9 | - | - | - |
| HD 112164 | 248127641 | 63033 | 5.89 | Centaurus | 193.7 | −44.2 | 897.2 ± 23.6 | 50.6 ± 0.9 | - | 2 | - |
| 112 Psc | 422679659 | 9353 | 5.89 | Pisces | 30.0 | 3.1 | 1248.9 ± 86.8 | 67.4 ± 2.1 | - | - | - |
| HD 59984 | 6677245 | 36640 | 5.9 | Monoceros | 113.0 | −8.9 | 1139.0 ± 35.5 | 59.3 ± 1.0 | - | 2 | - |
| HD 193664 | 403585118 | 100017 | 5.91 | Draco | 304.4 | 66.9 | 3174.6 ± 201.7 | 138.5 ± 2.8 | C | - | 2 |
| HD 57006 | 453144504 | 35509 | 5.91 | Canis Minor | 109.9 | 7.1 | 591.6 ± 29.5 | 35.0 ± 1.2 | - | - | - |
| HD 52711 | 91686663 | 34017 | 5.93 | Gemini | 105.9 | 29.3 | 2583.3 ± 99.1 | 122.3 ± 0.9 | - | - | - |
| 58 UMa | 56939464 | 56148 | 5.94 | Ursa Major | 172.6 | 43.2 | 586.7 ± 29.4 | 34.8 ± 1.3 | - | - | - |
| 35 Leo | 95360265 | 50319 | 5.95 | Leo | 154.1 | 23.5 | 985.2 ± 55.0 | 54.3 ± 0.9 | - | - | 5 |
| HD 38529 | 200093173 | 27253 | 5.95 | Orion | 86.6 | 1.2 | 622.5 ± 27.9 | 35.6 ± 0.9 | - | 32, 2 | 3, 4 |
| HD 21722 | 31799975 | 15968 | 5.96 | Hydrus | 51.4 | −69.3 | 1618.1 ± 175.1 | 78.6 ± 2.0 | - | - | 2 |
| HD 33093 | 169396790 | 23831 | 5.97 | Lepus | 76.9 | −12.5 | 856.0 ± 48.8 | 49.1 ± 1.5 | - | 2 | - |
| 21 Eri | 301558151 | 17027 | 5.97 | Eridanus | 54.8 | −5.6 | 460.3 ± 5.6 | 27.3 ± 0.9 | - | 2, 7 | - |
| HD 29645 | 156157340 | 21847 | 5.97 | Perseus | 70.5 | 38.3 | 1392.7 ± 44.6 | 69.2 ± 1.0 | - | - | - |
| HD 18262 | 387541497 | 13679 | 5.97 | Cetus | 44.1 | 8.4 | 1184.6 ± 42.3 | 62.4 ± 1.7 | - | - | - |
| HD 98560 | 467957174 | 55280 | 5.99 | Carina | 169.8 | −64.6 | 1260.6 ± 167.7 | 66.1 ± 1.6 | - | - | - |
| 16 Cyg A | 27533341 | 96895 | 5.99 | Cygnus | 295.5 | 50.5 | 2236.5 ± 97.9 | 103.5 ± 1.1 | - | 33 | 2, 4, 5 |
| HD 152303 | 233503400 | 81854 | 5.99 | Ursa Minor | 250.8 | 77.5 | 1689.5 ± 49.6 | 82.2 ± 1.5 | - | - | 2 |
| HD 121384 | 208789160 | 68101 | 6.0 | Centaurus | 209.1 | −54.7 | 425.6 ± 8.2 | 28.6 ± 0.6 | - | 2, 7 | 5 |

**Notes.** Table 1 is published in its entirety in the machine-readable format at the CDS via anonymous ftp to cdsarc.u-strasbg.fr (130.79.128.5) or via http://cdsweb.u-strasbg.fr/cgi-bin/qcat?J/A+A/. A portion is shown here for guidance regarding its form and content. The table provides the measured global asteroseismic parameters for the sample, with stars sorted according to their visual magnitude ("*V*"). The first three columns provide identifiers for the stars in the form of their Bayer/Flamsteed designation (or primary name according to Simbad) in addition to their TESS ("TIC") and Hipparcos ("HIP") IDs. The "HWO" column indicates if the star is found in the HWO target list and provides the tier (A, B, or C). The last two columns provide references to the primary sources of previous seismic detections if they exits (in all cases we have indicated if a given star is contained in the Hatt et al. (2023), Zhou et al. (2024), and/or Corsaro et al. (2024) samples), and if a given star is listed in one of the other tables in the paper on "PLATO" (Table 2), "Exoplanets" (Table 3), "Interferometry" (Table 4), or "Binarity" (Table 5).

**References.** (1) Kjeldsen et al. (1995); (2) Hatt et al. (2023); (3) Corsaro et al. (2024); (4) Martić et al. (2001); (5) Bedding et al. (2001); (6) Carrier et al. (2001); (7) Zhou et al. (2024); (8) Bonanno et al. (2008); (9) Grundahl et al. (2017); (10) Carrier & Eggenberger (2006a); (11) Kjeldsen et al. (2005); (12) Carrier et al. (2005); (13) Kjeldsen et al. (2008); (14) Mosser et al. (2008); (15) Huber et al. (2022); (16) Metcalfe et al. (2023); (17) Guzik et al. (2016); (18) Hon et al. (2024); (19) Ball et al. (2022); (20) Deal et al. (2017); (21) Chontos et al. (2021); (22) Bouchy et al. (2005); (23) Metcalfe et al. (2020); (24) Bedding et al. (2006); (25) Carrier et al. (2007); (26) Metcalfe et al. (2021); (27) Metcalfe et al. (2024); (28) Delrez et al. (2021); (29) Mosser et al. (2005); (30) Appourchaux et al. (2008); (31) Nielsen et al. (2020); (32) Ball et al. (2020); (33) Metcalfe et al. (2012).